



저작자표시-비영리-변경금지 2.0 대한민국

이용자는 아래의 조건을 따르는 경우에 한하여 자유롭게

- 이 저작물을 복제, 배포, 전송, 전시, 공연 및 방송할 수 있습니다.

다음과 같은 조건을 따라야 합니다:



저작자표시. 귀하는 원저작자를 표시하여야 합니다.



비영리. 귀하는 이 저작물을 영리 목적으로 이용할 수 없습니다.



변경금지. 귀하는 이 저작물을 개작, 변형 또는 가공할 수 없습니다.

- 귀하는, 이 저작물의 재이용이나 배포의 경우, 이 저작물에 적용된 이용허락조건을 명확하게 나타내어야 합니다.
- 저작권자로부터 별도의 허가를 받으면 이러한 조건들은 적용되지 않습니다.

저작권법에 따른 이용자의 권리는 위의 내용에 의하여 영향을 받지 않습니다.

이것은 [이용허락규약\(Legal Code\)](#)을 이해하기 쉽게 요약한 것입니다.

[Disclaimer](#)

PH.D DISSERTATION

MAGNETIC PROGRAMMABLE
POLYMER-NANOPARTICLE
COMPOSITE FOR
MICROSTRUCTURE ACTUATION

자성 조절이 가능한
고분자-나노복합체를 이용한
미세 구조물의 제어

BY

JIYUN KIM

AUGUST 2013

DEPARTMENT OF ELECTRICAL ENGINEERING AND
COMPUTER SCIENCE
COLLEGE OF ENGINEERING
SEOUL NATIONAL UNIVERSITY

PH.D DISSERTATION

MAGNETIC PROGRAMMABLE
POLYMER-NANOPARTICLE
COMPOSITE FOR
MICROSTRUCTURE ACTUATION

자성 조절이 가능한
고분자-나노복합체를 이용한
미세 구조물의 제어

BY

JIYUN KIM

AUGUST 2013

DEPARTMENT OF ELECTRICAL ENGINEERING AND
COMPUTER SCIENCE
COLLEGE OF ENGINEERING
SEOUL NATIONAL UNIVERSITY

MAGNETIC PROGRAMMABLE
POLYMER-NANOPARTICLE COMPOSITE
FOR MICROSTRUCTURE ACTUATION

자성 조절이 가능한
고분자-나노복합체를 이용한
미세 구조물의 제어

지도교수 권 성 훈

이 논문을 공학박사 학위논문으로 제출함

2013 년 8 월

서울대학교 대학원

전기컴퓨터 공학부

김 지 윤

김지윤의 공학박사 학위논문을 인준함

2013 년 8 월

위 원 장 : _____ 이 신 두 _____

부위원장 : _____ 권 성 훈 _____

위 원 : _____ 조 규 진 _____

위 원 : _____ 김 성 재 _____

위 원 : _____ 백 창 옥 _____

Abstract

MAGNETIC PROGRAMMABLE POLYMER-NANOPARTICLE COMPOSITE FOR MICROSTRUCTURE ACTUATION

In this dissertation, I introduce a new magnetic nanocomposite material system and in situ fabrication process that is not shape limited and allows the programming of heterogeneous magnetic anisotropy at the microscale. The key idea is to combine the self-assembling behavior of superparamagnetic nanoparticles, which have stronger magnetization than that of general paramagnetic materials, with a spatially modulated photopatterning process. By repetitively tuning the nanoparticle assembly and fixing the assembled state using photopolymerization, I fabricate microactuators for which all parts move in different directions under a homogeneous magnetic field. To show the feasibility of this concept, I demonstrate polymeric nanocomposite actuators capable of two-

dimensional and three-dimensional complex actuations that have rarely been achieved using conventional microactuators. This approach greatly simplifies the manufacturing process and also offers effective rules for designing novel and complex microcomponents using a nanocomposite material with engineered magnetic anisotropy.

First, I investigate the self-assembling behavior of both ferrimagnetic magnetite nanoparticles and superparamagnetic nanoparticles using Monte Carlo simulation. Magnetic materials used to fabricate magnetic polymer composite include ferrimagnetic magnetite nanoparticles with 50nm of averaged diameter and superparamagnetic magnetite nanoparticles with 280nm of averaged diameter. Magnetic particle interactions, that critically affect to the self-assembling behavior of the magnetic nanoparticles, such as particle-field interaction, particle-particle dipole interaction, magnetic anisotropy and steric layer repulsion are considered. I adopt cluster-moving Monte Carlo simulation method to analyze the magnetic self-assembly of magnetic nanoparticles and investigate the self-assembling behavior of the magnetite nanoparticles varying the intensity of the applied magnetic field during the chain formation and the concentration of the magnetic nanoparticles. The result shows that the well-defined magnetic chains are formed as both the intensity of the applied magnetic field and the magnetic nanoparticle concentration increase.

Also, a novel method to fabricate magnetic nanoparticle embedded polymer composite microstructure is introduced. Briefly, the combination of photocurable

polymer and magnetic nanoparticles is photopolymerized to immobilize the various states of magnetic nanoparticles. I especially adopt a system called optofluidic maskless lithography system to fabricate various shapes of polymeric microstructures within a second. Also, I develop a model system to describe the actuation of a magnetic polymer composite. The magnetic torque, the derivative of system energy, of the composite microstructure embedding magnetic chains is calculated based on the expanded Monte Carlo simulation result. And, the steady-state elastic modulus of the magnetic composite microbeam is induced by utilizing the simulated torque and cantilever bending experiment result. The movement of cantilever type microstructure is investigated at equilibrium state that the magnetic torque equals to the mechanical restoring torque.

As an application, I demonstrate multiaxial microactuators. Polymeric microcomponents are widely used in microelectromechanical systems (MEMS) and lab-on-a-chip devices, but they suffer from the lack of complex motion, effective addressability and precise shape control. To address these needs, I fabricated polymeric nanocomposite microactuators driven by programmable heterogeneous magnetic anisotropy. Spatially modulated photopatterning was applied in a shape independent manner to microactuator components by successive confinement of self-assembled magnetic nanoparticles in a fixed polymer matrix. By freely programming the rotational axis of each component, I demonstrate that the polymeric microactuators can undergo predesigned, complex two- and three-dimensional motion.

Finally I also introduce a novel color changing microactuators based on the self-assembling behavior of the magnetic nanoparticles. I propose a color-tunable microactuator utilizing the optical and magnetic behaviors of one-dimensionally assembled superparamagnetic nanoparticles that play the role of a one-dimensional Bragg reflector and establish a magnetic easy axis. By combining these properties with rapid photopolymerization, I developed red, blue, and green micropixels whose colors could be tuned by the application of an external magnetic field. This strategy offers very simple methods for the fabrication and operation of soft color-tunable surfaces with high resolution.

Keywords: Magnetic polymer-nanoparticle composite, Microstructure actuation, Magnetic self-assembly, Photolithography

Student Number: 2010-20779

Contents

Abstract	i
Contents	v
List of Figures	vii
List of Tables	xxi
Chapter 1 Introduction	1
1.1 Polymer Nanocomposite	4
1.2 Magnetic Polymer Composite	7
1.3 Magnetic Self-assembly	11
1.4 Main Concept	15
Chapter 2 Magnetic Nanoparticle Self-assembly	18
2.1 Material Specification	19
2.1.1 Crystalline Structure of Magnetite	19

2.1.2 Synthesis of Superparamagnetic Nanoparticles	22
2.1.3 Magnetic Anisotropy of Magnetite Nanoparticles	23
2.2 Interacting Magnetic Nanoparticle with MC Simulation	27
2.2.1 Interaction Energy of Magnetic Nanoparticles	27
2.2.2 2D Cluster-moving Monte Carlo Simulation	31
2.3 Self-assembly of Magnetic Nanoparticles	34
2.3.1 Self-assembly of Ferrimagnetic Nanoparticles	36
2.3.2 Self-assembly of Superparamagnetic Nanoparticles	41
2.4 Conclusion	46
Chapter 3 Magnetic Nanoparticle Embedded Polymer Composite	47
3.1 Optofluidic Maskless Lithography	48
3.2 <i>In-situ</i> Fabrication Process	50
3.3 Torque on Magnetic Composite Structure	54
3.3.1 Magnetic Torque from Self-assembled Nanoparticles	54
3.3.2 Magnetic Torque on Arbitrary Structure	59
3.3.3 Elastic Modulus of Magnetic Composite Beam	61
3.4 Design Principles	65
3.4.1 Simple Cantilever	66
3.5 Conclusion	70
Chapter 4 Multiaxial Microactuators	71
4.1 Fabrication	72
4.1.1 Various Types of Microfluidic Devices	74

4.1.2 Micropatterning of PDMS Thin Film on Glass Substrate	76
4.1.3 Grey Mask for Flexible Hinge	77
4.2 Microfluidic Components	79
4.3 Various Types of Multiaxial Microactuators	82
4.4 Rotating Microstructures	87
4.5 Microrobot	89
4.6 Conclusion	92
Chapter 5 Magneto-chromatic Microactuators	93
5.1 Fabrication	94
5.2 Structural Color Generation	97
5.3 Color Change of Microsurface	100
5.4 Micropatterns	103
5.5 Conclusion	105
Conclusion and Future Work	106
Bibliography	109
국문 초록	119

List of Figures

Figure 1.1 Nanocomposite material in nature. (a) Inner shell of an oyster shows beautiful structural color because it is composed of repetitive layers of organic and inorganic material. (b) Bone of also naturally occurring hierarchical nanocomposite material composed of ceramic tablets and organic binders. Due to this composition, bone shows superior mechanical property even with porous structure. (c) Wood also obtains layers of organic material, thus showing the directional mechanical properties. 5

Figure 1.2 Magnetic self-assembly. (a) Ferrofluid is composed of ferromagnetic nanoparticles and carrier fluid. Ferrofluid shows interesting cooperative behavior by the application of the external magnetic field. (b) The magnetostatic interaction between effectively diamagnetic and paramagnetic particles within a magnetized ferrofluid enables to organize a diverse set of colloidal particles into highly reproducible, rotationally symmetric arrangements. (c) Flat elastomer sheets, patterned with magnetic dipoles, are self-assembled into free-standing three-dimensional objects by a competition between mechanical and magnetic

interactions..... 11

Figure 1.3 Self-assembling behavior of magnetic nanoparticles. Magnetic nanoparticles are randomly dispersed and magnetic moments are also randomly rotating without the magnetic field. When an external magnetic field is applied to the system, the magnetic nanoparticles assemble forming chain-like nanostructures to reduce the total energy of the system. If the direction of the magnetic field changes, the chain-like nanostructure rotates to reduce the increased magnetic interaction energy of the system following the changed direction of the applied magnetic field..... 13

Figure 1.4 Main concept of this thesis: the self-assembled state of magnetic nanoparticles is immobilized in various directions in polymer matrix by adopting dynamic photopolymerization process, especially called optofluidic maskless lithography system. With this methodology, polymeric microstructures can obtain various directions of magnetic anisotropy in it, which enable to actuate the microstructures in multiple directions under the homogeneous magnetic field. These types of magnetic microstructures have a potential to be useful for many microsystem applications especially requiring functional microactuators. 16

Figure 2.1 Crystal structure of magnetite. (a) Magnetite whose chemical formula is Fe_3O_4 is a representative ferromagnetic material with a cubic lattice. Magnetite has three $\langle 1,1,1 \rangle$ directions which are the magnetic easy axes of this material. $\langle 1,1,0 \rangle$ directions are intermediate axes and $\langle 1,0,0 \rangle$ directions are hard axes. This crystalline magnetic anisotropy critically determines the behavior of

the intrinsic magnetic moments. (b) At room temperature, the critical diameter for single-domain is 80nm and the diameter for superparamagnetic behavior is approximately 30nm, for the magnetite nanoparticle. 20

Figure 2.2 Magnetite nanoparticles and material properties. (a) The averaged size of the magnetite nanoparticle cluster is 282.6nm with the standard deviations of 27. (b) The magnetization curve of the magnetic nanoparticles was measured using SQUID. (c) As a result, the saturation magnetization of this nanoparticle is 72.78 emu/g and the magnetic mass susceptibility is 0.082 emu/gOe..... 22

Figure 2.3 Magnetic anisotropy (a) Crystalline magnetic anisotropy of magnetite. (b) Demagnetization field in a magnetic material. 24

Figure 2.4 Schematic of two interacting magnetic nanoparticles. The interactions including particle-field interaction, particle-particle dipole interaction, magnetic anisotropy and steric layer repulsion are considered to analyze the self-assembling behavior of the magnetic nanoparticles. 28

Figure 2.5 Cluster-moving Monte Carlo simulation process. The nanoparticles are uniformly distributed at each lattice point and their diameters are assigned following the Gaussian distribution. Directions of the magnetic anisotropy and moment are also randomly assigned for each particle. When the external magnetic field is applied on y-axis, particle location and magnetic moment direction and magnetic anisotropy direction of a single particle are perturbed within the range of 10 degree. All interaction energies are calculated and whether this state can be accepted or not is

determined by the probability, and this processes are repeated until the simulation is terminated. 32

Figure 2.6 Example of Monte Carlo simulation result. As the step number becomes 200000 times, the particles assemble forming chain-like nanostructure, but chains show branched structure..... 33

Figure 2.7 Monte Carlo simulation of ferrimagnetic magnetite nanoparticles according to the applied magnetic field intensity. As the applied magnetic field intensity increases, the assembled nanoparticles form clear straight chain structure. This appearance is comparable to the experimental chain formation. As the applied magnetic field intensity decreases, chain formation time increases and the assembled chains represent highly aggregated shape..... 36

Figure 2.8 MC simulation result of ferromagnetic magnetite nanoparticles according to the nanoparticle concentration. As nanoparticle number in a unit area increases, the assembled nanoparticles form clear and straight chain structure. This nanostructure morphology is comparable to the experimental chain formation. As the interparticle distance decreases, chain formation time decreases and the assembled chains represent long and clear shape..... 38

Figure 2.9 Self-assembly of ferrimagnetic nanoparticles with the averaged diameter of 53.2nm. Ferrimagnetic nanoparticles are assembled along the applied magnetic field direction. Length of the microchains is a function of the exposure time to an external magnetic field of 0.001, 0.01 and 0.1T. The magnetic nanoparticle concentration is 0.01g/cm³..... 39

Figure 2.10 Self-assembly of ferromagnetic nanoparticles with the averaged diameter of 53.2nm. Length of the microchains increases as the applied magnetic field intensity and the nanoparticle concentration increase. Sample includes 50 chains for each case. 40

Figure 2.11 MC simulation result of superparamagnetic nanoparticles. As the applied magnetic field intensity increases, the assembled nanoparticles form clear straight chain structure. As the applied magnetic field intensity decreases, chain formation time increases and the assembled chains represent aggregated shape. 42

Figure 2.12 MC simulation result of superparamagnetic magnetite nanoparticles. As the interparticle distance decreases, the assembled nanoparticles form clear straight chain structure. This appearance is comparable to the experimental chain formation. As the nanoparticle number per unit area decreases, chain formation time increases and the assembled chains represent quite aggregated shape due to the decrease of magnetic interaction energy proportional to three square of interparticle distance. 43

Figure 2.13 Self-assembly of superparamagnetic nanoparticles with the averaged diameter of 282.3nm. Superparamagnetic nanoparticles are assembled along the applied magnetic field direction. Length of the microchains is a function of the exposure time to an external magnetic field of 0.001, 0.01 and 0.1T. The magnetic nanoparticle concentration is 0.01g/cm³. 44

Figure 2.14. Self-assembly of ferromagnetic nanoparticles with the averaged diameter of 282.3nm. Length of the microchains increases as the applied magnetic field intensity and the nanoparticle

concentration increase. Sample includes 50 chains for each case. 45

Figure 3.1 Schematic of Optofluidic Maskless Lithography System (OFML) and the polymeric microparticles with various shapes. OFML system is composed of three major parts: UV light source, DMD modulator which patterns the injected UV light, and objective lens which focus the patterned UV light into the microfluidic channel. The focused UV light polymerize the photocurable polymer in the microfluidic channel and various shapes of microparticles can be fabricated within a second. 49

Figure 3.2 Fabrication process. By repetitive freezing of magnetic nanoparticles in photocurable resin using OFML system, magnetic polymer-nanoparticle composite material can be fabricated. 50

Figure 3.3 (a) Conventional MEMS process for cantilever fabrication. (b) Fabrication process of magnetic polymer composite actuator. (i) Patterning of a PDMS layer on slide glass. (ii) Introduction of MN-containing UV curable resin into a PDMS microfluidic channel bonded to the patterned PDMS glass. (iii) Photopatterning of the actuator using a single exposure via the OFML system. An oxygen inhibition layer is generated, preventing polymerization between the microstructure and the substrate. (iv) Washing of uncured resin..... 51

Figure 3.4 Surface of Photopolymerized superparamagnetic nanocomposite (SEM image, scale bar: 50 μ m). (a) Microparticle which contains randomly distributed magnetic nanoparticles. (b) Microparticle which contains aligned magnetic nanoparticles. Roughness is caused by the nanoparticle alignment. (c) Microparticle which shows two adjacent nanoparticle alignments..... 52

Figure 3.5 Rotation of magnetic polymer-nanoparticle composite. Ring-shaped composite microparticles rotate until the microchains fixed in the structure becomes parallel to the applied magnetic field direction..... 54

Figure 3.6 Magnetic interaction energy and induced magnetic torque of ferrimagnetic magnetite nanoparticles. Theoretically, magnetic torque from single domain material is the cross product of magnetic moment and the applied magnetic field, which means the torque is proportional $\sin\theta$. The simulation result also shows the function of $\sin\theta$ 55

Figure 3.7 Magnetic constant K_{ferri} for ferromagnetic nanoparticle composite. For all cases, the number of the magnetic nanoparticles in MC simulation was the same as 144 and interparticle distances vary according to the nanoparticle density. As a result, it turns out that K_{ferri} only depends on the absolute number of the magnetic nanoparticles in the material, not on the self-assembled state of them. 56

Figure 3.8 Magnetic interaction energy and induced magnetic torque of superparamagnetic magnetite nanoparticles. Theoretically, magnetic anisotropic torque from single domain material is proportional $\sin 2\theta$. The simulation result also shows the function of $\sin 2\theta$ 57

Figure 3.9 Magnetic constant $K_{\text{superpara}}$ for superparamagnetic nanoparticle composite. For all cases, the number of the magnetic nanoparticles in MC simulation was the same as 144 and interparticle distances vary according to the nanoparticle density. As a result, it turns out that $K_{\text{superpara}}$ depends on the magnetic

nanoparticle density, thus inferring that the magnetic torque increases as the nanoparticle number per chain increases. Therefore, $K_{\text{superpara}}$ relies on the self-assembled state of magnetic nanoparticles in composite structure. 58

Figure 3.10 Strategy to expand 2D MC simulation result to calculate the torque from 3D microstructure. The 3D total torque from this strategy determines the total magnetic torque of a model cantilever... 60

Figure 3.11 Pseudo Rigid Body Modeling to calculate the mechanical restoring torque of large-bending cantilever structure. It assumes that the magnetic composite cantilever follows the end-moment loading..... 62

Figure 3.12 Parameters for model system. Magnetic field for nanoparticle assembly, elastic modulus and magnetite nanoparticle are given. Controllable variables include actuator geometry, nanoparticle density, magnetic field for rotation and bending angle..... 65

Figure 3.13 Simple cantilever. In this shape, cantilever geometry and the relationship between the magnetic torque and the mechanical restoring torque are defined. The magnetic field required to achieve a specific bending angle can be calculated using this relationship. Also, the magnetic field intensity required to actuate the microcantilever ranges from 0.01 to 0.1T which general permanent magnet is able to afford..... 67

Figure 4.1 Actuator fabrication process. Schematics of the actuator fabrication process and photopolymerization set-up. The fabricated structure is anchored to the pure glass surface while it remains unattached above the PDMS coated region on the substrate due to

the inhibition layer.	72
Figure 4.2 Various types of microfluidic devices to fabricate versatile microactuators such as microcomponents for microfluidic system, microrobot and rotating microparticles.....	74
Figure 4.3 Patterned PDMS. (a) Chemical patterning of thin PDMS film (b) Mechanical patterning of thin PDMS film. (Scale bar: 500 μ m)	76
Figure 4.4 Connecting joints using gray scale mask: Leg-like actuators. (Left) Leg-like actuation the absence of a magnetic field. (Middle) Bending of warm leg-like actuators with gray-scale mask connecting joint. The color of the connecting joints is lighter than other parts, which means that the mechanical stiffness of that part is lower relative to other parts of the actuator. (Right) Bending of leg- like actuators without gray-scale mask connecting joints is not easy as the joints are stiffer than other parts. (Scale bar: 100 μ m).....	77
Figure 4.5 Connecting joints using a gray-scale mask: trapper (Left) The benders without a magnetic field. (Right) Bending of warm leg-like actuators with a gray-scale mask connecting joint. The color of the connecting joints is brighter than other parts, which means that the mechanical stiffness of that part is lower relative to other parts of the actuator. (Scale bar: 100 μ m)	78
Figure 4.6 Various magnetic actuation mechanisms. (Top) Free-floating particle sorter. At the intersect of three microfluidic channels, the nonmagnetic particle is sorted to a selected branch of the channel by rotating the actuator in a counterclockwise direction. (Middle) Finned microvalve for two-phase microfluidics. When the magnetic field is applied to the actuator, the rail-guided valve actuator moves	

along the rail toward the field direction and blocks one of two food dye streams (each food dye is diluted in deionized water). (i) Blue stream is blocked. (ii) Red streams are blocked. (Middle) Sorting magnetic structures. At branch points, each circular finned microstructure chooses the next rail branch according to the field direction..... 80

Figure 4.7 A microactuator containing four different easy axes recoils like a snake when a magnetic field is applied. (Scale bar 100um.) Each part of the structure bends in different directions, owing to artificial easy axes made by magnetic microchains. 83

Figure 4.8 Arrow-like magnetic actuator. Five identical arrow-like actuators bend in five different directions under the uniform magnetic field line. (Scale bar 50um.) Also, magnetic tweezer contains both a pure polymer region and a magnetic anisotropy programmed region. 83

Figure 4.9 Blooming flower-like actuator on circularly patterned PDMS. When the magnetic field is applied perpendicular to the substrate surface, the flower closes in on itself, bending its eight identical petals. (Scale bar: 500µm)..... 84

Figure 4.10 Heterogeneous cantilever actuation. Three identical cantilevers bend at different angles because their magnetic nanoparticle chain directions are different. (Scale bar: 100µm)..... 85

Figure 4.11 Heterogeneous cantilever actuation. The cantilever contains three bodies and three joints. Each body has a different magnetic axis, so it bends in different directions under the applied magnetic field. The final configuration of the cantilever would be very difficult to

achieve using conventional magnetic actuators. (Scale bar: 100 μ m) ...	85
Figure 4.12 Artificial centipede legs. Each leg is composed of two parts with different magnetic nanoparticle chain directions. As the magnetic field line direction is changed, legs move as if they were crawling on the substrate. (Scale bar: 100 μ m).....	86
Figure 4.13 Microswimmer. Two arms of the actuator are closed under the magnetic field. The two arms bend creating a space which can contain particles. As a result, the microswimmer can swim following the external magnetic field gradient closing its arms by the external magnetic field line direction. (Scale bar: 100 μ m).....	86
Figure 4.14 Color-barcoded magnetic microparticles under vertical magnetic-field lines. The particle codes are displayed on the 2D surface of the vial. Rotating color-barcoded magnetic microparticles. Non-rotating particle has no 1D chain structures in it.	87
Figure 4.15 Polymeric micro-looper. Sequential movement of a micro-looper (Scale bars 100 μ m). (a)-(b) The micro-looper creeps on the substrate as the external magnetic field is applied. First, a weak and slightly tilted magnetic field is applied. The micro-looper starts to bend and the tail moves towards the head. As the magnetic field becomes stronger and clearly vertical, the micro-looper completely arches. When the magnetic field is slightly tilted in the opposite direction, head proceeds forward and the tail sticks to the substrate. After the magnetic field is removed, a sequential crawling process is finished. The micro-looper can crawl on the substrate as this process is repeated. (c) Schematics of micro-looper movement. The micro-looper is composed of four bodies having different magnetic axis,	

such that choosing an appropriate magnetic field direction and intensity enables to achieve the desired configuration..... 90

Figure 4.16 Design optimization of a polymeric micro-looper. The micro-looper with initial design shows unnecessary twisting by the application of the magnetic field. The initial micro-looper design was changed to have ladder-like joints with bigger bodies. The head and tail have perpendicular chain direction to the substrate and arching bodies have a parallel chain direction to the substrate. (Scale bar: 100 μ m)..... 91

Figure 5.1 Process for the fabrication of a magnetically tunable chromatic microactuator. The dispersed super-paramagnetic nanoparticles (SNs) self-assemble under an applied external magnetic field to produce a structural red color, and these colored nanostructures are then lithographically fixed in a cantilever-shaped microstructure. 95

Figure 5.2 Structural color due to self-assembly of super-paramagnetic CNCs. The intrinsic color of M-ink is brown, but its color changes by the application of the external magnetic field because the CNCs assemble to form chain-like nanostructure capable of playing a role of one-dimensional photonic crystal. 97

Figure 5.3 Figure 5.3 Principles of color generation and color change. The self-assembled magnetic nanoparticles reflect a specific wavelength because of their periodicity and form artificial magnetic easy axes to regulate the chromatic microactuator. 98

Figure 5.4 Red-colored microactuator and its color change. The reflective structural color is changed as the deflection angle of the

microactuator changes, owing to the angular dependence of the structural color. (scale bar: 50 μ m)	100
Figure 5.5 Spectra of the red microactuator. The self-assembled nanoparticles have a resonant peak at a green wavelength; therefore, the highest intensity occurs when the color of the microactuator becomes green. Bending angle determines the color of the microactuator.....	101
Figure 5.6 Green and blue microactuators. I can choose the original color of the microactuators by varying the intensity of the applied magnetic field during the fabrication process. (scale bar: 50 μ m).....	102
Figure 5.7 Color surface with multiple pixels of various colors. The surface is scalable, because the original color can be determined during the fabrication process within a half-second (scale bar: 50 μ m)	103
Figure 5.8 Synactuation of blue-colored microactuators. All seven microactuators begin with a blue color and change their color simultaneously upon the application of the external magnetic field..	104

List of Tables

Table 1.1 Microfabrication techniques for polymer nanocomposite structure.....	6
Table 1.2 Magnetic polymer-nanoparticle composite for microsystem.....	8
Table 1.3 Comparison of magnetic forces working on magnetic structure. ..	9
Table 2.1 Basic parameters for MC simulation	35
Table 3.1 Parameters for magnetic torque calculation.....	63

Chapter 1

Introduction

In this dissertation, I introduce a new magnetic nanocomposite material system and in situ fabrication process that is not shape limited and allows the programming of heterogeneous magnetic anisotropy at the microscale. The key idea is to combine the self-assembling behavior of superparamagnetic nanoparticles, which have stronger magnetization than that of general paramagnetic materials, with a spatially modulated photopatterning process. By repetitively tuning the nanoparticle assembly and fixing the assembled state using photopolymerization, I fabricate microactuators for which all parts move in different directions under a homogeneous magnetic field.

In chapter 1, I describe the advantages of polymer based nanocomposite material, especially incorporating magnetic nanoparticles. And, several types of self-assembling behavior of the magnetic particulates, such as ferrofluids, are introduced because the key of this technology is to program the magnetic easy axis in polymer by fixing the self-assembled magnetic nanoparticles. Lastly, the main concept of this research is described, which combine the magnetic nanoparticle

self-assembly and photolithography.

In chapter 2, the self-assembling behavior of the magnetic nanoparticles is analyzed using Monte Carlo simulation. Chain formation of both ferrimagnetic nanoparticles with the averaged diameter of 50nm and superparamagnetic nanoparticles with the averaged diameter of 280nm is investigated in terms of the applied magnetic field intensity and the initial magnetic nanoparticle concentration. The tendency to the magnetic microchain elongation observed from the Monte Carlo simulation properly corresponds to the experimental result.

In chapter 3, magnetic torque working on the polymer-nanoparticle composite structure is investigated based on the simulation result in chapter 2. Also, the advantages of in-situ fabrication method using optofluidic maskless lithograph system are described, compared to conventional lithography for the development of microactuators. Composite incorporating ferromagnetic nanoparticles rotate due to the magnetic moment-field interaction regardless of the self-assembled state of the nanoparticles, while composite incorporating superparamagnetic nanoparticles induces the torque from the magnetic moment-moment interaction. Based on the magnetic torque calculated from the simulation, the static model system for a simple cantilever is developed.

In chapter 4, to show the feasibility of this technology, various types of polymeric nanocomposite actuators are demonstrated, capable of two-dimensional and three-dimensional complex actuations that have rarely been achieved using conventional microactuators.

In chapter 5, magnetochromatic microactuators are introduced, which utilize the structural color generation and the magnetic easy axis implanting of self-assembled nanoparticles. Microchains composed of superparamagnetic nanoparticles play both roles of one-dimensional photonic crystal reflecting

structural color and magnetic easy axis providing the rotational axis in the microstructure. A surface composed of several color changing pixels is fabricated and its spectral characteristic is also analyzed.

I envision that this approach greatly simplifies the manufacturing process and also offers effective rules for designing novel and complex microcomponents using magnetic axis engineering.

1.1 Polymer Nanocomposite

Polymeric material has become an indispensable part of our life as being compartments of various objects such as furniture, containers, versatile casings, and study materials. They have attracted a great deal of attention, as they are lightweight, flexible and easily processed. Pristine polymers, however, often suffer from low durability, weak mechanical property and flammability. [1] For example, the high water content and flexibility of hydrogel polymers lead to inferior mechanical stability limiting their applications. Thus, there has been an increasing demand for novel strategies to build new materials that satisfy several functions for a specific application.

Nanocomposite materials have attracted great attention of scientists and engineer in recent years. These materials have clear advantages over those used to produce homogeneous large-grained materials. The inclusion of nanosized building blocks in a specific matrix provide new ways to create novel materials with superior physical, chemical and electrical properties such as improved mechanical durability, good conductivity, and optical selectivity. [2] The most convincing examples of such materials are naturally occurring structures such as bone and seashell. Bone has outstanding mechanical stability due to the hierarchical arrangement of ceramic tablets and organic binder. [3] Inner surface of oyster is composed of repeated layers of organic and inorganic materials, thus representing metallic structural colors. The composition and the arrangement of nanosize building blocks facilitate various functions of the composite material, and this strategy to tailor the material property using nanosized building blocks has been investigated in several interdisciplinary fields. [4-7]

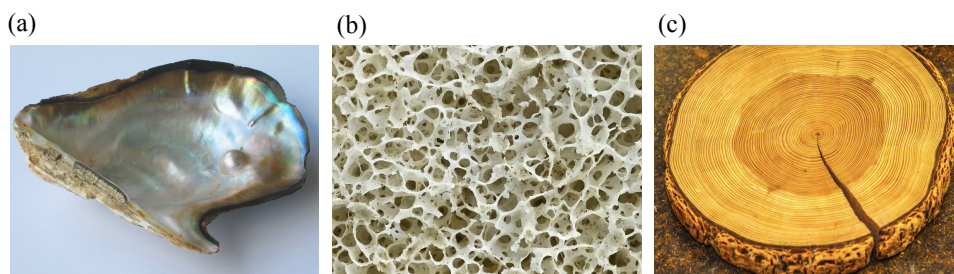


Figure 1.1 Nanocomposite material in nature. (a) Inner shell of an oyster shows beautiful structural color because it is composed of repetitive layers of organic and inorganic material. [8] (b) Bone is also naturally occurring hierarchical nanocomposite material composed of ceramic tablets and organic binders. Due to this composition, bone shows superior mechanical property even with porous structure. [3] (c) Wood also obtains layers of organic material, thus showing the directional mechanical properties. [9]

A nanocomposite is considered multiphase solid material where one of the phases having nano-scale repeat distances between the different phases which composes the material. Examples include copolymers, porous media, gels and colloids. These materials typically consist of an organic host material containing inorganic particulate or vice versa. [10] They also combine more than two phases to form a multiphase solid. Multiphase materials with nanosized building blocks are able to demonstrate different but better mechanical, electrical, optical, and catalytic properties than those of individual homogeneous materials. In other words, multifunctional behavior derived from the synergic combination of various phases, not expected from the simple sum of the individual phases, benefit to fabricate a novel material for a specific purpose. [11]

Table 1.1 Microfabrication techniques for polymer nanocomposite structure [10]

Principle	Mold	Light	Ablation	Bottom-up
Technology	Hot embossing Nanoimprint Casting Injection molding	Photolithography Streolithography 2-photon Lithography	Laser Plasma etching	Electrospinning Inkjet printing

Polymer based nanocomposites are easy to fabricate using conventional fabrication technologies, thus having attracted attention due to the potential to address specific microsystem challenges. Polymeric structures are usually fabricated using injection molding, photolithography, etching, printing, electrospinning and so on, and polymeric nanocomposites can be obtained by simply incorporating various types of nanoparticulates such as metallic nanoparticles and carbon nanotubes into a polymer matrix during the fabrication process. The acquirement of nanosized functional building blocks results in unique properties such as improved mechanical strength, stimuli-responsive behaviors and enhanced biological interactions. [12] For instance, the incorporation of nanosized hydroxyapatite in polymer hydrogels has improved the mechanical properties, thus made this nanocomposite useful for a broad range of tissue engineering. In addition, polymeric material can be made responsive to external stimuli by incorporating stimuli-specific nanoparticulates. To that end, a variety of approaches using magnetic nanoparticles, gold nanoparticles or carbon nanotubes have been employed to impart remote controlled capabilities to composite materials [13-21], because these materials can eliminate the need to be physically wired to additional inorganic electrodes or control devices. In this dissertation, photolithography is adopted to fabricate magnetic composite microstructure. [22]

1.2 Magnetic Polymer Composite

The advantages of polymers and magnetic materials can be merged into one material by embedding magnetic fillers in the polymer matrix. Polymeric materials can be easily processed because they are light, flexible and easy to structure. Their optical transparency and biocompatibility also allow to broaden the spectrum of potential applications. Magnetic materials can be controlled without any additional apparatus having physical contact with the structure. As long as the actuation environment is magnetically transparent, they can be operated in many different media including air, vacuum, conducting and non-conducting media. Therefore, magnetic composite material systems benefit from both outstanding physical and chemical properties of the polymer and remote controllability of magnetic fillers. [23] The flexibility of magnetic actuation in conjunction with the advantages of polymeric materials makes magnetically driven metal-polymer composites attractive for many applications such as magnetic beads in bioassays and magnetic gating valves in microfluidic control systems. Magnetic polymer composite can be also utilized for microactuators which manipulate biological particulates in liquid environment and free microrobots that transport and release drugs to a specific target. [24, 25] Furthermore, microfluidic systems often exploit magnetic polymer composites as actuating microcomponents including pumps, mixers and remote sensors. [26-29]

Table 1.2 Magnetic polymer-nanoparticle composite for microsystem.

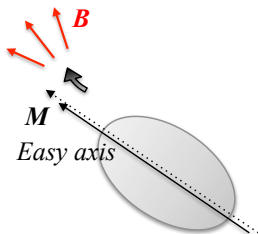
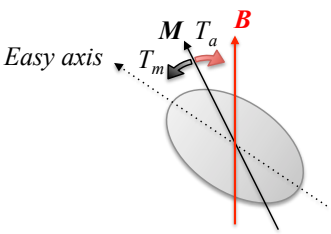
Polymer	MN	MN Size	MN Type	Fabrication	Dimension	Utilization	Ref
PDMS	Fe ₃ O ₄	200nm	Ferro	casting	~200μm	Micro stirrer	[30]
PDMS	Fe ₃ O ₄	10nm	Superpara	Spin-coating	4000x36μm	Membrane	[31]
PDDA	γ-Fe ₂ O ₃	50nm	Ferro	Nano self-assembly	200x500x0.2μm	Cantilever	[32]
Acrylic Resin	Fe ₃ O ₄	50nm	Ferro	Stereo lithography	8x8x4mm	Flow sensor	[33]
SU8	Ni	~100nm	Ferro	Photolitho	1000x300x70μm	Micromirror	[34]
SU8	Ni	100nm	Ferro	Photolitho	430x130x15μm	Torsion actuator	[35]
SU8	γ-Fe ₂ O ₃	10nm	Superpara	Photolitho	3x3x12μm	Cell sorting	[36]
Methyl Acrylate	Fe ₃ O ₄	10nm	Superpara	Two-photon litho.	14μm	Microturbine	[37]
ETPTA	α-Fe ₂ O ₃	330nm	Ferro	Photolitho	~100μm	Separation	[38]
SU8	Fe ₃ O ₄	50nm	Ferri	Photolitho	100x110x50μm	Transporter	[39]

The incorporated particulates should be well dispersed to achieve uniform material properties in the structure. [26] One of the most frequently used methods to bring magnetic behavior into polymeric materials is to mix specific magnetic fillers with the polymer. The relevant magnetic materials used for the fabrication of magnetic nanocomposite include typical inorganic materials such as Fe, Fe₂O₃, Fe₃O₄, Co and Ni. [25]

Most technologies for polymeric structure fabrication can be adopted to manufacture magnetic nanocomposite structure, even though particle dispersion and aggregation limit the minimum feature size of the magnetic composite structure as well as critically influence the uniformity in mechanical and magnetic properties. One of the most promising microfabrication technologies capable of applying to magnetic composite fabrication is photolithography. [27-29] This

process allows cost-effective batch-fabrication of microstructures with small feature sizes as well as various shapes. For example, ferromagnetic nanoparticles have been incorporated in the photocurable polymer SU-8 to create a magnetic nanocomposite for the use of micromirror or torsion microactuator. [40, 41] Other applications include microturbines, microstirrers, microvalves, microsorter, microgrippers, micromotors and flow sensors, and these results show that engineered magnetic polymer composites offer a high potential for various microsystem applications.

Table 1.3 Comparison of magnetic forces working on magnetic structure.

	Magnetic Force	Magnetic Torque	Magnetic Anisotropy Torque
			
Driving Equation	$F = m \cdot \nabla B$	$T_m = m \times B$	$T_a = K \sin 2\theta$
Advantages	-Translational movement	-Rotational movement	-Rotational movement
Disadvantages	-Strong -Low controllability	-Strong -Difficult to engineer	-Weak -Difficult to engineer

Three types of magnetic forces are capable of manipulating polymeric magnetic composite structure. First, the magnetic translational force is general rule that magnetic materials are usually attracted or repelled into regions of stronger magnetic field depending on the orientation of the magnets. [42] Second, under the magnetic field derived from a magnet, the other magnetic material near the first is allowed to turn and promptly rotates to align itself with the magnetic field line. In

this case, the free magnetic material experiences a magnetic torque because the magnetic field of the stationary magnet creates the interacting force. This magnetic torque, which is proportional to the applied magnetic field intensity and the magnetic moment of the magnetic material, works until the magnetic moment of the free magnetic material align with the magnetic field line. [42] Lastly, there exists another type of magnetic torque which arises from the magnetic anisotropy of the material. A magnetically isotropic material has no preferential direction for its magnetic moment in the absence of an applied magnetic field. On the other hand, a magnetically anisotropic material obtains energetically favorable directions which are called magnetic easy axes in it, thus tending to align its magnetic moment with one of the easy axes. When the magnetic moment deviates from the easy axis, the magnetic anisotropic torque works to minimize the magnetic interaction energy of the material system. [43]

The conventional magnetic microcomponents reported so far have only offered simple motions such as monotonous translation and rotation, owing to intrinsic limitations in their actuation principles. The utilization of the magnetic translational force and the magnetic torque presents inherent difficulties in the design of multi-directionally moving microcomponents because it becomes harder to control the spatial variation of the magnetic field at the microscale. This confines feasible motions capable of achieving using typical magnetic forces to simple rotation or bending. [44-49] More importantly, patterning multiple magnetic moments with different directions in a magnetic structure is difficult to achieve with conventional micromachining process. Even if each functional part of a magnetic structure has a differently oriented magnetic moment, they will attract each other without the external magnetic stimulation and result in unwanted aggregation of the microcomponents even before the actuation. Therefore,

achieving complicated actuation with precise shape control as well as large deflection requires another type of energy transduction mechanism and corresponding material systems.

1.3 Magnetic Self-assembly

Magnetic particulates interact each other with and without the external magnetic stimuli, thus creating various superstructure according to the material property, the particulate size, and the external magnetic stimuli. Sometimes randomly dispersed magnetic particulates forms an organized structure or pattern as a consequence of specific magnetic interactions among the particulates, and these superstructures are able to provide functionality to a specific material system. There exist several cases which utilize the self-assembling behavior of the magnetic particulates to build more complicated and sensitive system.

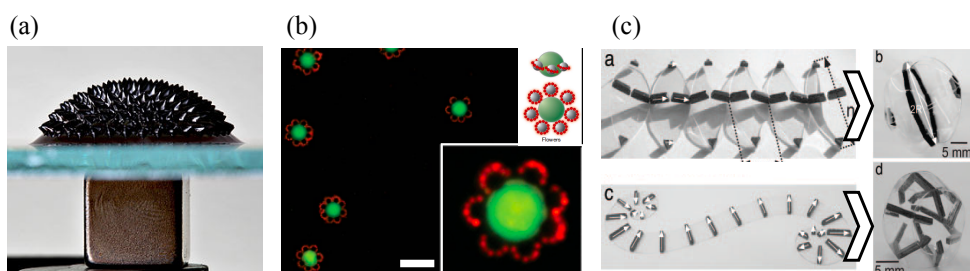


Figure 1.2 Magnetic self-assembly. (a) Ferrofluid is composed of ferromagnetic nanoparticles and carrier fluid. Ferrofluid shows interesting cooperative behavior by the application of the external magnetic field. [50] (b) The magnetostatic interaction between effectively diamagnetic and paramagnetic particles within a magnetized ferrofluid enables to organize a diverse set of colloidal particles into highly reproducible, rotationally symmetric arrangements. [51] (c) Flat elastomer sheets, patterned with magnetic dipoles, are self-assembled into free-standing three-dimensional objects by a competition between mechanical and magnetic interactions. [52]

Ferrofluids are colloidal liquids composed of nanoscale ferromagnetic particles and a carrier fluid, which become strongly magnetized in the presence of an external magnetic field. Each particle is completely coated with a surfactant and magnetic interaction of particles is weak enough that surfactants' Van der Waals force can prevent magnetic agglomeration in the absence of external magnetic field. [50] Therefore, ferrofluids are usually classified as superparamagnetic material rather than ferromagnetic material because they hardly retain magnetization with an externally applied magnetic field. When the external magnetic field is applied, the ferrofluids change the morphology into more organized and periodic form.

Also, as shown in figure 1.2, colloidal magnetic particles can be organized into highly reproducible and rotationally symmetric arrangements under the external magnetic field. Magnetostatic interaction between diamagnetic and paramagnetic particles results to build various multipolar configurations such as axial quadrupoles, axial octupoles, linear quadrupoles and mixed multiple arrangements within a magnetized ferrofluid. These superstructures resemble electrostatic charge configurations, but have been hardly represented using this technique. [51]

In macro scale, the spontaneous assembling of two dimensional elastomeric sheets was achieved using magnetic interaction. The flat sheet patterned with permanent magnets is folded into a three dimensional object that is topologically equivalent of spherical shells. The competition between mechanical and magnetic interactions determines the process of self-assembly. This strategy obtains a potential for the fabrication of three dimensional electronic devices which generate a simple electrical circuit surrounding a spherical cavity. [52]

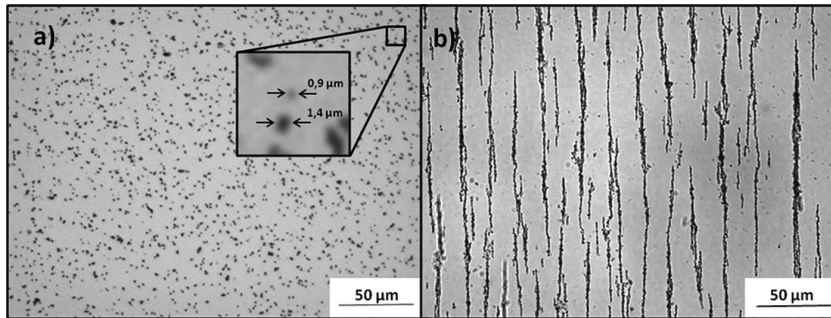


Figure 1.3 Self-assembling behavior of magnetic nanoparticles. Magnetic nanoparticles are randomly dispersed and magnetic moments are also randomly rotating without the magnetic field. When external magnetic field is applied to the system, the magnetic nanoparticles assemble forming chain-like nanostructures to reduce the total energy of the system. If the direction of the magnetic field changes, the chain like nanostructure rotate to reduce the increased magnetic interaction energy of the system following the changed direction of the applied magnetic field. [53]

Formation of microchains is a widely known self-assembling behavior of the magnetic nanoparticles. In the absence of external magnetic field, the nanoparticles are randomly dispersed in a liquid, and have no preferential directions of aggregation. When the external magnetic field is applied, the magnetic nanoparticles self-assemble, forming chain-like nanostructures along the magnetic field lines to minimize the magnetic interaction energy of the system. Remarkably, when the magnetic field direction is changed, all chains rapidly rotate or realign along the changed magnetic field direction. The principle of rotation varies according to the types of magnetic nanoparticles. Ferromagnetic or ferromagnetic microchains rotate due to the magnetic moment-field interaction while

superparamagnetic microchains rotate due to the magnetic moment-moment interaction. In both cases, these magnetic microchains can play a role of artificial magnetic easy axes when these arrangements are fixed in a solid structure. [54]

1.4 Main Concept: Programmable Magnetic Composite

Conventional magnetic composites mostly utilize magnetic translational attraction to make a magnetic structure function. This is because patterning multiple magnetic moments with different directions in a microstructure is very difficult to achieve using a conventional micromachining process. Also, if each functional part of a microcomponent has a differently oriented magnetic moment, microcomponents will attract each other in the absence of the external magnetic stimulation, resulting in unwanted configuration of the system even before the actuation. Therefore, to achieve complex actuations with large deflection and precise shape control, other energy transduction mechanisms should be introduced and a corresponding magnetic material system should be developed to apply such mechanisms.

By adopting a superparamagnetic material, precisely controlled multi-directional movements in a microactuator can be achieved. Theoretically, superparamagnetic material aligns its magnetic moment with the external magnetic field direction without spontaneous magnetization as well as magnetic hysteresis. Thus, if I can pattern various directions of magnetic anisotropy in a solid structure, each part of a superparamagnetic microactuator which obtains a different magnetic anisotropy does not respond without the external magnetic field, but can rotate to make its own magnetic easy axis parallel to the orientation of the external magnetic field. This strategy provides an effective energy transduction mechanism for solid

structure actuation. This property, however, has not yet been used because the conventional magnetic anisotropic torque is relatively small compared with other magnetic forces. Furthermore, the direction of an intrinsic magnetic easy axis is firmly determined by the shape and the magnetocrystalline structure of the magnetic material, and thus cannot be controlled in natural magnetic materials.

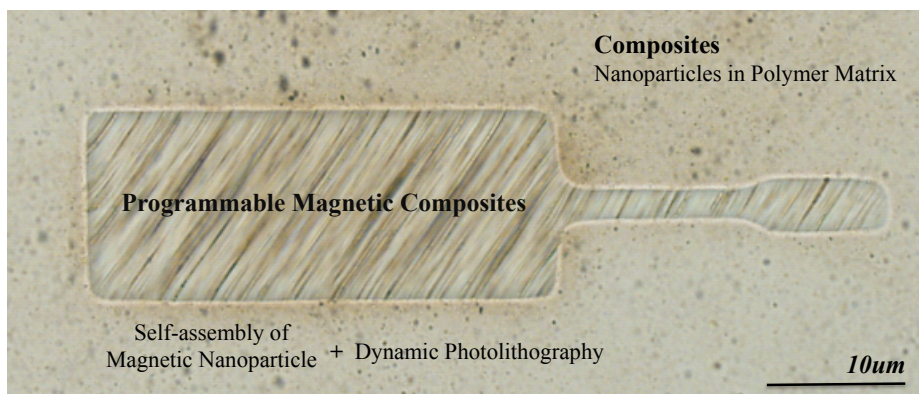


Figure 1.4 Main concept of this thesis: the self-assembled state of magnetic nanoparticles is immobilized in various directions in polymer matrix by adopting dynamic photopolymerization process, especially called optofluidic maskless lithography system. With this methodology, polymeric microstructures can obtain various directions of magnetic anisotropy in it, which enable to actuate the microstructures in multiple directions under the homogeneous magnetic field. These types of magnetic microstructures have a potential to be useful for many microsystem applications especially requiring functional microactuators.

In this dissertation, I develop a new magnetic nanocomposite material system and in situ fabrication process that allows the programming of heterogeneous magnetic anisotropy at the microscale in a shape independent manner. The key idea is to combine self-assembling behavior of superparamagnetic nanoparticles, which have stronger magnetization than that of same sized paramagnetic materials, with a spatially modulated photopatterning process. By repetitively tuning the nanoparticle assembly and fixing the assembled state using photopolymerization, microactuators for which all parts move in different directions under a homogeneous magnetic field can be fabricated. To show the feasibility of the concept, polymeric nanocomposite actuators capable of two-dimensional and three-dimensional complex actuations that have rarely been achieved using conventional microactuators are demonstrated. This approach greatly simplifies the manufacturing process and also offers effective rules for designing novel and complex microcomponents using a nanocomposite material with engineered magnetic anisotropy.

Chapter 2

Magnetic Nanoparticle Self-Assembly

In this chapter, the self-assembling behavior of magnetite nanoparticles is investigated using Monte Carlo simulation. In the simulation, particle interactions, which affect to the self-assembling behavior of the magnetic nanoparticles, such as particle-field interaction, particle-particle dipole interaction, magnetic anisotropy and steric layer repulsion, are considered. Based on the previous research, cluster-moving Monte Carlo method is realized using Python to investigate aggregate structure of magnetic fluid system. Self-assembling behavior of the magnetite nanoparticles vary according to the intensity of the applied magnetic field during the chain formation and the concentration of the magnetic nanoparticles. The result shows that well-defined magnetic chains are formed as both the intensity of the applied magnetic field and the magnetic nanoparticle concentration increase, which is well-fitted to experimental result. Also, magnetite with 50nm diameter shows cooperative ferromagnetic behavior and magnetite with 280nm diameter represents superparamagnetic behavior, as expected in the theoretical investigation.

2.1 Material Specification

In the chapter 2.1, the material properties of the magnetite nanoparticle, which are fundamental to analyze the self-assembling behavior of the magnetic nanoparticles, are investigated. First, the crystalline structure of the magnetite which causes various magnetic properties is investigated. The superparamagnetic nanoparticles with the averaged diameter of 280nm are synthesized in Biophotonics and nanoengineering laboratory, and the magnetic characteristics such as the magnetic susceptibility and the saturation magnetization are measured using the superconducting quantum interference device (SQUID). Also, the magnetic anisotropy of these nanoparticles, which determines the self-assembling behavior as well as the magnetic anisotropic torque working on the magnetic polymer composite, is defined.

2.1.1 Crystalline Structure of Magnetite

Magnetite is a well-known mineral as both one of the common naturally occurring iron oxides and one of the strongest magnetic materials among all the naturally occurring minerals on Earth. It has black or brownish-black color with a metallic gloss. The chemical formula is Fe_3O_4 , the chemical IUPAC name is iron (II,III) oxide and the common chemical name is ferrous-ferric oxide. [55] Magnetite is a common ferrimagnetic oxide, and its structural formula is $[\text{Fe}^{3+}]_T[\text{Fe}^{3+}, \text{Fe}^{2+}]_O\text{O}_4$. In ionic compounds, including oxides, complex forms of magnetic ordering can occur as a result of the crystal structure, and one type of magnetic ordering is called ferrimagnetism.

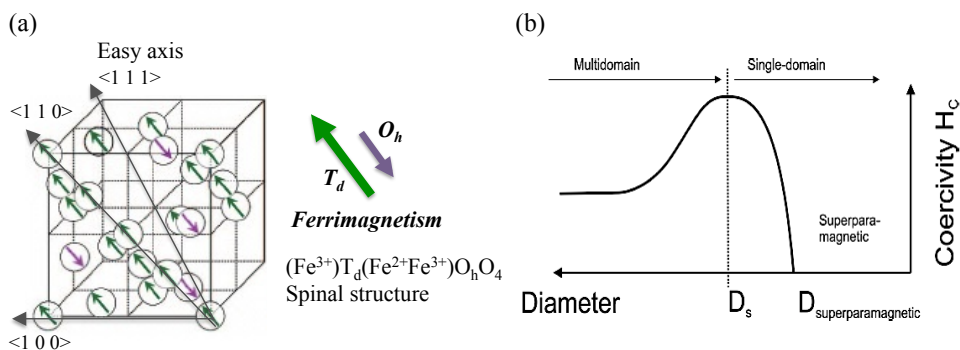


Figure 2.1 Crystal structure of magnetite. (a) Magnetite whose chemical formation is Fe_3O_4 is representative ferromagnetic material with cubic lattice. Magnetite has three $\langle 1,1,1 \rangle$ directions which are the magnetic easy axes of this material. $\langle 1,1,0 \rangle$ directions are intermediate axes and $\langle 1,0,0 \rangle$ directions are hard axes. This crystalline magnetic anisotropy critically determines the behavior of the intrinsic magnetic moments. (b) At room temperature, the critical diameter for single-domain is 80nm and the diameter for superparamagnetic behavior is approximately 30nm, for the magnetite nanoparticle. [56, 57]

A simple representation of the magnetic spins in a ferrimagnetic oxide is shown in figure 2.1. The magnetic structure is composed of two magnetic sublattices separated by oxygens. Oxygen anions mediate the superexchange interactions resulting in an antiparallel alignment of spins between the sublattices. In ferrimagnets, therefore, the magnetic moments of the sublattices are not equal and result in a net magnetic moment. Ferrimagnetism exhibits all the hallmarks of ferromagnetic behavior spontaneous magnetization, Curie temperatures, hysteresis, and remanence. The larger oxygen ions are closely packed in a cubic lattice and the smaller Fe ions fill in the gaps, thus magnetite, Fe_3O_4 crystallizes with the spinel structure. [58]

In nanoscale, magnetite changes its magnetic state from ferromagnetic to superparamagnetic. In general, thermal fluctuation depending on the material temperature causes the magnetization to fluctuate in a random manner, but energy barrier proportional to the material volume inhibits the magnetization of a material to flip from one state to another. When the thermal fluctuation overcomes the intrinsic energy barrier of the magnetic material at specific temperature and volume, this material appears to be blocked showing ferromagnetic behavior. And opposite, if the energy barrier gets small at the same temperature, the magnetic moment can jump from state to state fast enough to make the material superparamagnetic. As a result, the competition between the thermal energy and the magnetic barrier plays a key role to determine the magnetic behavior of a magnetic material. The temperature which thermal energy balances magnetic barrier energy is called blocking temperature. Also, the volume at this state can be thought of as the volume at which blocking temperature is lower than room temperature.

On the contrary, as size of the magnetic material increases, the homogeneous ferrimagnetic state incurs an increasing energy cost because of the demagnetizing field. Demagnetizing field tends to rotate the magnetization in a way that reduces the total moment of the magnet, and this energy is balanced by the exchange interaction energy that tends to keep magnetic spins aligned. Therefore, there exists a critical size at which the balance tips in favor of the demagnetizing field and the multi-domain state is favored. In larger materials than its critical size, the magnetization is organized in magnetic domains. In the case of spherical magnetite particles, the critical diameter, which the transition between superparamagnetism and single-domain state occur, is 30nm at room temperature. Also, the single-domain nanoparticle becomes multi-domain state over the size of 80nm. [59]

2.1.2 Synthesis of Superparamagnetic Nanoparticles

Superparamagnetic nanoparticles with the averaged diameter of 280nm are synthesized in Biophotonics and Nanoengineering Laboratory. The sequential process for the superparamagnetic nanoparticle synthesis is as follows. A FeCl_3/DEG stock solution is prepared by dissolving 20mmol FeCl_3 in 50mL of DEG and heating it at 120°C for 1 hour under a nitrogen atmosphere. A NaOH / DEG stock solution is also prepared by dissolving 125mmol of NaOH in 50 mL of DEG and heating it at 120°C for 1h under a nitrogen atmosphere. [60]

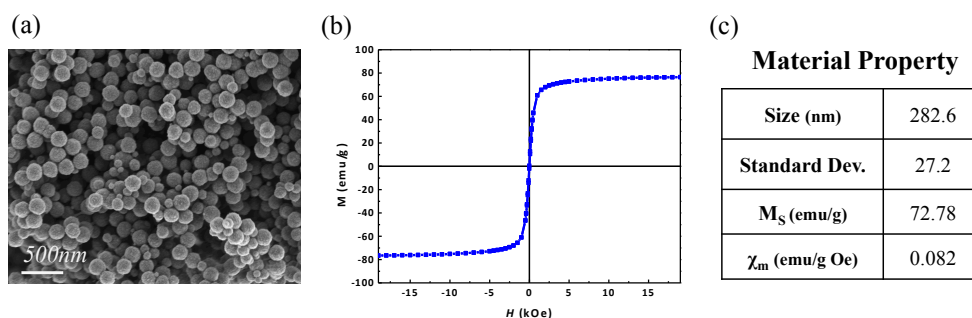


Figure 2.2 Magnetite nanoparticles and material properties. (a) The averaged size of the magnetite nanoparticle cluster is 282.6nm with the standard deviations of 27. (b) The magnetization curve of the magnetic nanoparticles was measured using SQUID. (c) As a result, the saturation magnetization of this nanoparticle is 72.78 emu/g and the magnetic mass susceptibility is 0.082 emu/gOe.

Superparamagnetic Fe_3O_4 core nanoparticles with tunable size are synthesized by using a high-temperature hydrolysis reaction with PAA as a surfactant. In a typical synthesis, a mixture of 288 mg of PAA, 1mL of FeCl_3 stock solution and 15mL of DEG is heated to 220°C in a nitrogen atmosphere for 90min with

vigorous stirring to form a transparent, light yellow solution. Then, 1.8mL of NaOH/DEG stock solution is injected into the above solution which slowly turns black after about 2min. The resulting mixture is further heated for 1h to yield about 120nm Fe₃O₄ colloids. The synthesized Fe₃O₄ colloids are first washed with a mixture of deionized (DI) water and ethanol, then with pure water several times, and finally dispersed in 3mL of DI water. [60]

The averaged diameter of magnetite nanoparticles in figure 2.2 is 282.6nm with the standard deviation of 27. The total sample numbers are 239. Also, the magnetic mass susceptibility and the saturation magnetization of 280nm magnetite nanoparticle are measured as 0.082 emu/g Oe and 72.78 emu/g, respectively.

2.1.3 Magnetic Anisotropy of Magnetite Nanoparticles

In common ferromagnetic material, the magnetization vector M prefers to align with its energetically favorable direction, known as the easy axis. An easy axis is determined by the various sources of magnetic anisotropy, which is the function of material properties and structure geometry. The magnetic-anisotropy energy is minimized when the magnetization vector points in either direction along the easy axis, and the magnetic anisotropy energy approaches zero when the magnetization vector becomes parallel to the easy axis. In the absence of an applied magnetic field, a magnetically anisotropic material will align its moment with one of the easy axes, while a magnetically isotropic material has no preferential direction for its magnetic moment. In the presence of an applied magnetic field, the magnetization vector of the magnetically anisotropic material establishes rotational equilibrium under the influence of both magnetic moment-field interaction energy and magnetic anisotropy energy. The anisotropy energy is expressed as

$$U_a = vK \sin^2 \theta$$

with the magnetic material volume v , the magnetic anisotropy constant K , and the angle θ away from the easy axis. Magnetic anisotropy is originated from various causes such as crystalline structure, shape and stress of the magnetic material. [61]

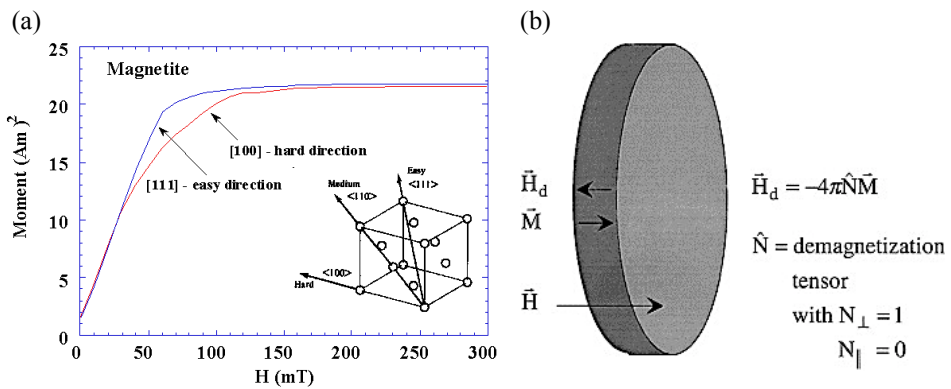


Figure 2.3 Magnetic anisotropy (a) Crystalline magnetic anisotropy of magnetite. (b) Demagnetization field in a magnetic material.

Crystalline anisotropy arises from spin-orbit coupling, the interaction of the spin magnetic moment with the crystal lattice, which is independent of material size and shape. Crystalline anisotropy emerges from the magnetization curve along the crystallographic orientation because the magnetization reaches saturation in different intensities of the applied magnetic fields depending on the crystallographic orientation of the sample. In magnetite above 130 K, <111> is the easy direction of magnetization, <100> is the hard direction of magnetization and <110> is the intermediate direction of magnetization. Crystalline anisotropy is defined as the energy necessary to deflect the magnetic moment from the easy to

the hard direction in a single crystal, and in cubic crystals like magnetite, it is given by a series expansion in terms of the angles between the direction of magnetization and the cube axes. First two coefficients of the series expansion are sufficient to represent the anisotropy energy in an arbitrary direction. At 300 K, the first term K_1 is -1.35×10^5 ergs/cm³ and the second term K_2 is -0.44×10^5 ergs/cm³. [62]

The shape anisotropy is originated from the shape of the magnetic material. It attempts to align the easy axis with the longest axis of a structure. Demagnetizing field is usually adopted to explain this anisotropy. A magnetic structure produces magnetic charges at the surface, which becomes another source of a magnetic field called the demagnetizing field. The effect of the demagnetizing field will be minimized when the magnetization is along the longest axis, thus producing an easy axis of magnetization along the long axis. Thus, the magnitude of shape anisotropy is dependent on both saturation magnetization and material geometry. For magnetite, bigger than about 20 microns, shape anisotropy is less important than the crystalline anisotropy. In smaller sized materials than 20 microns, shape anisotropy becomes the dominant form of anisotropy. However, in the case of spherical particles, the shape anisotropy can be ignored because a sphere has no preferentially long axes in any direction. [63]

Surface anisotropy is also affected by shape of the material because imbalance of surface stress causes the anisotropy of the magnetic moments. The magnetic material with uneven surfaces obtains larger surface anisotropy than the material with flat surfaces. The surface anisotropy is important when the size of the material decreases. As the surface/volume ratio dramatically increases, surface imbalance critically distorts the magnetic moments of the material. As with the shape anisotropy, the surface anisotropy becomes theoretically zero in the case of perfectly spherical particle because there is no imbalance of surfaces. [64]

In this dissertation, the magnetite nanoparticles are regarded as perfect spheres. Therefore shape and surface anisotropy can be neglected and the crystalline anisotropy is only considered to simulate the cooperative behavior of magnetic nanoparticles in liquid under the applied magnetic field.

2.2 Interacting Magnetic Nanoparticles with MC Simulation

In the chapter 2.2, Interactions among the magnetic nanoparticles in liquid were investigated by adopting Monte Carlo method. To simplify the case, the magnetite nanoparticle is idealized to be uniaxial stable single domain particle with a single easy axis. Essential magnetic interactions including magnetic dipole-field interaction, dipole-dipole interaction and steric layer repulsion are defined. Using Monte Carlo Simulation, the self-assembling behavior of both ferromagnetic nanoparticles and superparamagnetic nanoparticles are analyzed in terms of magnetic chain formation and magnetic anisotropy torque. Mostly I combine the methods of Aoshima et. al. (2005) and Bertoni et. al. (2011) to perform Monte Carlo Simulation for the investigation of self-assembling behavior of superparamagnetic nanoparticles. [65, 66]

2.2.1 Interaction Energy of Magnetic Nanoparticles

Spherical magnetite nanoparticles are idealized to have uniaxial single domain particle with a single easy axis. The interaction energy between these magnetic particles, which depends on the relative position of the objects, contributes to the total energy of the system. If the magnetic moment of particle i and the uniform magnetic field strength are denoted by \mathbf{m}_i , ($m_i=|\mathbf{m}_i|$) and \mathbf{H} ($H=|\mathbf{H}|$), respectively, the interaction energy between particle i and the magnetic field u_i^H , the magnetic anisotropy energy u_i^A , the interaction energy of two magnetic dipoles u_{ij}^m , and the interaction energy due to the overlapping of the steric layers, u_{ij}^v , are expressed as follows. [65, 66]

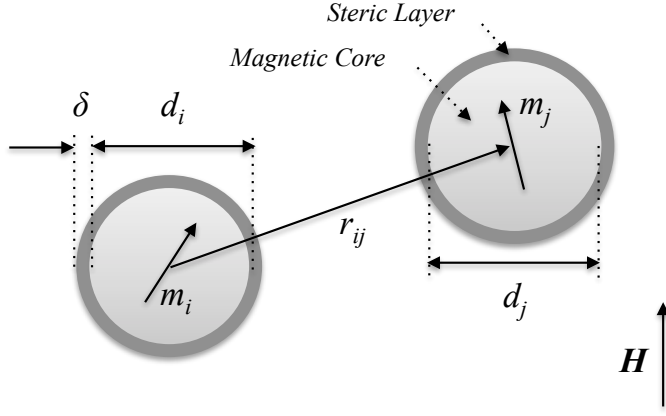


Figure 2.4 Schematic of two interacting magnetic nanoparticles. The interactions including particle-field interaction, particle-particle dipole interaction, magnetic anisotropy and steric layer repulsion are considered to analyze the self-assembling behavior of the magnetic nanoparticles.

$$u_i^H = -kT\xi_i \mathbf{n}_i \cdot \frac{\mathbf{H}}{H}$$

$$u_i^A = K_i(1 - (\mathbf{n}_i \cdot \mathbf{a}_i)^2)$$

$$u_{ij}^m = -kT\lambda_{ij} \frac{d_0^3}{r_{ji}^3} \{ \mathbf{n}_i \cdot \mathbf{n}_j - 3(\mathbf{n}_i \cdot \mathbf{t}_{ji})(\mathbf{n}_i \cdot \mathbf{t}_{ji}) \}$$

$$u_{ij}^v = \frac{\lambda_{vi}kT}{2} \left\{ 2 - \frac{2C_i}{t_{\delta i}} \ln \left(\frac{t_{\delta i} + 1}{C_i} \right) - 2 \frac{C_i - 1}{t_{\delta i}} \right\} + \frac{\lambda_{vj}kT}{2} \left\{ 2 - \frac{2C_i}{t_{\delta i}} \ln \left(\frac{t_{\delta i} + \frac{d_j}{d_i}}{C_i} \right) - 2 \frac{C_i - \frac{d_j}{d_i}}{t_{\delta i}} \right\}$$

in which,

$$C_i = \frac{(1 + t_{\delta i})^2 - (d_j/d_i + t_{\delta i})^2 + 4r_{ji}^2/d_i^2}{4r_{ji}/d_i}$$

$$C_j = \frac{(d_j/d_i + t_{\delta i})^2 - (1 + t_{\delta i})^2 + 4r_{ji}^2/d_i^2}{4r_{ji}/d_i}$$

Where k is Boltzmann's constant, T is the absolute temperature of the fluid, r_{ij} is the magnitude of the vector \mathbf{r}_{ji} drawn from particles i to j , and \mathbf{n}_i and \mathbf{t}_{ji} denote the unit vectors given by $\mathbf{n}_i = \mathbf{m}_i/m_i$ ($m_i = |\mathbf{m}_i|$) and $\mathbf{t}_{ji} = \mathbf{r}_{ji}/r_{ji}$. The parameters t is the ratio of the steric layer thickness to the radius of the solid portions of particle i , and is expressed as $2\delta/d_i$. C_i is the repulsion constant depending on the particle size, relative distance and steric layer thickness. To make the simulation parameters easy to handle, several parameters are combined into dimensionless parameters. The dimensionless parameters are as follows.

$$\xi_{av} = \frac{\mu_{av} m_{av} H}{kT}$$

$$\lambda_{av} = \frac{\mu_{av} m_{av}^2 H}{4\pi d_0^3 kT}$$

These parameters include all the information about the magnetic moments and their interaction with the environment. ξ describes the magnetic interaction with the external magnetic field and λ focuses on the magnetic dipole interactions. The magnitude of the magnetic moment of particles, $m(=|\mathbf{m}|)$, is assumed to be in

proportion to its particle volume $\pi d^3/6$, then the dimensionless parameters ξ_i and λ_{ij} should be multiplied by the volume ratio. Then, the evaluation of the total interaction energy in this system is as follows.

$$u^{total} = \sum_i u_i^{total} = \sum_i u_i^H + \sum_i u_i^A + \frac{1}{2} \sum_i \sum_{j(i \neq j)} u_{ij}^m + \frac{1}{2} \sum_i \sum_{j(i \neq j)} u_{ij}^v$$

Total interacting energy of the system, which includes the magnetic moment-field interaction energy, the magnetic moment-moment interaction energy, magnetic anisotropy energy and steric layer repulsion energy in a system, is utilized to simulate the self-assembling behavior of magnetic fluid in the presence of the external magnetic field. Previous researches include other interactions expected to affect to the total energy of the system and the assembling behavior of the nanoparticles in a fluid, such as Van der Waals interaction and isotropic interaction, but these factors can be regarded to be negligible in this case. All magnetic interactions should be considered to investigate the magnetic fluid containing ferromagnetic nanoparticles. In contrast to the ferrimagnetic nanoparticle, the thermal energy of the superparamagnetic nanoparticle overcomes the crystalline anisotropic energy of this material and the orientation of the induced magnetic moment becomes almost parallel to the applied magnetic field direction, thus ignoring the particle-field interaction and the magnetic anisotropy. This difference makes the superparamagnetic polymer composite exploits magnetic anisotropy torque arisen from the magnetic moment-moment interaction, while the ferromagnetic polymer composite moves using the conventional magnetic torque caused by the interaction between magnetic moment and magnetic field. This characteristic will be considered later in this chapter.

2.2.2 2-D Cluster-moving Monte Carlo Simulation

Monte Carlo method is one of the widely used computational algorithms that rely on repeated random sampling to obtain numerical results. They can be suited in such problems that it is impossible to obtain a closed-form expression or infeasible to apply a deterministic algorithm. These problems include optimization, numerical integration and sample generation from a probability distribution. Investigations on polydispersity of the aggregate structures are indispensable for clarifying the self-assembling morphology and aggregated structures of magnetic nanoparticles in the presence of the external magnetic field. Aoshima et. al. and Bertoni et. al. investigated a normal distributed polydisperse system of ferromagnetic particles and clarified the influence of the particle-size distribution on the aggregate structure. [65, 66] Conventional Monte Carlo algorithm hardly reproduces physically reasonable aggregate structures for the case of a system with a strong particle-particle interaction. This is due to the fact that a particle movement rarely overcomes particles interactions to escape from its cluster to form larger clusters. Therefore, they developed the cluster-moving Monte Carlo algorithm for the use in the simulation of a strongly interacting system by allowing a cluster to move as a composite single particle.

I adopted the cluster-moving Monte Carlo algorithm, a powerful technique for generating microscopic thermodynamic equilibrium states, which is indispensable for investigating the formation of microchains in a strong interacting system. The basic algorithms are as follows.

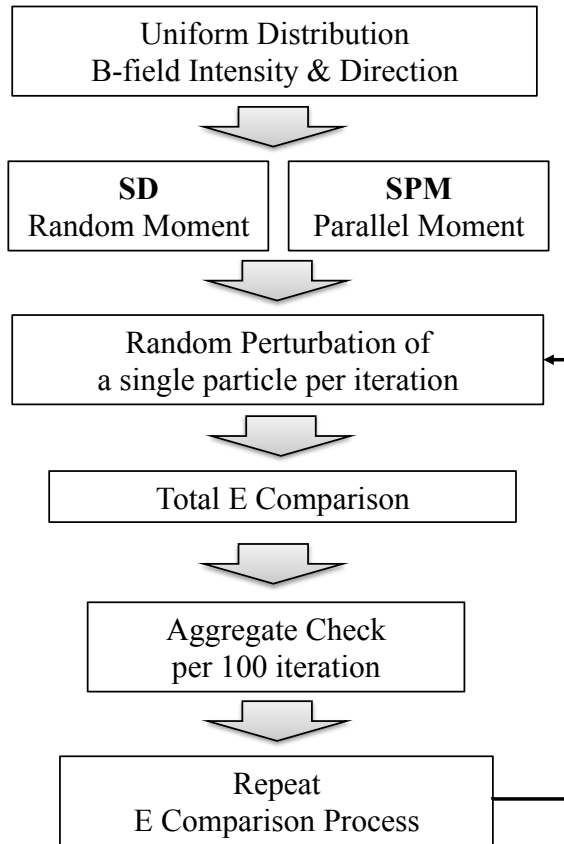


Figure 2.5 Cluster-moving Monte Carlo simulation process. The nanoparticles are uniformly distributed at each lattice point and their diameters are assigned following the Gaussian distribution. Directions of the magnetic anisotropy and moment are also randomly assigned for each particle. When the external magnetic field is applied on y-axis, particle location and magnetic moment direction and magnetic anisotropy direction of a single particle are perturbed within the range of 10 degree. All interaction energies are calculated and whether this state can be accepted or not is determined by the probability, and this processes are repeated until the simulation is terminated.

The magnetic nanoparticles are assigned to have varied diameters with a corresponding magnetic anisotropy and moment and periodically distributed in its initial state. When the external magnetic field is applied, the particle location and the direction of the magnetic moment of a single particle are randomly perturbed within a certain range, and its acceptability is then determined by a probability in proportion to the Boltzmann factor $\exp(-\Delta U/kT)$, where ΔU is the change in the total energy of the system before and after the movement. In other words, the next configuration of the system is determined by the change of total magnetic interaction energy. This process is repeated until the simulation is terminated. [66] Python was utilized to realize this procedure and visualize the result.

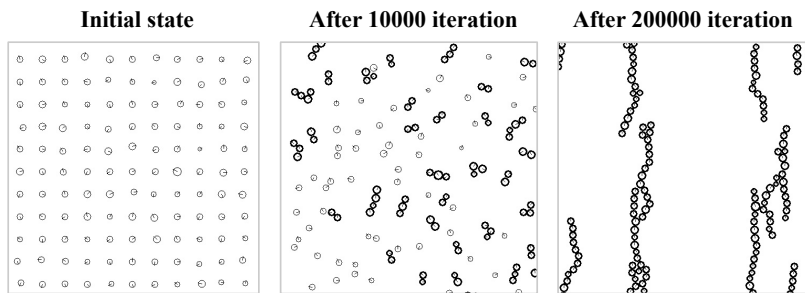


Figure 2.6 Example of Monte Carlo simulation result. As the step number becomes 200000 times, the particles assemble forming chain-like nanostructure, but chains show branched structure.

This result shows the example result of aggregate moving Monte Carlo simulation. The average diameter of the nanoparticle is 10nm, the inter-particle distance is 40nm and the applied magnetic field intensity is 0.01T. As the simulation conducted 200000 iterations, the particles assemble forming chain-like nanostructure with branches.

2.3 Self-assembly of Magnetic Nanoparticles

In the presence of the external magnetic field, the magnetic nanoparticles are self-assembled forming chain-like nanostructures due to the magnetic interactions mentioned above. Here, the self-assembling behavior of both ferromagnetic nanoparticles and superparamagnetic nanoparticles are investigated based on the Monte Carlo simulation. Self-assembly of superparamagnetic nanoparticles only requires magnetic dipole-dipole interactions to form chain-like structure, while self-assembly of ferrimagnetic nanoparticles depends on magnetic dipole-field interaction, magnetic anisotropy as well as magnetic dipole-dipole interaction. As a result, magnetic torque working on the ferromagnetic composite is dominantly caused by the magnetic moment-field interaction, while magnetic torque working on the superparamagnetic composite is caused by the magnetic dipole-dipole interaction, which provides a high potential for engineering.

Magnetite nanoparticles with the diameter of 40~60nm are bought from Sigma Aldrich. The averaged diameter is 53.2nm with the standard deviation of 5 (sample number=239). In the simulation, this particle is assumed to have uniaxial single domain with the saturation magnetization of 88 emu/g. Then, the magnetic moment is the multiple of the saturation magnetization and the volume of the material. Superparamagnetic nanoparticle with the diameter of 280nm are synthesized in Biophotonics and Nanoengineering Laboratory. The averaged diameter is 282.2nm with the standard deviation of 27. Superparamagnetic nanoparticles follows the relationship that the magnetization is the multiple of magnetic field and magnetic volume susceptibility. The detailed parameters for the simulation are as follows.

Table 2.1 Basic parameters for MC simulation

	Parameter	SPM	FERRI	Scale
χ_m	Mass susceptibility	8.20×10^{-2}	-	emu/g Oe
χ_v	Volume susceptibility	4.24×10^{-1}	-	emu/cm ³ Oe
M_s	Saturation magnetization	7.28×10^1	8.80×10^1	emu/g
d_{av}	Averaged diameter	2.82×10^2	5.32×10^1	nm
<i>Std.</i>	Standard deviation of d_{av}	27	5	dimensionless
B	Magnetic field intensity	0.001 - 0.1	0.001 - 0.1	T=Wb/m ² =N/Am ³
μ_0	Vacuum permeability	1.26×10^{-6}	1.26×10^{-6}	Wb/Am
μ_r	Relative permeability	6.33	-	dimensionless
μ	Permeability	7.95×10^{-6}	-	Wb/Am
H	Magnetic field	7.96×10^4	7.96×10^4	A/m
k	Boltzman constant	1.38×10^{-23}	1.38×10^{-23}	m ² Kg/s ² K=Nm/K
T	Temperature	3.00×10^2	3.00×10^2	K
d	Magnetite density	5.17	5.17	g/cm ³
V	Volume	1.15×10^{-20}	6.55×10^{-23}	m ³
M	Magnetization	6.70×10^4	4.55×10^5	A/m
m	Magnetic moment	7.70×10^{-16}	2.98×10^{-17}	Am ²

Based on these parameters, the self-assembling behavior of both ferromagnetic nanoparticles and superparamagnetic nanoparticles is investigated experimentally. The length of the magnetic chain increases as the exposure time to the external magnetic field increases. The chain length also depends on the applied magnetic field intensity and the initial concentration of the magnetic nanoparticles in a media. Using Monte Carlo simulation, the characteristic of magnetic microchain formation was also investigated for both ferromagnetic magnetite nanoparticles and superparamagnetic magnetite nanoparticles. Experimental result for the magnetic chain elongation shows that this simulation properly describes the magnetic self-assembly phenomena. Therefore, the principle magnetic torques working on the magnetic self-assembly was also verified for both cases of ferromagnetic and superparamagnetic nanoparticles using Monte Carlo simulation.

2.3.1 Self-assembly of Ferrimagnetic Nanoparticles

In the absence of the external magnetic field, the ferromagnetic nanoparticles are randomly dispersed, and all magnetic moments point random direction. By the application of the external magnetic field, the magnetic microchains elongate along the magnetic field line due to the magnetic interactions of magnetic nanoparticles. When the applied magnetic field direction changes, the microchains rotate following the changed direction, especially to minimize the magnetic moment-field interaction energy. Therefore in this case, self-assembly depends on magnetic dipole-dipole interaction as well as the magnetic dipole-field interaction, while the magnetic chain rotation relies on only magnetic dipole-field interaction.

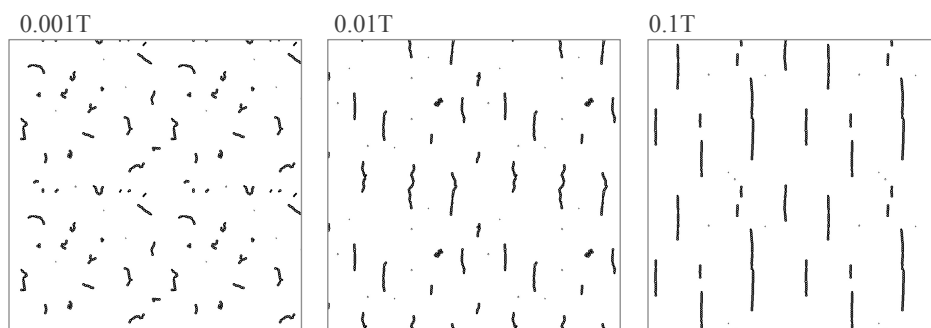


Figure 2.7 Monte Carlo simulation of ferrimagnetic nanoparticles according to the applied magnetic field intensity. As the applied magnetic field intensity increases, the assembled nanoparticles form clear straight chain structure. This appearance is comparable to the experimental chain formation. As the applied magnetic field intensity decreases, chain formation time increases and the assembled chains represent highly aggregated shape.

First, the magnetic chain elongation according to the applied magnetic field intensity is investigated. Density of the magnetic nanoparticle, which determines the interparticle distance in the initial state as the experimental density of the polymer fluid containing magnetic nanoparticles, is 0.01g/cm^3 . The applied external magnetic field to induce the self-assembling behavior of the magnetic nanoparticles is defined to be 0.001T , 0.01T and 0.1T respectively. The interparticle distance is 323.44nm based on the density 0.01g/cm^3 and the total lattice length is $3.88\mu\text{m}$.

Figure 2.7 shows the self-assembling behavior of ferrimagnetic nanoparticles under the various magnetic field intensities. After 350000 iterations, the system becomes stable without any further configuration change. Due to their magnetic moment-moment interaction, the nanoparticles aggregate each other without directional preferences under the external magnetic field of 0.001T . Their magnetic moments do not depend on the applied external magnetic field intensity unlike the magnetic moments of the superparamagnetic nanoparticles. However, as the energy of particle-field interaction increases, they assemble parallel to the magnetic field direction forming chain-like nanostructures.

Secondly, the magnetic chain formation according to the initial concentration of the magnetite nanoparticles is investigated. The applied magnetic field intensity is chosen to be 0.1T , which determines the particle-field interaction energy. The density of the magnetic fluid is defined as 0.001 , 0.05 , 0.01 and 0.02g/cm^3 , respectively. The interparticle distance changes 267.45 , 323.44 , 407.51 and 696.84nm as the nanoparticle density varies 0.02 , 0.01 , 0.005 and 0.001g/cm^3 respectively.

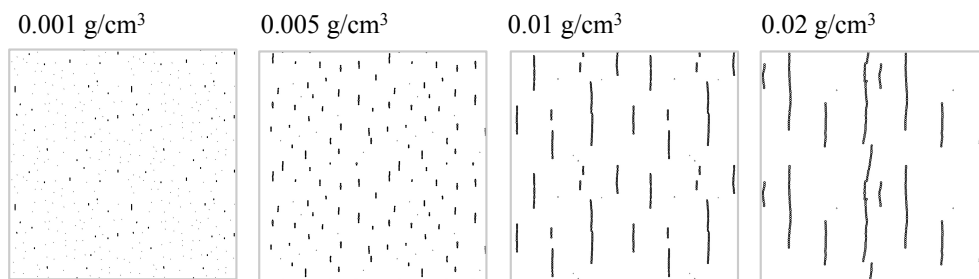


Figure 2.8 MC simulation result of ferromagnetic magnetite nanoparticles according to the nanoparticle concentration. As nanoparticle number in a unit area increases, the assembled nanoparticles form clear and straight chain structure. This nanostructure morphology is comparable to the experimental chain formation. As the interparticle distance decreases, chain formation time decreases and the assembled chains represent long and clear shape.

Figure 2.8 shows the self-assembling behavior of ferrimagnetic nanoparticles under the various nanoparticle densities. After 350000 iterations, the system becomes stable without any further configuration change. Interparticle distance affects to the particle-particle dipole interaction because the particle-particle dipole interaction is in inverse proportion to the interparticle distance. When the nanoparticle density decreases, the interparticle distance increases diminishing the chances for the magnetic nanoparticles to meet and interact. The simulation result shows that the critical factor for chain formation is dipole-dipole interaction because, at low density, ferrimagnetic nanoparticles whose magnetic moments are almost independent to the external magnetic field intensity hardly form chains even under the relatively strong external magnetic field.

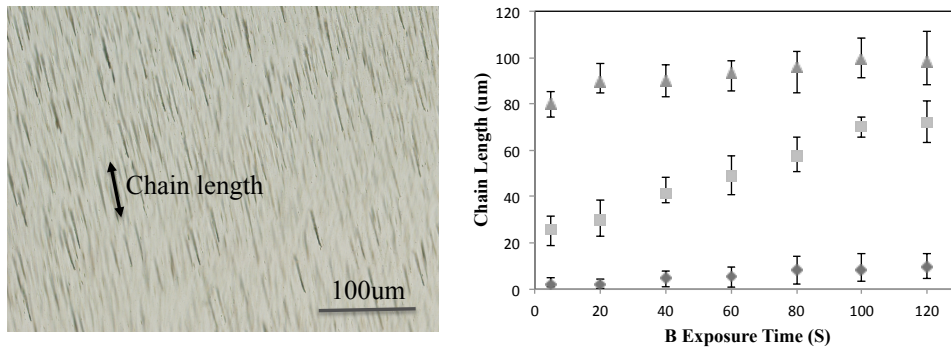


Figure 2.9 Self-assembly of ferrimagnetic nanoparticles with the averaged diameter of 53.2nm. Ferrimagnetic nanoparticles are assembled along the applied magnetic field direction. Length of the microchains is a function of the exposure time to an external magnetic field of 0.001, 0.01 and 0.1T. The magnetic nanoparticle concentration is 0.01g/cm³.

The characteristic of magnetic chain formation is also investigated through experiments. By the application of the external magnetic field, the magnetic nanoparticles gradually assemble and elongate. The length of the magnetic chain increases as the exposure time to the external magnetic field increases. The chain length also depends on the applied magnetic field intensity and the initial concentration of the magnetic nanoparticles in a media.

In figure 2.9, chain length increases as the exposure time to external magnetic field increases. The magnetic nanoparticle density in a media is 0.01g/cm³. Magnetic chain length becomes saturated over a certain time because interchain distance becomes too far to create the chains. In the application of the strong magnetic field, the magnetic chain length reaches to its stable length within several seconds after the application of the external magnetic field. Under the weak magnetic field, the magnetic nanoparticles are hardly assembled. As expected, the

saturated magnetic chain length increases as the applied magnetic field intensity increases. These magnetic microchains also aggregate each other due to their magnetic moment-moment interaction.

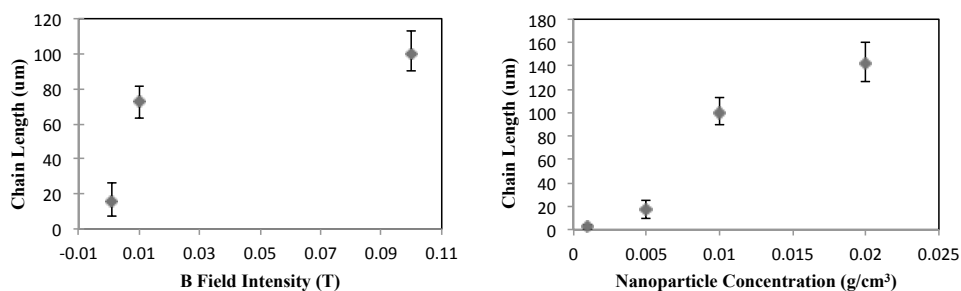


Figure 2.10 Self-assembly of ferromagnetic nanoparticles with the averaged diameter of 53.2nm. Length of the microchains increases as the applied magnetic field intensity and the nanoparticle concentration increase. Sample includes 50 chains for each case.

Figure 2.10 shows the relationship between magnetic chain elongation and the applied magnetic field intensity. Also, the magnetic chain length according to the initial nanoparticle density is measured. The magnetic nanoparticle density is 0.01g/cm^3 . The chain length was measured 120 seconds after the application of the external magnetic field. The total sampling number was 100 chains in the 100x optical microscopy image. As expected, the magnetic chain length is determined by both the external magnetic field intensity and the initial magnetic nanoparticle density increase.

2.3.2 Self-assembly of Superparamagnetic Nanoparticles

In the absence of the external magnetic field, the superparamagnetic nanoparticles are randomly dispersed, and its apparent magnetic moments are negligible. This is because the thermal energy overcomes the magnetic anisotropy energy in the superparamagnetic material. By the application of the external magnetic field, the magnetic moments of the nanoparticles are fixed and their directions become parallel to the applied magnetic field orientation. The magnetic microchains elongate along the magnetic field line due to the magnetic interactions of magnetic nanoparticles. When the applied magnetic field direction changes, the magnetic moment direction in each magnetic nanoparticle also changes to be parallel to the changed magnetic field direction. As a result, microchains rotate following the changed direction, especially to minimize the magnetic particle-particle dipole interaction energy. The magnetic moment direction follows the applied magnetic field direction, therefore both self-assembly of superparamagnetic nanoparticles and the rotation of magnetic chains only depends on magnetic dipole-dipole interaction.

First, the superparamagnetic chain elongation according to the applied magnetic field intensity is investigated. Density of the magnetic nanoparticle is 0.01g/cm^3 . The applied external magnetic field to induce the self-assembling behavior of the magnetic nanoparticles is defined to be 0.001T, 0.01T and 0.1T respectively. The interparticle distance is 1811.29nm based on the density 0.01g/cm^3 and the total lattice length is $21.74\mu\text{m}$.

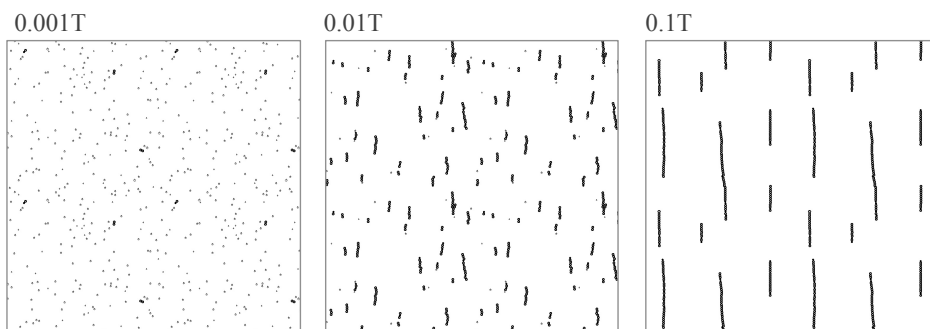


Figure 2.11 MC simulation result of superparamagnetic nanoparticles. As the applied magnetic field intensity increases, the assembled nanoparticles form clear straight chain structure. As the applied magnetic field intensity decreases, chain formation time increases and the assembled chains represent aggregated shape.

Figure 2.11 shows the self-assembling behavior of superparamagnetic magnetite nanoparticles with the averaged diameter of 280nm under the various magnetic field intensities. After 350000 iterations, the system shows stable state. They are still randomly dispersed under 0.001T of weak magnetic field. Because the magnetic moment of superparamagnetic nanoparticles critically depends on the applied magnetic field intensity, the particles hardly interact with each other under the weak magnetic field, unlike the ferromagnetic nanoparticles which interact with each other with the applied external magnetic field. As the energy of particle-field interaction increases, they assemble parallel to the magnetic field direction forming chain-like nanostructures. As the magnetic particle-field interaction increases, the length of the nanostructure becomes longer.

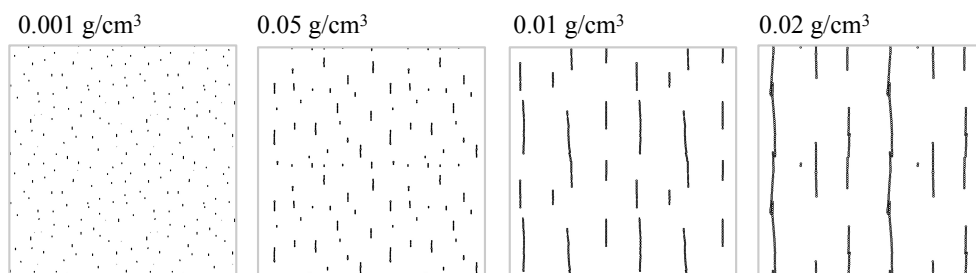


Figure 2.12 MC simulation result of superparamagnetic magnetite nanoparticles. As the interparticle distance decreases, the assembled nanoparticles form clear straight chain structure. This appearance is comparable to the experimental chain formation. As the nanoparticle number per unit area decreases, chain formation time increases and the assembled chains represent quite aggregated shape due to the decrease of magnetic interaction energy proportional to three square of interparticle distance.

Secondly, the magnetic chain formation according to the initial concentration of the magnetite nanoparticles is investigated. The applied magnetic field intensity is chosen to be 0.1T, which determines the particle-field interaction energy. The density of the magnetic fluid is defined as 0.001, 0.05, 0.01 and 0.02 g/cm^3 , respectively. The interparticle distance changes 1002.45, 1811.29, 2282.08 and 3902.30nm as the nanoparticle density varies 0.02, 0.01, 0.005 and 0.001 g/cm^3 respectively.

Figure 2.12 shows the self-assembling characteristics of superparamagnetic magnetite nanoparticles under the various nanoparticle densities. The applied magnetic field intensity is 0.1T. After 350000 iterations, the system shows stable state. Interparticle distance only affects to the particle-particle dipole interaction. The simulation result shows that, as the nanoparticle number per unit area decreases, chain formation time increases.

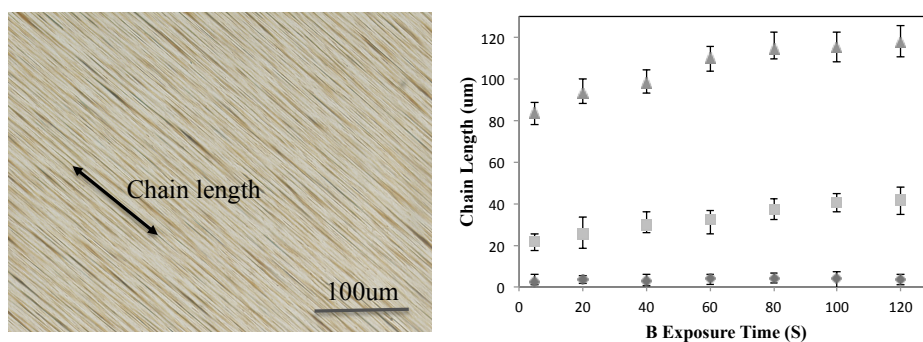


Figure 2.13 Self-assembly of superparamagnetic nanoparticles with the averaged diameter of 282.3nm. Superparamagnetic nanoparticles are assembled along the applied magnetic field direction. Length of the microchains is a function of the exposure time to an external magnetic field of 0.001, 0.01 and 0.1T. The magnetic nanoparticle concentration is 0.01g/cm³.

The characteristic of superparamagnetic chain formation is also investigated through experiments. Under the application of the external magnetic field, the magnetic nanoparticles assemble and elongate as time goes by. The length of the magnetic chain increases as the exposure time to the external magnetic field increases. The chain length also depends on the applied magnetic field intensity and the initial concentration of the magnetic nanoparticles in a media.

In figure 2.13, chain length increases as the exposure time to external magnetic field increases. The magnetic nanoparticle density in a media is 0.01g/cm³. Magnetic chain length becomes saturated over a certain time because interchain distance becomes too far to make the chains to interact each other. Under the large magnetic field intensity, the magnetic chain length reaches to its stable length within several seconds after the application of the external magnetic

field. Under the low magnetic field intensity, the magnetic nanoparticles are hardly assembled and the stable chain length is shorter than the chain length of the ferromagnetic nanoparticles. However, at high magnetic field intensity, the magnetic chains are longer and sharper than the magnetic chains composed of the ferromagnetic nanoparticles. As expected, the saturated magnetic chain length increases as the applied magnetic field intensity increases.

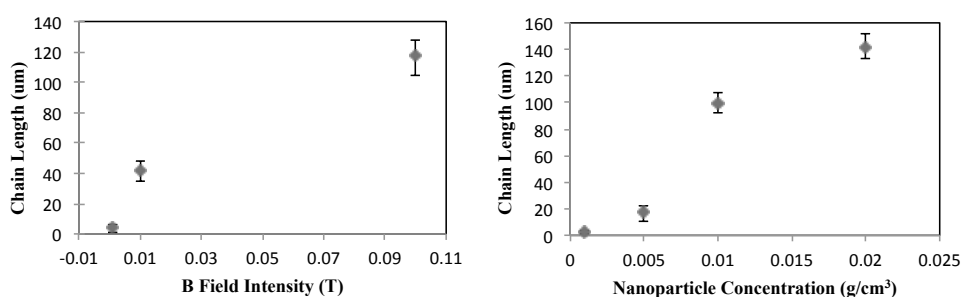


Figure 2.14 Self-assembly of ferromagnetic nanoparticles with the averaged diameter of 282.3nm. Length of the microchains increases as the applied magnetic field intensity and the nanoparticle concentration increase. Sample includes 50 chains for each case.

Figure 2.14 shows the relationship between magnetic chain elongation and the applied magnetic field intensity. Also, the magnetic chain length according to the initial nanoparticle density is measured. The magnetic nanoparticle density is 0.01g/cm^3 . The chain length was measured 120 seconds after the application of the external magnetic field. The total sampling number was 100 chains in the optical microscopy image. As expected, the magnetic chain length increases as both the external magnetic field intensity and the initial magnetic nanoparticle density increase.

2.4 Conclusion

In chapter 2, I investigated the magnetic properties of magnetite and the self-assembling behavior of magnetite nanoparticles using Monte Carlo simulation. Magnetite nanoparticle is strong ferromagnetic material with crystalline anisotropy. The magnetic chain formation through self-assembly was realized by considering magnetic moment-field interaction, magnetic moment-moment interaction and steric layer repulsion, and analyzed in terms of the applied magnetic field intensity and the magnetic nanoparticle concentration. According to the previous research, cluster-moving Monte Carlo method was adopted using Python. The result shows that magnetic chains are formed as both the intensity of the applied magnetic field and the magnetic nanoparticle concentration increase, which correspond to experimental result. Also, magnetite with 50nm diameter shows cooperative ferromagnetic behavior and magnetite with 280nm diameter represents superparamagnetic behavior, as expected in the theoretical investigation.

Chapter 3

Magnetic Nanoparticle Embedded Polymer Composite

In chapter 3, a novel method to fabricate magnetic nanoparticle embedded polymer composite microstructure is introduced. Optofluidic maskless lithography system is adopted, enabling to fabricate various shapes of polymeric microstructures within a second. Based on the Monte Carlo simulation result, the torque, the derivative of interaction energy, of the magnetic chain embedded microstructure is calculated, and the torque from two-dimensional Monte Carlo simulation was expanded to calculate three-dimensional composite microstructure. Also, the steady-state elastic modulus of the magnetic composite microbeam is induced by utilizing the simulated torque and cantilever bending experiment result. Based on these results, a model system for the magnetic polymer composite actuation is developed.

3.1 Optofluidic Maskless Lithography

Optofluidic maskless lithography (OFML) is a flow-lithography technique that can synthesize free-floating microstructures in microfluidic channels. It is the combination of digital-micromirror device based UV projection system and a microfluidic channel for stream of UV-curable resin, and a microscope for inspection as shown in figure 1.1. The overall experimental setup is very similar to conventional maskless lithography, except that a microfluidic channel is used as the exposure substrate instead of a wafer. A 10× microscope objective lens having a numerical aperture (NA) of 0.28 projects the computer-controlled image pattern on the MEMS SLM to the final object plane with a demagnification factor of approximately 8.9. Since the pitch of the micromirror array is 13.68 μm in the SLM plane, the pixel size in the object plane is approximately $1.54 \times 1.54 \mu\text{m}^2$. The common object plane of the projection system is adjusted to meet the microfluidic channel on the microscope. [67, 68]

The microfluidic channels used in all experiments are fabricated using a standard soft lithography technique with polydimethylsiloxane (PDMS) elastomer. It is important to note that since PDMS is a highly permeable material, thin layer of oxygen near PDMS channel surface prevent the photopolymerization at the vicinity of the walls, and thus allow the formation of free-flowing polymeric microstructures without adhering to the channel surface. The thickness of oxygen inhibition layer is approximately less than a few micrometers, thus not significantly affecting the thickness of the particles which normally exceeds 20μm. [69]

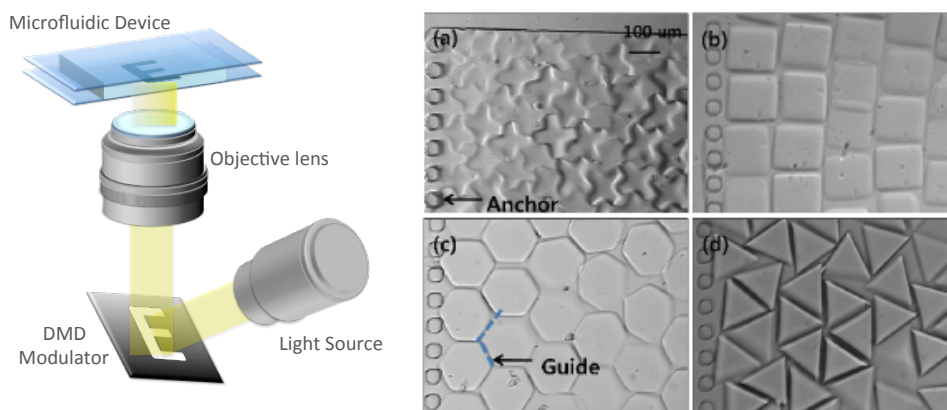


Figure 3.1 Schematic of Optofluidic Maskless Lithography System (OFML) and the polymeric microparticles with various shapes. OFML system is composed of three major parts: UV light source, DMD modulator which patterns the injected UV light, and objective lens which focus the patterned UV light into the microfluidic channel. The focused UV light polymerize the photocurable polymer in the microfluidic channel and various shapes of microparticles can be fabricated within a second. [67]

The use of SLM for dynamic mask provides precise spatial and temporal control of fabrication within the field-of-view. Combined with the dynamic nature of resin flow, versatile fabrication can be achieved. Figure 3.1 shows various examples of dynamic fabrication with the control of the geometry. Extruded polymeric microstructures are fabricated by selectively solidifying the liquid-phase photocurable oligomer stream with the UV light exposure through the slide glass substrate. Using this device, the self-assembled state of the magnetic nanoparticles can freeze in polymer in a moment in any shape, and this advantage enables to sequentially immobilize the various directions of magnetic nanoparticles chains in polymer.

3.2 In-situ Fabrication Process

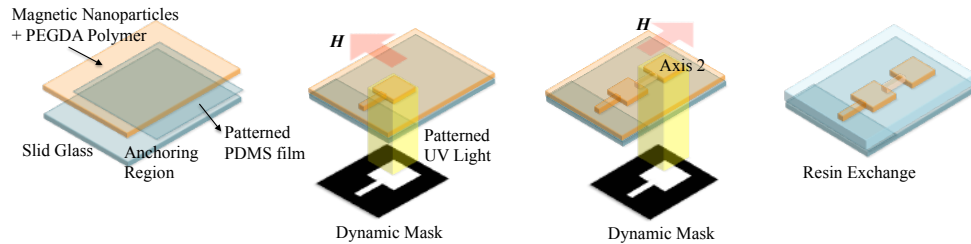


Figure 3.2 Fabrication process. By repetitive freezing of magnetic nanoparticles in photocurable resin using OFML system, magnetic polymer-nanoparticle composite material can be fabricated.

With this system, a sequential process is used to manufacture miniaturized polymeric actuators. First, a glass substrate is coated with PDMS, which is responsible for the inhibition layer used for generating the free-floating part of the component. The coated PDMS is partially removed to create the anchoring region where the structures are permanently attached to the intrinsic glass substrate. Then, the microfluidic channel is attached on the PDMS coated glass substrate and filled with a mixture of poly (ethylene glycol) diacrylate (PEGDA), photoinitiator and superparamagnetic nanoparticles. A homogeneous magnetic field is applied across the microfluidic channel, which causes the superparamagnetic nanoparticles in the resin to form chains along the direction of the applied magnetic field. The resin is photopolymerized within a second, thus freezing the superparamagnetic nanoparticle alignments in the polymerized region. [54, 70]

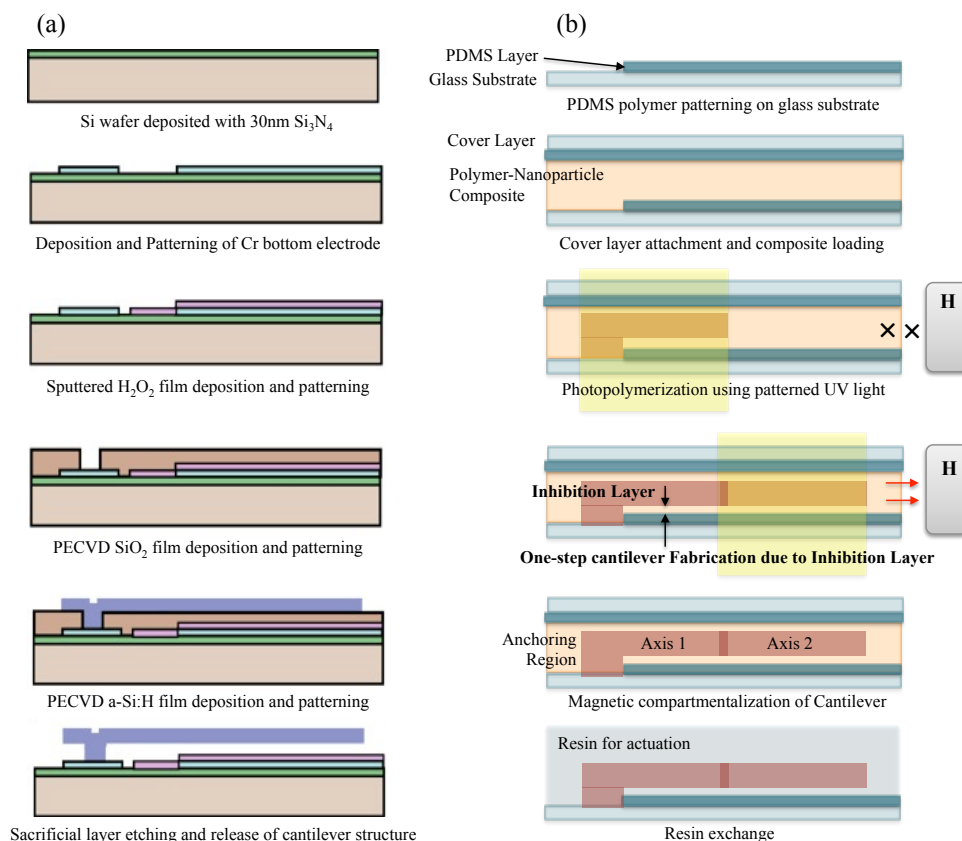


Figure 3.3 (a) Conventional MEMS process for cantilever fabrication. (b) Fabrication process of magnetic polymer composite actuator. (i) Patterning of a PDMS layer on slide glass. (ii) Introduction of MN-containing UV curable resin into a PDMS microfluidic channel bonded to the patterned PDMS glass. (iii) Photopatterning of the actuator using a single exposure via the OFML system. An oxygen inhibition layer is generated, preventing polymerization between the microstructure and the substrate. (iv) Washing of uncured resin. [54]

Existence of inhibition layer dramatically simplifies the microactuator fabrication process. Patterned PDMS glass is used as a substrate for the anchored magnetic cantilever. The oxygen inhibition layer on PDMS surface prevents the polymeric structure from adhering to the substrate, thus making free-floating actuation possible. In the absence of a PDMS layer, the synthesized region adheres to the glass, functioning as an anchor. Therefore, a complex monolithic magnetic actuator, such as an anchored cantilever beam, can be easily fabricated within a single exposure. Since both anchored and unanchored parts are simultaneously fabricated in situ, the oxygen inhibition layer plays a role of a sacrificial layer. Therefore, this technique is very simple and effective for the fabrication of polymeric microstructure in fluidic system compared to the conventional micromachining process. The actuator can be simply controlled by manipulating the direction of the applied magnetic field using a permanent magnet.

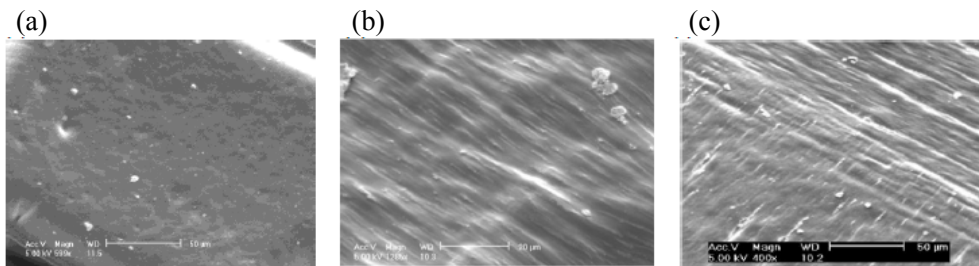


Figure 3.4 Surface of Photopolymerized superparamagnetic nanocomposite (SEM image, scale bar: 50 μ m). (a) Microparticle which contains randomly distributed magnetic nanoparticles. (b) Microparticle which contains aligned magnetic nanoparticles. Roughness is caused by the nanoparticle alignment. (c) Microparticle which shows two adjacent nanoparticle alignments. A microstructure can obtain various directions of magnetic chains.

Figure 3.4 shows that the surface morphology of composite structure containing magnetic nanoparticles. By freezing the dispersed nanoparticles in hydrogel matrix using the dynamic photolithography device, the composite structure in figure 3.4 (a) obtains randomly dispersed magnetic nanoparticles. If the arrangements of magnetic nanoparticles are fixed in the matrix under the application of the external magnetic field, the composite structure in figure 3.4(b) obtains self-assembled magnetic nanoparticles.

In the absence of a magnetic field, the cantilever beam rests above the PDMS substrate. By applying a weak magnetic field perpendicular to the substrate, the cantilever beam bends slightly toward the field while the end of the beam is anchored to the glass. When a strong vertical magnetic field is applied, the cantilever pulls more strongly, overcoming the mechanical torque to straighten the beam. In this process, only the unanchored part of the cantilever beam is lifted. The overall fabrication steps take only a few minutes because complex fabrication steps such as electroplating for a sacrificial layer are not required. In addition, photopatterning of magnetic structures is executed at the same place as the actuation area. Therefore, the entire process is very simple and fast, allowing in situ fabrication and real-time magnetic actuation.

3.3 Torque on Magnetic Composite Structure

In chapter 3.3, the magnetic torque of the magnetic polymer composite is investigated based on the simulation result in chapter 2. Both ferrimagnetic and superparamagnetic composite structure show similar response to the external magnetic field, but the principle interactions which plays a role of inducing torque are different.

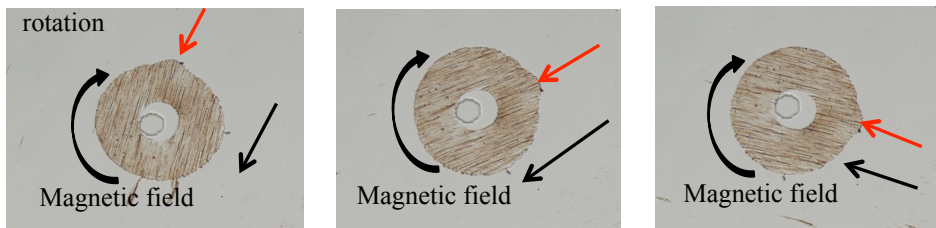


Figure 3.5 Rotation of magnetic polymer-nanoparticle composite. Ring-shaped composite microparticles rotate until the microchains fixed in the structure becomes parallel to the applied magnetic field direction. [70]

3.3.1 Magnetic Torque from Self-assembled Nanoparticles

Using the Monte Carlo simulation result mentioned in chapter 2, the magnetic torque working on the magnetic composite can be calculated according to the applied actuating magnetic field and the angle between the chain and the applied magnetic field direction. For both cases including ferrimagnetic and superparamagnetic magnetite nanoparticle, the total energy of the system and the induced torque in a given simulation lattice area are analyzed.

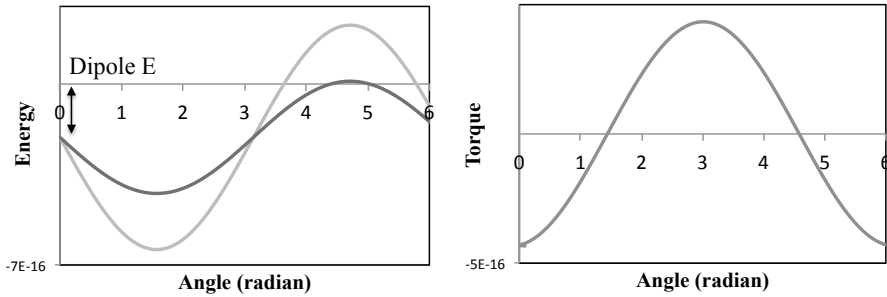


Figure 3.6 Magnetic interaction energy and induced magnetic torque of ferrimagnetic magnetite nanoparticles. Theoretically, magnetic torque from single domain material is the cross product of magnetic moment and the applied magnetic field, which means the torque is proportional $\sin\theta$. The simulation result also shows the function of $\sin\theta$.

In the case of ferrimagnetic magnetite nanoparticles, the direction of the magnetic moment and the locations of magnetic nanoparticles are fixed. Total energy of the system varies according to the orientations of the applied magnetic field. Theoretically, magnetic torque from single domain material is the cross product of magnetic moment and the applied magnetic field, which means the induced magnetic torque is proportional $\sin\theta$. The simulation result also represents the function of $\sin\theta$ and the simulation well explains the expected phenomena and the magnetic torque induced by the self-assembled single domain nanoparticles is dominated by the particle-field interaction. In Figure 4.3, the magnetic energy is the function of $(\sin\theta + \alpha)$ and ' α ' is caused by the particle-particle dipole interaction. The upper graph represents the magnetic energy from the self-assembled nanoparticle under 0.1T of the external magnetic field, and the lower graph describes the magnetic energy from the self-assembled nanoparticles under 0.05T. Even though they show different level of total energy of the system,

the energy induced when the chain orientation is parallel to the magnetic field direction is the same. In the simulation for the ferrimagnetic material, the relative directions of the magnetic moment of all particles are fixed and the value of the magnetic moment only depends on the volume of the nanoparticles. This means that their particle-particle dipole interactions are constant under any circumstances. Therefore, this result infers that the magnetic torque working on the ferromagnetic composite critically depends on the magnetic particle-field interaction.

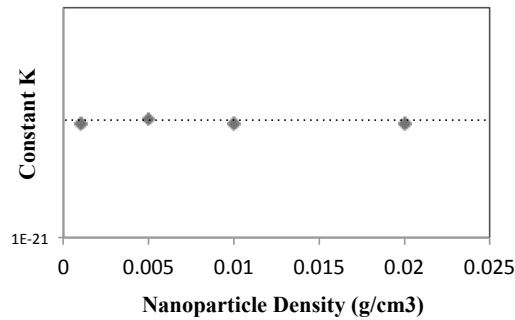


Figure 3.7 Magnetic constant K_{ferri} for ferromagnetic nanoparticle composite. For all cases, the number of the magnetic nanoparticles in MC simulation was the same as 144 and interparticle distances vary according to the nanoparticle density. As a result, it turns out that K_{ferri} only depends on the absolute number of the magnetic nanoparticles in the material, not on the self-assembled state of them.

The magnetic torque working on the ferromagnetic chain in the simulation area can be expressed as follows: $T_{ferri} = K \sin\theta = K_{ferri} H \sin\theta$. In the example case, the applied magnetic field intensity for nanoparticle self-assembly is 0.1T and the magnetic nanoparticle density varies as 0.001, 0.005, 0.01 and 0.02g/cm³. The

magnetic torque working on each self-assembled state is calculated under the applied working magnetic field 0.001, 0.005, 0.01, 0.05 and 0.1T, for the angle between the chain and the applied field direction $0\sim 2\pi$. The total number of nanoparticles in the simulation area is the same for all cases as 144. As a result, the constant K_{ferri} is invariable according to the nanoparticle density which determines the interparticle distance. Therefore, the magnetic constant for ferromagnetic composite, K_{ferri} , depends on the total number of nanoparticles regardless of their relative positions and arrangement, and K_{ferri} can be regarded as the superposition of the total magnetic moments of the ferromagnetic nanoparticles in the matrix. In this case, K_{ferri} turns out to be $5.51 \times 10^{-21} (\text{Nm}^2/\text{A})$. And it can be assumed that the total K of a ferromagnetic composite structure only depends on the absolute number of magnetic nanoparticles in it, regardless of the self-assembled state of the magnetic nanoparticles.

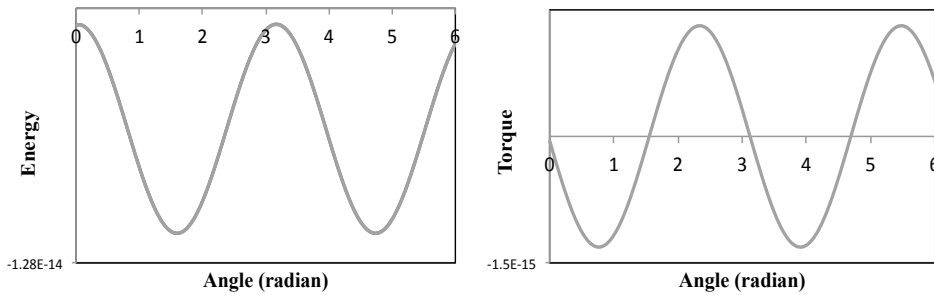


Figure 3.8 Magnetic interaction energy and induced magnetic torque of superparamagnetic magnetite nanoparticles. Theoretically, magnetic anisotropic torque from single domain material is proportional $\sin 2\theta$. The simulation result also shows the function of $\sin 2\theta$.

In the case of superparamagnetic magnetite nanoparticles, the direction of the magnetic moment is defined to be parallel to the direction of the external magnetic field and fix the locations of magnetic nanoparticles. Total energy of the system was calculated according to the orientation of the applied external magnetic field. Theoretically, magnetic anisotropic torque from superparamagnetic material is proportional $\sin 2\theta$. The simulation result also shows the function of $\sin 2\theta$ and the simulation well explains the expected phenomena and this represents that the magnetic torque of superparamagnetic nanoparticles is dominated by the particle-particle dipole interaction. When $\sin 2\theta$ obtains its maximum value, the magnetic torque value equals to the magnetic constant K .

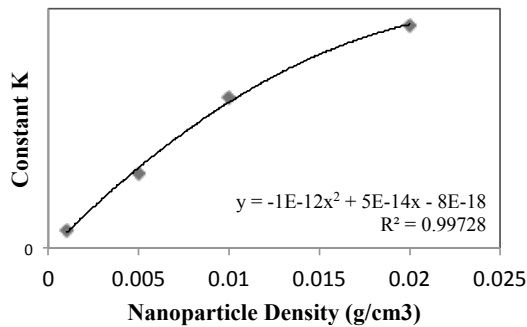


Figure 3.9 Magnetic constant $K_{\text{superpara}}$ for superparamagnetic nanoparticle composite. For all cases, the number of the magnetic nanoparticles in MC simulation was the same as 144 and interparticle distances vary according to the nanoparticle density. As a result, it turns out that $K_{\text{superpara}}$ depends on the magnetic nanoparticle density, thus inferring that the magnetic torque increases as the nanoparticle number per chain increases. Therefore, $K_{\text{superpara}}$ relies on the self-assembled state of magnetic nanoparticles in composite structure.

The magnetic torque working on the ferromagnetic chain in the simulation lattice can be expressed as follows: $T_{superpara} = K \sin 2\theta = K_{superpara} H^2 \sin 2\theta$. In the example case, the applied magnetic field intensity for nanoparticle self-assembly is 0.1T and the magnetic nanoparticle density varies as 0.001, 0.005, 0.01 and 0.02g/cm³. The magnetic torque working on each self-assembled state is calculated under the applied working magnetic field 0.001, 0.005, 0.01, 0.05 and 0.1T, for the angle between the chain and the applied field direction $0 \sim 2\pi$. The total number of nanoparticles in the simulation area is the same for all cases as 144. As a result, the constant $K_{superpara}$ is invariable according to the nanoparticle density which determines the interparticle distance. $K_{superpara}$ depends on the total number of nanoparticles regardless of their relative positions and arrangement, and can be regarded as the superposition of the total magnetic moments of the ferromagnetic nanoparticles in the matrix.

3.3.2 Magnetic Torque on Arbitrary Structure

Torque calculated from the two dimensional Monte Carlo simulation can be utilized to approximately predict the total torque of the three dimensional micro-sized magnetic nanocomposite structure. In addition, at equilibrium, the magnetic torque equals to the mechanical restoring torque, therefore the elastic modulus of micro-sized magnetic composite beam can be induced from this result.

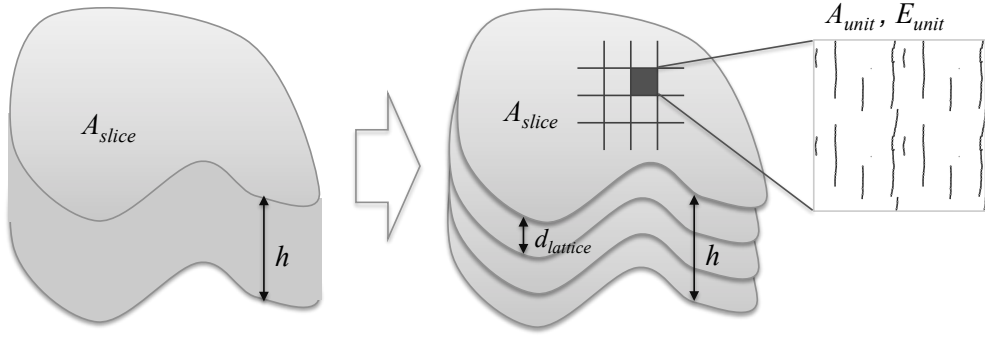


Figure 3.10 Strategy to expand 2D MC simulation result to calculate the torque from 3D microstructure. The 3D total torque from this strategy determines the total magnetic torque of a model cantilever.

The simple process to calculate the torque of three-dimensional microstructure based on the simulation result is as follows. It is assumed that the two dimensional layers of self-assembled nanoparticles are stacked per lattice interval which is the initial interparticle distance of the simulation.

$$E_{slice} = \frac{A_{slice}}{A_{unit}} E_{unit}$$

$$\frac{dE_{slice}}{d\theta} = T_{slice} = \frac{A_{slice}}{A_{unit}} \frac{dE_{unit}}{d\theta} \frac{A_{slice}}{A_{unit}} T_{unit}$$

$$T_{m_total} = N_{slice} T_{slice} = \frac{h}{d_{lattice}} T_{slice}$$

$$d_{latt} = \frac{0.01}{\sqrt[3]{C/d_{den}V}} = 3.902 \times 10^{-7} C^{(-\frac{1}{3})} = c_{latt} C^{(-\frac{1}{3})}$$

Therefore, the total magnetic torque on the composite material can be induced from the simulated torque and the composite structure geometry. At the equilibrium, magnetic torque of the magnetic composite microstructure equals to the mechanical restoring torque. To evaluate the elastic modulus of the microsized magnetic composite beam, total magnetic torque on the microstructure and the other mechanical parameters should be calculated.

3.3.3 Elastic Modulus of Magnetic Composite Beam

In addition to the magnetic torque, the mechanical restoring torque should be assigned. To calculate the mechanical restoring torque of large bending structure, I adopt the pseudo rigid body model. In the past, elliptic integrals have been used to analyze end-loaded large deflection cantilever beams in order to obtain closed-form solutions. However, this mathematical approach is difficult to use and produces little insight about the motion or stiffness of the beam. As a result, alternative methods of determining the beam deflection path have been developed, one of these alternative methods is a parametric approximation model called the Pseudo-Rigid-Body Model (PRBM). This method consists in describing the compliant member's motion and stiffness by replacing it with a rigid-link analogue that has approximately the "same motion and stiffness for a known range of motion and to a known mathematical tolerance". In other words, the PRBM "provides a simplified but accurate method of analyzing the deflection of flexible beams and provides the designer a means of visualizing the deflection", meaning that given a compliant beam, its motion can be found by treating it as a mechanism with rigid links or given a specific motion, a PRBM that performs the same motion can be developed and transformed into its compliant analogue. After the identification of the PRBM

of the compliant member, its kinematic and elastic parameters are optimized and validated so that its range of applicability and level of error are known and acceptable. [71-74]

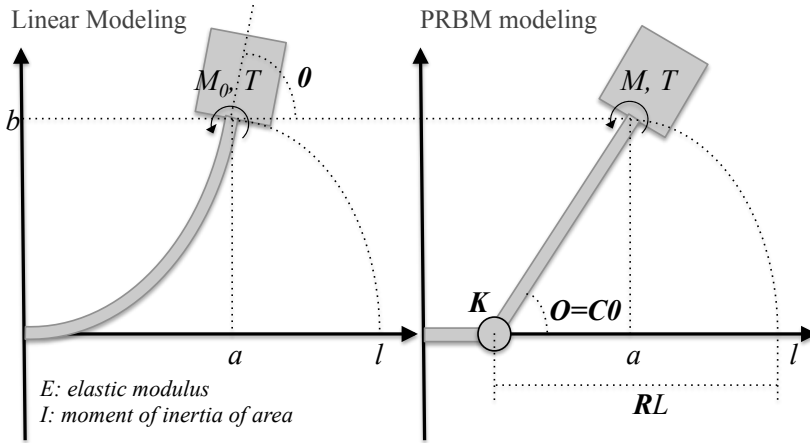


Figure 3.11 Pseudo Rigid Body Modeling to calculate the mechanical restoring torque of large-bending cantilever structure. It assumes that the magnetic composite cantilever follows the end-moment loading.

For the cuboid structure which is anchored in an end and load the moment in the other end, the PRBM model equation is as follows. [71]

$$T_{prbm} = K\theta = \gamma K_{\theta} \frac{E_y I_y}{l} \theta = \left(\gamma K_{\theta} \frac{wD^3}{12l} \theta \right) E_y$$

Mechanical torque of simple beam is expressed where k_{θ} is the mechanical stiffness and θ is deflection angle of the simple beam. And the mechanical stiffness is the function of elastic modulus and moment inertia. The moment of inertia is correlated with beam geometry. In the case of end-moment loading, γ is

approximately 0.7346 and k_{θ} is approximated to 2.0643. Mechanical restoring force can be regulated by changing the beam geometry such as the length, thickness and width. In addition, the elastic modulus can be controlled because it is correlated with a intrinsic nature of the polymer and the photocuring condition.

Based on these relationships, a simple experiment was performed to calculate the elastic modulus of the magnetic composite beam. The nanoparticle density of this composite is 0.01g/cm^3 . The applied magnetic field intensity to assemble the dispersed nanoparticles is 0.1T and the applied magnetic field intensity to actuate the structure is also 0.1T. The geometry of the cantilever head is $200 \times 150 \times 60\text{um}^3$ and the geometry of the bending beam is $400 \times 20 \times 60\text{um}^3$. The detailed parameters are in table 3.1.

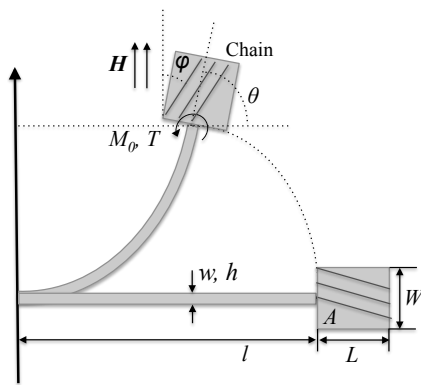
Table 3.1 Parameters for magnetic torque calculation.

	Parameters	Value	Scale
B_A	M field for assembly	0.1	T
B_W	M field for rotation	0.1	T
h	Particle height	6.00×10^{-5}	m
L	Particle length	4.00×10^{-4}	m
w	Particle width	2.00×10^{-5}	m
A_{tot}	Particle top area	3.00×10^{-8}	m^2
C	Particle concentration	0.01	g/cm^3
d_{simul}	Interparticle distance	1.81×10^{-6}	m
L_{simul}	One side length	2.17×10^{-5}	m
A_{simul}	Simulation area	4.72×10^{-10}	m^2
A_{Ratio}	A_{tot}/A_{simul}	63.50	-
h_{Ratio}	Number of slices	33.13	-
T_{Ratio}	$A_{Ratio} \times h_{Ratio}$	2.10×10^3	-
$T_{m\ simul}$	Simulated torque	6.55×10^{-16}	Nm
T_m	Total torque on structure	1.38×10^{-12}	Nm

As a result, when we apply the magnetic field of 0.05T perpendicular to the magnetic chain direction, the resulting bending angle is 0.96 rad in average and the induced magnetic torque is 0.66pNm. Also, when we apply the magnetic field of 0.1T perpendicular to the magnetic chain direction, the resulting bending angle is 1.40 rad in average and the induced magnetic torque is approximately 1pNm. From these two cases, the elastic modulus of the magnetic composite beam is 523.85 Pa in average. However, the elastic modulus of the magnetic composite beam is very flexible because it depends on many factors including the initial magnetic nanoparticle density, the magnetic field intensity applied when the nanoparticles are arranged, the projected ultra-violet light intensity during photopolymerization, and the projection time of ultra-violet light of photopolymerization.

3.4 Design Principles

Here, the model equation for the superparamagnetic composite actuator is described. At the equilibrium, major forces which determine the final location of the actuator are the magnetic torque and the mechanical restoring torque. Before inducing the equation, several parameters are fixed. Magnetic field intensity for magnetic nanoparticle self-assembly is 0.1T, elastic modulus of the bending part is 523.85Pa, and magnetite nanoparticle diameter is 280nm. The relationship between the magnetic torque and the mechanical torque can be expressed in terms of the actuator geometry, the magnetic nanoparticle density in the composite, the applied magnetic field intensity for actuation, and the rotating angles.



Parameters	Symbol	Value	Scale
M field for assembly	B_A	0.1	T
Elastic modulus	E_Y	5.24×10^2	Pa
Particle diameter	d	2.80×10^{-7}	m
Magnetic susceptibility	χ_v	0.42	emu/cm ³ Oe

Variables	Symbol	Scale
Cantilever geometry	$A, l, w, h \dots$	m
Nanoparticle density	C	g/cm ³
M field for rotation	H	A/m
Rotation angle	θ, φ	rad

Figure 3.12 Parameters for model system. Magnetic field for nanoparticle assembly, elastic modulus and magnetite nanoparticle are given. Controllable variables include actuator geometry, nanoparticle density, magnetic field for rotation and bending angle.

The magnetic torque and the mechanical torque are described in chapter 3, and they can be expressed as

$$T_{prbm} = \gamma K_{\theta} E_y I_y \theta = \gamma K_{\theta} E_y \frac{wh^3}{12l} \theta$$

$$T_m = A \frac{h}{d_{unit}} T_{unit}(\varphi, H, C) = \left(\frac{1}{c_{latt}}\right) (Ah) KC^{(-\frac{1}{3})} H^2 \sin 2\varphi$$

where θ is the bending angle of the beam part of the actuator, φ is the angle between the magnetic chain direction fixed in the composite and the applied magnetic field line. A is the area of magnetic composite part parallel to the magnetic chains and h is the thickness of the magnetic composite part where magnetic chains lie. T_{unit} is the magnetic torque per area, induced from the composite part, is the function of φ , the applied magnetic field intensity H , and the magnetic nanoparticle concentration in the composite structure. Using these equations, the movement of various types of magnetic actuators can be expected.

3.4.1 Simple Cantilever

Here, simple cantilever made of magnetic nanoparticle composite is analyzed. The cantilever is composed of two parts: first part is magnetic head that induces magnetic anisotropy torque, and second part is bending beam that induces mechanical restoring torque. The geometry of the superparamagnetic composite cantilever is defined as follows.

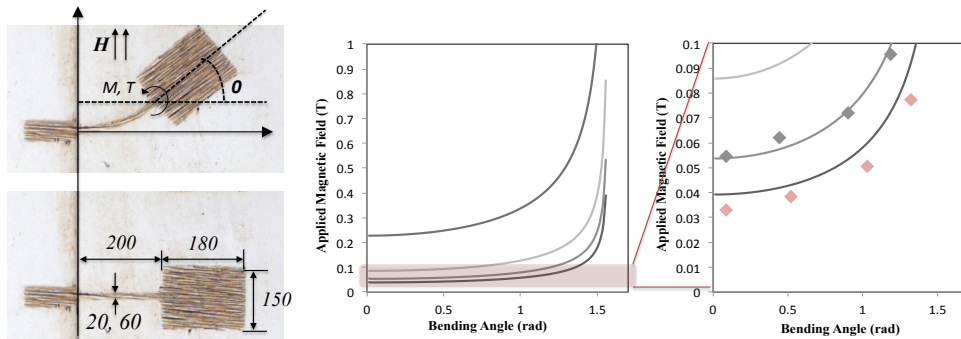


Figure 3.13 Simple cantilever. In this shape, cantilever geometry and the relationship between the magnetic torque and the mechanical restoring torque are defined. The magnetic field required to achieve a specific bending angle can be calculated using this relationship. Also, the magnetic field intensity required to actuate the microcantilever ranges from 0.01 to 0.1T which general permanent magnet is able to afford.

In this case, if the magnetic field is applied to the perpendicular to the longitudinal axis of the magnetic actuator, the relationship between the magnetic torque and the mechanical restoring torque can be expressed as follows.

$$\varphi = \frac{\pi}{2} - \theta$$

$$T_m = \left(\frac{1}{c_{latt}}\right)(Ah)KC^{(-\frac{1}{3})}H^2 \sin\left(2\left(\frac{\pi}{2} - \theta\right)\right) = \left(\frac{1}{c_{latt}}\right)(LWh)KC^{(-\frac{1}{3})}H^2 \sin 2\theta$$

At equilibrium,

$$T_{prbm} = T_m$$

$$\left(\frac{\gamma K_\theta E_y}{12}\right) \left(\frac{wh^3}{l}\right) \theta = \left(\frac{1}{c_{latt}}\right) (LWh) KC^{\frac{1}{3}} H^2 \sin 2\theta$$

$$\left(\frac{\gamma K_\theta E_y c_{latt}}{24}\right) \left(\frac{wh^2}{LlW}\right) K^{-1} C^{(-\frac{1}{3})} H^{-2} = \frac{\sin 2\theta}{2\theta} = \text{sinc} 2\theta$$

$$c_{ca\Box til} \left(\frac{wh^2}{LlW}\right) K^{-1} C^{(-\frac{1}{3})} H^{-2} = \text{sinc} 2\theta$$

$$H = \left(c_{cantil} \frac{\left(\frac{wh^2}{LlW}\right)}{KC^{\left(\frac{1}{3}\right)} \text{sinc} 2\theta} \right)^{1/2}$$

According to this equation, the magnetic actuator capable of performing the desired function can be designed. c_{cantil} is constant, which is applicable for all cases that the magnetic nanoparticles are self-assembled under 0.1T of the magnetic field intensity and the magnetic nanoparticle is superparamagnetic nanoparticle with the diameter of 280nm. The numerator of this equation represents the geometrical parameter of the magnetic composite actuator. C is the initial concentration of the magnetic nanoparticles in the composite, and K , which is a function of the magnetic nanoparticle concentration C , is the magnetic torque constant per area induced from the Monte Carlo simulation. Using this equation, the appropriate

intensity of the applied magnetic field to achieve the bending angle of the actuator can be calculated.

In figure 3.13, the required magnetic field intensity to achieve a bending angle is represented for the magnetic composite with various nanoparticle concentrations. It is obvious that the magnetic field intensity for the wanted actuation increases as the magnetic nanoparticle density decreases. Also, the bending angle of the magnetic composite microactuator can be regulated within 60 degree under the application of the magnetic field between 0~0.1T which permanent magnet is usually able to provide. In addition, red and grey dots represent the experimental bending angle of a magnetic composite cantilever, and this shows that the actuation of magnetic composite structure can be properly described with the modeling result.

3.5 Conclusion

In chapter 3, in-situ fabrication method of magnetic nanoparticle embedded polymer composite microstructure is introduced, and novel model system of magnetic polymer-nanoparticle composite actuator is developed. Optofluidic maskless lithography system is adopted to fabricate various shapes of polymeric microactuators within a second. Based on the Monte Carlo simulation result and important experimental parameters, the magnetic torque of composite microstructure containing magnetic chains is calculated. Also, the mechanical restoring torque and the steady-state elastic modulus of bending beam are modeled using pseudo rigid body modeling. The magnetic polymer-nanoparticle composite actuator becomes static when the magnetic torque equals to the mechanical restoring torque. A model system for the magnetic polymer composite actuation is developed in the case of simple cantilever using this relationship.

Chapter 4

Multiaxial Microactuators

Chapter 4 introduces multiaxial microactuators composed of superparamagnetic composite compartments. Polymeric microcomponents are widely used in micro electro mechanical systems (MEMS) and lab-on-a-chip devices, but they suffer from the lack of complex motion, effective addressability and precise shape control. To address these needs, I fabricated polymeric nanocomposite microactuators driven by programmable heterogeneous magnetic anisotropy. Spatially modulated photopatterning was applied in a shape independent manner to microactuator components by successive confinement of self-assembled magnetic nanoparticles in a polymer matrix. By freely programming the rotational axis of each component, I demonstrate that the polymeric microactuators can undergo predesigned, complex two- and three-dimensional motion.

4.1 Fabrication

The fabrication process of multi-axial microactuators is based on the sequential immobilization of assembled magnetic nanoparticles in polymer matrix.

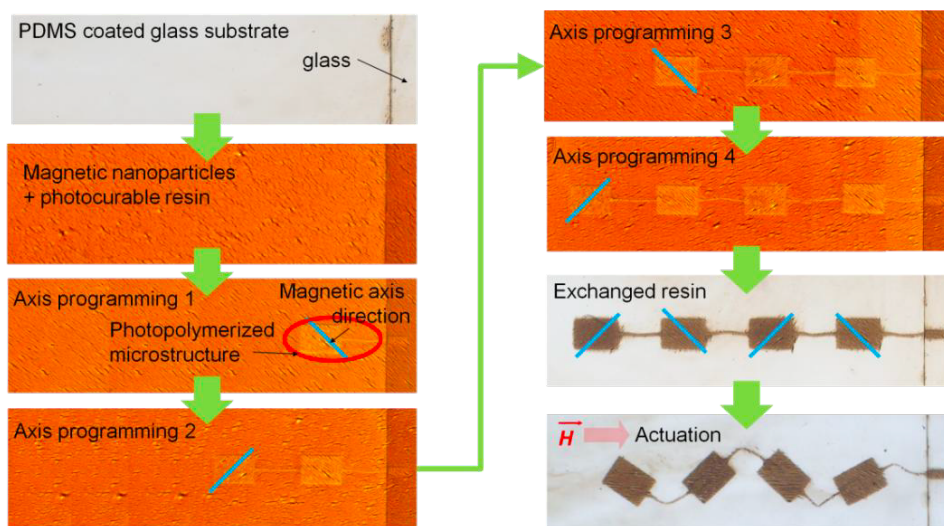


Figure 4.1 Actuator fabrication process. Schematics of the actuator fabrication process and photopolymerization set-up. The fabricated structure is anchored to the pure glass surface while it remains unattached above the PDMS coated region on the substrate due to the inhibition layer. [44]

The setup is composed of a high-speed optical projection system for dynamic ultraviolet (UV) photopatterning, a microfluidic channel for UV-photocurable acrylate oligomer stream, and a microscopic imaging system for inspection and monitoring. A high intensity mercury-xeon lamp (200W bulb) with a fiber-based light guide is used as a continuous wave light source for photopolymerization. A

10x microscope objective lens having a numerical aperture (NA) of 0.28 projects the computer-controlled image pattern on the MEMS SLM to the final object plane with a demagnification factor of approximately 8.9. Since the pitch of the micromirror array is $13.68\mu\text{m}$ in the SLM plane, the pixel size in the object plane is approximately $1.54 \times 1.54\mu\text{m}^2$. The optical projection system and imaging optics share the same objective lens and their light paths are separated by a beam splitter. Using this system, I can reliably synthesize polymeric microstructures with a single pixel resolution ($\sim 1.54 \times 1.54\mu\text{m}^2$) at 0.1s exposure time.

Moreover, using this fabrication process, I can produce the microactuator with programmed magnetic axes in large quantities. The time needed to form chain-like nanostructures under the applied magnetic field is about 0.5s and the time to photopolymerize a single microcompartment through this setup takes about 0.1s. Therefore total time to fabricate a microcompartment with a programmed magnetic axis is around 1s. Therefore, for example, if a uniform magnetic field is applied over an 8" wafer area and the mask size is within 4" \times 4" with a uniform light source, 10^6 microcantilevers with $50\mu\text{m} \times 50\mu\text{m} \times 30\mu\text{m}$ can be fabricated within a few seconds, and moreover this fabrication process can be repeated every second. This result means that our technique is both fast and extremely scalable compared to other polymer based microactuator fabrication methods and general magnetic actuator fabrication methods using conventional MEMS fabrication process.

4.1.1 Various Types of Microfluidic Devices

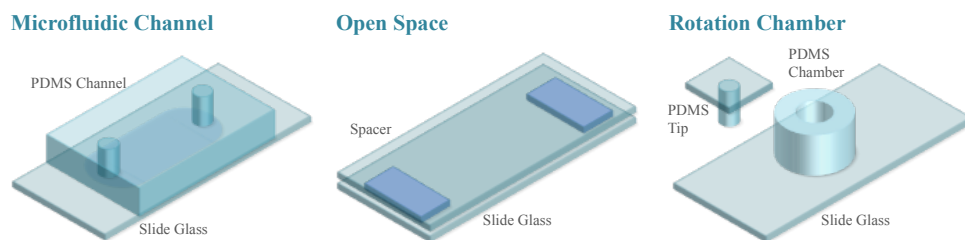


Figure 4.2 Various types of microfluidic devices to fabricate versatile microactuators such as microcomponents for microfluidic system, microrobot and rotating microparticles. [54, 70, 75-76]

The polymeric nanocomposite material used here is based on a combination of a photocurable polymer and magnetic nanoparticles. The superparamagnetic nanoparticles consist of several magnetite nanocrystals, their core capped with a negatively charged material in a silica shell. [77] Without an external magnetic field, the nanoparticles are randomly dispersed in a photocurable liquid resin. When the external magnetic field is applied, the superparamagnetic nanoparticles self-assemble, forming chain-like nanostructures along the magnetic field lines to minimize the magnetic dipole interaction energy of the system. Remarkably, when the magnetic field direction is changed, all chains rapidly rotate or realign along the changed magnetic field direction. Once polymerized, the chains induce cooperative torque, which is the driving force of microstructure actuation.

Optofluidic maskless lithography system, which is utilized to fabricate various shaped microstructures, is composed of a microfluidic channel, which determines the geometric dimension of the microstructure, and a permanent magnet, which generates an external magnetic field. With this system, a sequential process is used

to manufacture miniaturized polymeric actuators. First, a glass substrate is coated with polydimethylsiloxane (PDMS), which is responsible for the inhibition layer used for generating the free-floating part of the component. The coated PDMS is partially removed to create the anchoring region where the structures are permanently attached to the intrinsic glass substrate. Then, the microfluidic channel is attached on the PDMS coated glass substrate and filled with a mixture of poly (ethylene glycol) diacrylate (PEGDA), photoinitiator and superparamagnetic nanoparticles. A homogeneous magnetic field is applied across the microfluidic channel, which causes the superparamagnetic nanoparticles in the resin to form chains along the direction of the applied magnetic field. The resin is photopolymerized in a tenth of a second using an optofluidic maskless lithography system, thus freezing the superparamagnetic nanoparticle alignments in the polymerized region. After photopolymerization, the magnetic field direction is changed, leading to the rearrangement of superparamagnetic nanoparticle chains in the remaining region along the altered magnetic field lines. Then the photopolymerization process is carried out again, creating a newly polymerized part that has a different chain direction to the previous part. This repetitive tuning and fixing is done until the microactuator manufacturing is completed. Before use, the remaining resin is exchanged for the chosen resin to provide an appropriate liquid environment for microstructure actuation. In comparison to thermal curing, the photopolymerization process is instantaneous and can fix the self-assembled nanoparticles fast enough to maintain the assembled state, allowing for high resolution and multi-exposure patterning, with the total fabrication time determined by the time necessary to change the magnetic field. A 10× microscope objective lens having a numerical aperture (NA) of 0.28 projects the computer-controlled image pattern on the MEMS SLM to the final object plane with a demagnification

factor of approximately 8.9. Since the pitch of the micromirror array is $13.68\ \mu\text{m}$ in the SLM plane, the pixel size in the object plane is approximately $1.54 \times 1.54\ \mu\text{m}^2$. The common object plane of the projection system is adjusted to meet the microfluidic channel on the microscope.

4.1.2 Micropatterning of PDMS Thin Film on Glass Substrate

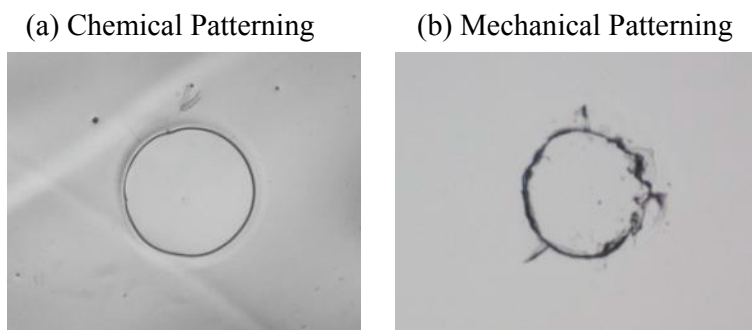


Figure 4.3 Patterned PDMS. (a) Chemical patterning of thin PDMS film (b) Mechanical patterning of thin PDMS film. (Scale bar: $500\ \mu\text{m}$)

There are two ways of using the PDMS patterning method on a glass substrate. In chemical patterning, PDMS is first spin coated on the glass substrate. To make the PDMS photosensitive, benzophenone is added to PDMS as a photosensitizer. Then the PDMS is patterned with UV light exposure, thermally cured and developed. Then, the region exposed to UV light is removed. This method offers a clear edge with high resolution, but the UV exposure time and the amount of benzophenone should be precisely regulated. Otherwise, PDMS is not completely removed. Mechanical patterning is a very simple and direct method. I can pattern PDMS film manually or use several cutters. However, a clear edge is hard to achieve if the patterning shape is complicated or the shape contains lots of curves.

In these designs I observed some ruffles at the edge of the pattern. Using these PDMS patterning methods, I can fabricate more varied microactuators. A blooming flower-like actuator on circularly patterned PDMS is also demonstrated. In this case, I used the mechanical patterning method. [54]

4.1.3 Grey Mask for Flexible Hinge

At connecting joints, the mechanical stiffness increases because the joint is polymerized two times. This effect may reduce actuator performance. Therefore, I decrease the photopolymerization intensity at connecting joints using a gray photomask. The gray-scale mask, as shown in Figure 5.5, results in diminished ultra violet light intensity by decreasing the number of DMD masks reflecting the light. Consequently, the mechanical stiffness of the connecting joints decreases. The use of grayscale mask lithography allows for the creation of leg-like actuators.

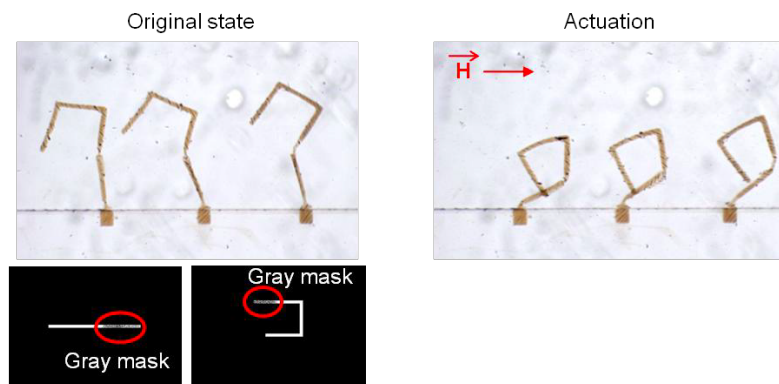


Figure 4.4 Connecting joints using a gray-scale mask: trapper (Left) The benders without a magnetic field. (Right) Bending of leg-like actuators with a gray-scale mask connecting joints. The mechanical stiffness of that part is lower relative to other parts of the actuator. (Scale bar: 100 μ m)

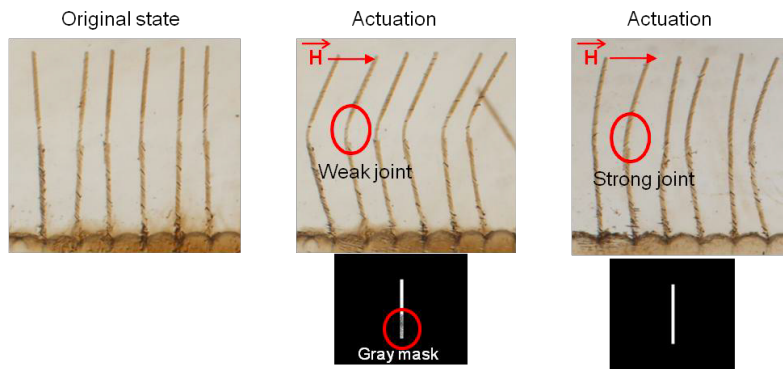


Figure 4.5 Connecting joints using gray scale mask: Leg-like actuators. (Left) Leg-like actuators in the absence of a magnetic field. (Middle) Bending of warm leg-like actuators with gray-scale mask connecting joint. The color of the connecting joints is lighter than other parts, which means that the mechanical stiffness of that part is lower relative to other parts of the actuator. (Right) Bending of leg-like actuators without gray-scale mask connecting joint is not easy as the joints are stiffer than other parts. (Scale bar: 100 μ m)

The color of the connecting joints is lighter than other parts, which means that the mechanical stiffness of that part is lower relative to other parts of the actuator. Bending of leg-like actuators without gray-scale mask connecting joint is not easy as the joints are stiffer than other parts. The color of the connecting joints is brighter than other parts, which means that the mechanical stiffness of that part is lower relative to other parts of the actuator. [54]

4.2 Microfluidic Components

A motor-type microactuator is generated by an OFML centering on a prefabricated PDMS hub, creating a structure capable of rotation. The magnetic field controls the rotational direction of the actuator. A hole at the center of the structure is generated during the polymerization due to the inhibition layer near the surface of the PDMS hub. It rotates in response to the rotating magnetic field induced by a magnet rotating around the channel. The rotating mechanism enables a simple micromotor-type actuator. At the intersection of three microfluidic branches, the magnetic sorter receives a free-floating nonmagnetic particle and sends it to the upper branch of the channel by rotating it in the counterclockwise direction. In addition to a particle-sorting magnetic actuator, I also unveil railed microfluidics-based actuators. Railed microfluidics is an agile method to guide and assemble microstructures within fluidic channels. By combining the guiding mechanism of railed microfluidics and the magnetic control of the magnetic microstructures, rail-guided actuators are demonstrated. The finned microstructure is fabricated on the rail, and it only travels on the rail; thus, the path of movement is determined by the geometry of the rail. By using this method, a rail-guided sliding microvalve actuator is used to alternately block a selected main stream. The position of the finned microvalve on the rail depends on the field direction of the magnet. When the magnetic field is applied perpendicular to the blue stream, the finned microvalve transits to the upper side of the channel along the rail and mainly blocks the blue stream.

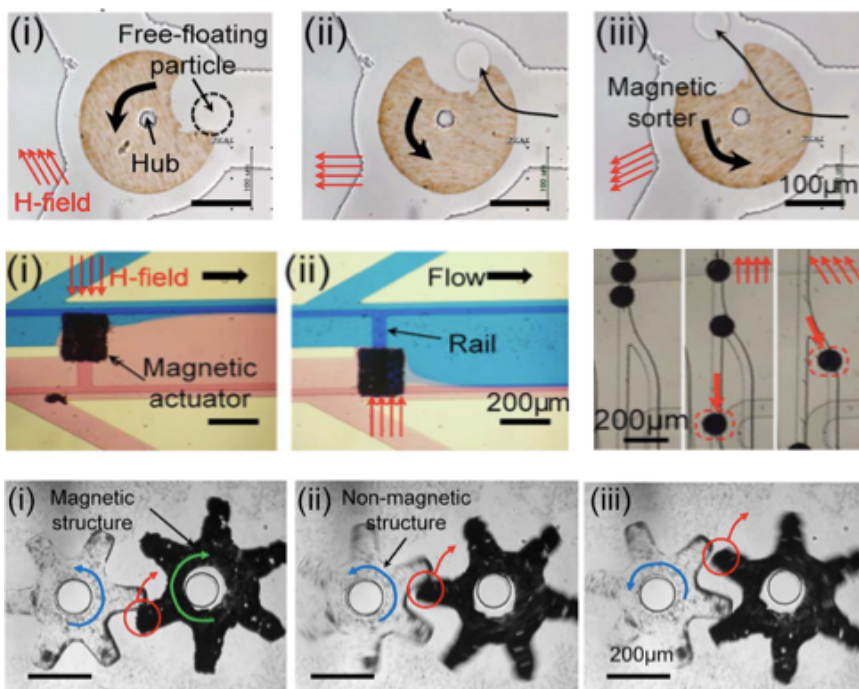


Figure 4.6 Various magnetic actuation mechanisms. (Top) Free-floating particle sorter. At the intersect of three microfluidic channels, the nonmagnetic particle is sorted to a selected branch of the channel by rotating the actuator in a counterclockwise direction. (Middle) Finned microvalve for two-phase microfluidics. When the magnetic field is applied to the actuator, the rail-guided valve actuator moves along the rail toward the field direction and blocks one of two food dye streams (each food dye is diluted in deionized water). (i) Blue stream is blocked. (ii) Red streams are blocked. (Middle) Sorting magnetic structures. At branch points, each circular finned microstructure chooses the next rail branch according to the field direction.

Therefore, I selectively block the unwanted main flow stream by moving the structure along the rail to change the fluid contents downstream in the channel. The rail-guided valve system can be used for layer-by-layer deposition application using a fast solution exchange scheme. By alternatively moving the magnetic structure on the rail, I can easily exchange main-stream flowing in the channels. I also show sorting of railed magnetic finned microstructures through the application of a magnetic field at channel branch sites. The moving direction of each approaching magnetic finned microstructure is controlled by the direction of the field at the branch point.

Applying the magnetic field from different sides of the device allows the structure to be sorted in different directions. By flowing particles while actively changing the field direction, numerous fabricated magnetic structures can be actively sorted inside ethyl alcohol buffer solution. In addition to single material actuation, I also demonstrate actuation of heterogeneous microstructures composed of magnetic and nonmagnetic components. They are fabricated by changing the resin in the channel, alternatively allowing selective magnetic actuation. Two toothed wheels alternate gear tooth contact with each other due to a rotating magnetic field. Here, only the magnetic wheel responds to the field which co-rotates the nonmagnetic wheel. [70]

4.3 Various Types of Multiaxial Microactuators

The significant advantage of this material system over conventional material systems for microsystems is that the magnetic properties of the polymeric microstructure, such as the direction of the magnetic easy axis or the amount of magnetization, are programmable. As mentioned above, the fixed alignment of magnetic nanoparticles in multiple polymerized regions creates magnetic anisotropy in the actuator. This enables a homogeneous magnetic field to independently actuate each part with the relative initial direction of chains in each component determining the final configuration of the actuator. Therefore, this principle enables the production of a variety of active polymeric microdevices by freely programming the rotational axis of each component.

The actuator in Figure 4.7 is composed of four parts, which have different magnetic easy axes. Each part rotates with a different direction and angle, responding to the homogeneous external magnetic field, and as a result, it moves like a crawling snake as the magnetic field line changes direction. The five identical actuators in Figure 4.8 bend at different angles, owing to the magnetic easy axes being programmed in different directions in each actuator. The magnetic microtweezer contains both a pure polymer region and a magnetic-anisotropy programmed region. These actuation examples show that, using our strategy, the design capability of polymeric magnetic actuators can be dramatically expanded.

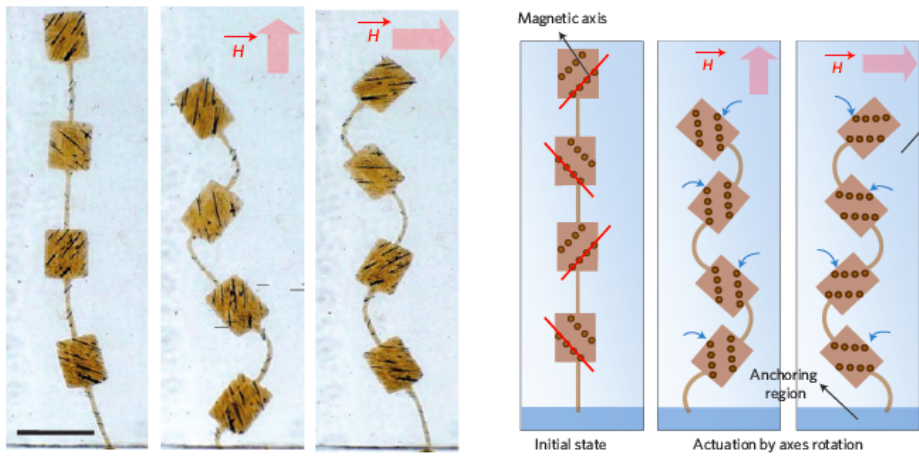


Figure 4.7 A microactuator containing four different easy axes recoils like a snake when a magnetic field is applied. (Scale bar 100 μ m.) Each part of the structure bends in different directions, owing to artificial easy axes made by magnetic microchains.

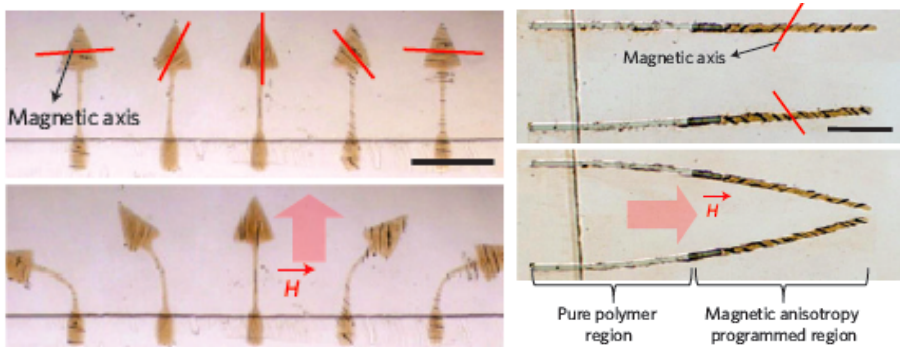


Figure 4.8 Arrow-like magnetic actuator. Five identical arrow-like actuators bend in five different directions under the uniform magnetic field line. (Scale bar 50 μ m.) Also, magnetic tweezer contains both a pure polymer region and a magnetic anisotropy programmed region.

Many magnetic axes can be implanted in a single polymeric microstructure as well as combine the magnetic actuator into other types of functional polymer. The superparamagnetic nanoparticles are arranged into one-dimensional chain-like nanostructures, and the nanostructures are uniformly distributed with constant spacings. Under a uniform magnetic field, the microstructure experiences a magnetic torque on the plate due to the cooperative response of the assembled nanostructures, and a mechanical restoring force due to the thin cantilever beam deflection. These forces become equal at the equilibrium state. Also, I am able to fabricate many different types of microactuators based on this technology. [54]



Figure 4.9 Blooming flower-like actuator on circularly patterned PDMS. When the magnetic field is applied perpendicular to the substrate surface, the flower closes in on itself, bending its eight identical petals. (Scale bar: 500 μ m)

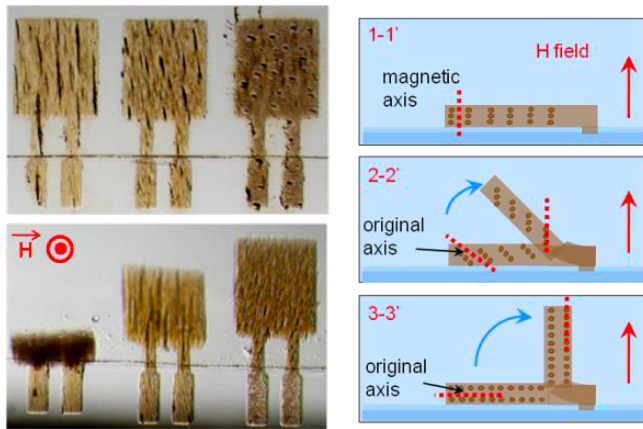


Figure 4.10 Heterogeneous cantilever actuation. Three identical cantilevers bend at different angles because their magnetic nanoparticle chain directions are different. (Scale bar: 100 μ m)

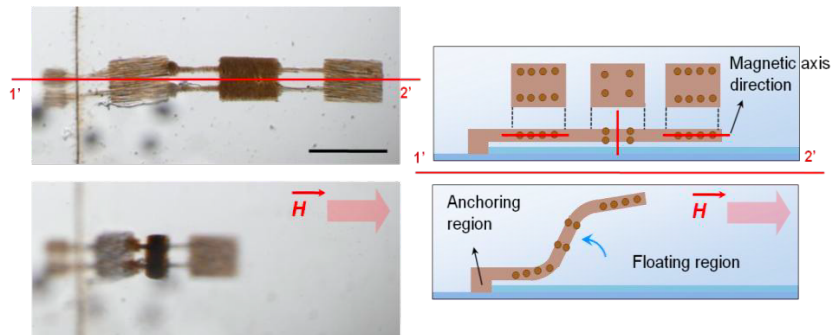


Figure 4.11 Heterogeneous cantilever actuation. The cantilever contains three bodies and three joints. Each body has a different magnetic axis, so it bends in different directions under the applied magnetic field. The final configuration of the cantilever would be very difficult to achieve using conventional magnetic actuators. (Scale bar: 100 μ m)

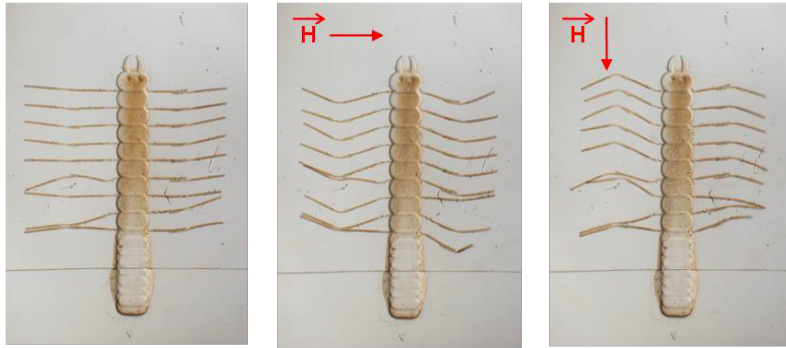


Figure 4.12 Artificial centipede legs. Each leg is composed of two parts with different magnetic nanoparticle chain directions. As the magnetic field line direction is changed, legs move as if they were crawling on the substrate. (Scale bar: 100 μ m)

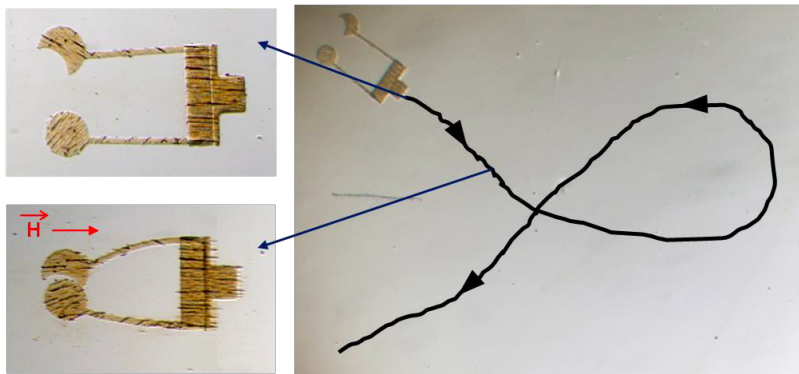


Figure 4.13 Microswimmer. Two arms of the actuator are closed under the magnetic field. The two arms bend creating a space which can contain particles. As a result, the microswimmer can swim following the external magnetic field gradient closing its arms by the external magnetic field line direction. (Scale bar: 100 μ m)

4.4 Rotating Microstructures

One significant advantage of color-barcoded magnetic microparticles over conventional magnetic beads is the capability of multi-axis rotation. This capability is obtained by virtue of the 1D chain structures of superparamagnetic CNCs embedded inside the microparticles. If I apply an external magnetic field to these 1D chain structures, a magnetic torque is induced and the microparticles are rotated as a result. The magnetic anisotropy of the particles can be controlled easily by setting the direction of the external magnetic field during the particle generation step. One non-rotating barcoded particle was intentionally fabricated without the chain formation step, whereas all other rotating barcoded particles were fabricated with aligned 1D CNC chains. This clearly shows that the 1D arrangement of the CNCs is necessary for rotation. [54, 76, 78]

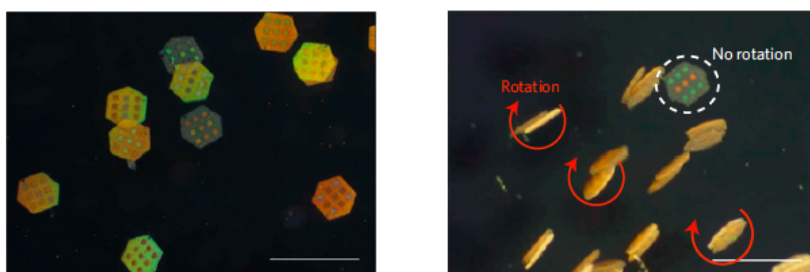


Figure 4.14 Color-barcoded magnetic microparticles under vertical magnetic-field lines. The particle codes are displayed on the 2D surface of the vial. Rotating color-barcoded magnetic microparticles. Non-rotating particle has no 1D chain structures in it.

Depending on the direction of the external magnetic-field lines, the color-barcoded magnetic microparticles can be rotated to lie horizontally with respect to the vial surface, enabling code identification or solution exchange. In addition to 2D positioning, particles can be rotated at a faster rate to create microscale rotating stirrers. A rotating external magnetic field within a horizontal plane rotates vertically aligned color-barcoded particles around their own vertical axes, allowing for rapid mixing and thus maximizing the reaction between the probe and the target in solution. Owing to the ability to hold the microparticles in place using simple magnetic control, this process can be repeated for multistep bioassays involving multistep solution exchanges. The total torque exerted on a microparticle having 1D chains of superparamagnetic nanoparticles under an external magnetic field is simply N times the torque on a single chain owing to the bilateral symmetry of the structure. The rotational speed of the particle is also affected by the viscosity of the surrounding medium. In typical solutions I found it possible to rotate the particles at a rotational frequency of several hundred revolutions per minute.

4.5 Microrobot

As a practical application, I apply our material system to demonstrate the polymeric microrobot. The polymeric microrobot is composed of two heads, two bodies and three joints. The inner two bodies have parallel magnetic easy axes and the outer two heads contain vertical magnetic easy axes with respect to the substrate. The three joints have a ladder structure to prevent unnecessary twisting. This microrobot engages in an arching motion through the application of an external magnetic field in a vertical direction to the substrate. To convert the arching motion into the net forward movement on the substrate, I use the frictional force between a head and the substrate. First, I apply the magnetic field at a slight tilt from the perfect vertical direction to the substrate. Thus, the two bodies bend in different directions while the floating head slowly moves to the other head, at which point it sticks to the substrate. As the magnetic field lines become vertical to the substrate, the microrobot arches like a looper caterpillar. Once the magnetic field becomes slightly tilted again, the head that has been stuck to the substrate following the initial state floats and moves forward, relaxing the arching of the bodies. Therefore, by carefully regulating the magnetic field direction, I can achieve forward crawling of the polymeric microrobot on the substrate.

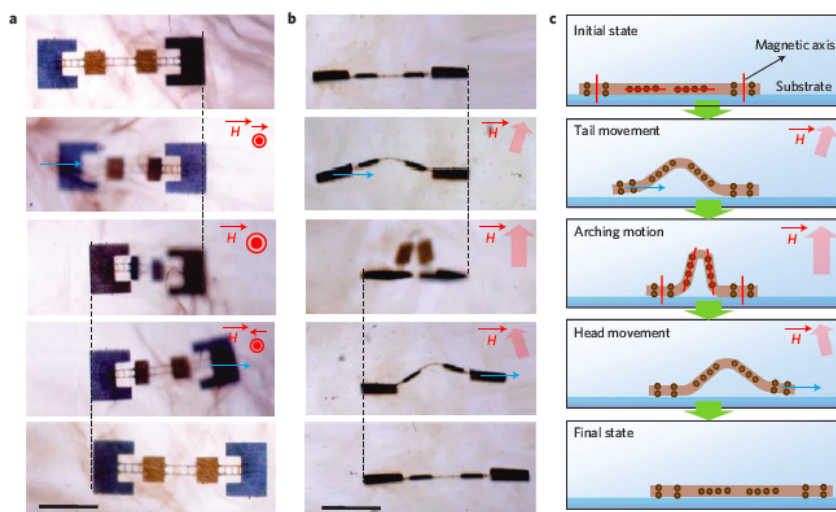


Figure 4.15 Polymeric micro-looper. Sequential movement of a micro-looper (Scale bars 100 μm). (a)-(b) The micro-looper creeps on the substrate as the external magnetic field is applied. First, a weak and slightly tilted magnetic field is applied. The micro-looper starts to bend and the tail moves towards the head. As the magnetic field becomes stronger and clearly vertical, the micro-looper completely arches. When the magnetic field is slightly tilted in the opposite direction, head proceeds forward and the tail sticks to the substrate. After the magnetic field is removed, a sequential crawling process is finished. The micro-looper can crawl on the substrate as this process is repeated. (c) Schematics of micro-looper movement. The micro-looper is composed of four bodies having different magnetic axis, such that choosing an appropriate magnetic field direction and intensity enables to achieve the desired configuration.

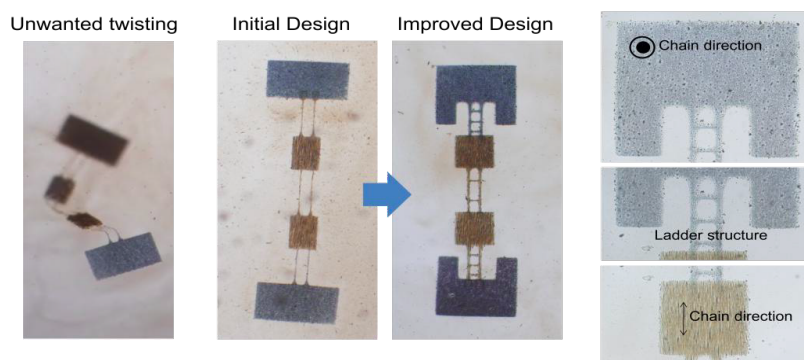


Figure 4.16 Design optimization of a polymeric micro-looper. The micro-looper with initial design shows unnecessary twisting by the application of the magnetic field. The initial micro-looper design was changed to have ladder-like joints with bigger bodies. The head and tail have perpendicular chain direction to the substrate and arching bodies have a parallel chain direction to the substrate. (Scale bar: 100 μ m)

The initial micro-looper is composed of four bodies and three joints. The head and the tail show a blue colour because they were fabricated using structural colour whose color can be seen in the vertical viewing angle. When, each joint is composed of two thin beams, they are easily broken and insufficient to prevent unnecessary movement. When the joints are twisted, head and tail are also easily turned over. To hinder the joint twisting, the ladder structure was added to the joint beam. Also, the head and tail size was made bigger both to increase the friction between the body and the substrate and to reduce the frequent disorientation of the micro-looper. The modified micro-looper shows improved performance. It is less frequently twisted and has an increased frictional force. [54]

4.6 Conclusion

In chapter 4, various types of multiaxial microactuators are demonstrated using the in-situ fabrication technology and the actuation model developed in previous chapters. Polymeric microcomponents are widely used in micro-electro-mechanical systems (MEMS) and lab-on-a-chip devices, but they suffer from the lack of complex motion, effective addressability and precise shape control. Polymer based multiaxial magnetic actuators have high potential to satisfy these needs. Successive confinement of self-assembled magnetic nanoparticles in a polymer matrix, using spatially modulated photopatterning, enables to fabricate polymeric microactuators in shape independent manner. By freely programming the rotational axis of each component, the polymeric microactuators capable of undergoing predesigned, complex two- and three-dimensional motion are demonstrated.

Chapter 5

Magneto-chromatic Microactuators

This chapter introduces a novel color changing microactuators based on the self-assembling behavior of the magnetic nanoparticles. Color-tunable microactuator, utilizing the optical and magnetic behaviors of one-dimensionally assembled super-paramagnetic nanoparticles that play the role of a one-dimensional Bragg reflector and establish a magnetic easy axis, is proposed. By combining these properties with rapid photopolymerization, I developed red, blue, and green micropixels whose colors could be tuned by the application of an external magnetic field. This strategy offers very simple methods for the fabrication and operation of soft color-tunable surfaces with high resolution.

5.1 Fabrication

Soft chromatic materials based on block copolymers [79-84], three-dimensional photonic crystal systems [85-89], and polymeric nanocomposites comprising inorganic nanoparticles [90-92] are currently under investigation, because they are lightweight, easy to produce, and easily applicable to various microsystems. However, most of the previously developed color-tuning schemes strongly depend on specific polymer properties or materials in the local environment and require external contact stimuli [93-95]; these hinder efforts to enhance their resolution and result in poor system scalability. Furthermore, the separation of the color-generation method and color-tuning scheme increases the complexity of the system. [96, 97] These problems can be solved if a material system is developed that can exploit both an optical property to display the color and another property to enable the color to be changed remotely, which could make both fabrication and operation easier.

Fabrication of color-tunable microstructures takes advantage of their magnetic behavior as well as the optical properties of the chain-like nanostructures mentioned above. The external magnetic field is oriented in a different direction can tilt a microstructure containing the immobilized chain-like nanostructures. This, in turn, changes the observed color: the wavelength of the light reflected from a tilted microstructure is blue-shifted owing to the different effective interparticle distance in the chain-like nanostructure. Such angular dependence is one of the basic characteristics of structural color.

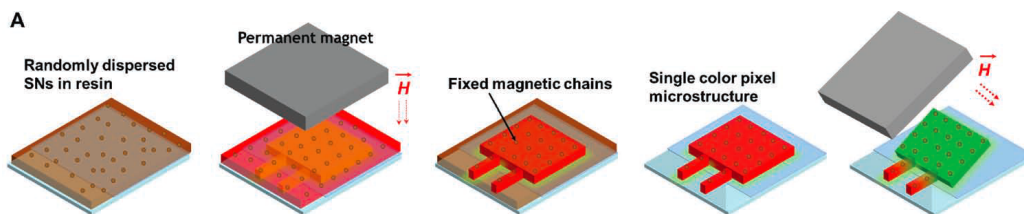


Figure 5.1 Process for the fabrication of a magnetically tunable chromatic microactuator. The dispersed super-paramagnetic nanoparticles (SNs) self-assemble under an applied external magnetic field to produce a structural red color, and these colored nanostructures are then lithographically fixed in a cantilever-shaped microstructure. [100]

Finally, rapid photopolymerization using an optofluidic maskless lithography system enables us to utilize the optical and magnetic properties of the assembled superparamagnetic colloidal nanocrystal clusters (CNCs) in the polymeric microstructure. Patterned UV light instantaneously immobilizes the assembled superparamagnetic CNCs in a polymer resin in a desired shape, so that the microstructure both has the desired initial structural color on its surface and includes the programmed magnetic easy axis in its body. Because the substrate is partially coated with a specific polymer, a small part of the microstructure can be anchored to the substrate, enabling the remaining part to be free-floating and easily susceptible to actuation. Moreover, the microstructure can be placed anywhere required with the desired initial surface color and magnetic axis during the manufacturing process. Therefore, both the color generation and color tuning of a microstructure can be achieved with a single material, the superparamagnetic CNCs, and the combination of these principles with OFML offers a simple and scalable method for in situ fabrication of a micropixelated color-tunable surface. [98-100]

Firstly, a glass substrate is coated with PDMS, which forms the inhibition layer used to generate the free-floating part of each microstructure. The coated PDMS is partially removed to create an anchoring region where the microstructure is permanently attached to the glass substrate. Then, a microfluidic channel is attached to the PDMS-coated glass substrate and filled with M-ink, a mixture of PEGDA, a photoinitiator, and magnetic nanoparticles. After an external magnetic field is applied, the patterned UV irradiation locally solidifies the M-ink, producing a colored microstructure at a specific region. The resulting microstructure has a cantilever shape and is partially attached to the glass substrate, while the remaining part is free-floating and capable of changing the reflected color. During this step, the initial color of the photopolymerized M-ink can be tuned by simply varying the intensity of the applied magnetic field. Here, the microactuators of various initial surface colors are generated under the magnetic field intensity from 200G to 700 G.

Color patterns with different structural colors can be easily generated through subsequent photopolymerization steps forming different colored microstructures in different locations. After a color pattern composed of several microstructures is generated on the substrate, the remaining M-ink is exchanged with an appropriate liquid. Upon the application of an external magnetic field, this color pattern can change its colors from their initial appearance. These structural colors are only shown under reflective light because the microactuator represents brownish color due to the intrinsic color of M-ink. [98, 99]

5.2 Structural Color Generation

The color-tunable liquid utilized in this work is called M-ink, the color of which is magnetically tunable and lithographically fixable. It is composed of superparamagnetic CNCs and a photocurable polymer resin. The superparamagnetic CNCs consist of several single-domain magnetite nanocrystals, and their core is capped with negatively charged material in a silica shell. Without an applied magnetic field, the CNCs are randomly dispersed in the polymeric resin and display an intrinsic brown color. When an external magnetic field is applied, the CNCs assemble to form chain-like nanostructures along the magnetic field lines to minimize the interaction energy of the magnetic dipoles. [78, 98, 100]

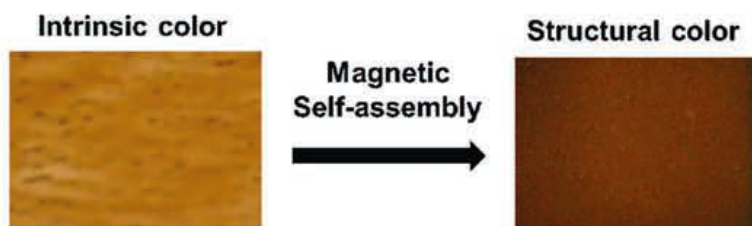


Figure 5.2 Structural color due to self-assembly of super-paramagnetic CNCs. The intrinsic color of M-ink is brown, but its color changes by the application of the external magnetic field because the CNCs assemble to form chain-like nanostructure capable of playing a role of one-dimensional photonic crystal.

More specifically, under the magnetic field, the attractive magnetic force due to the super-paramagnetic core is balanced with repulsive electrostatic and solvation forces, and the CNCs in the chain-like nanostructure dynamically

maintain an interparticle distance establishing equilibrium between these two opposing forces. This novel self-assembly behavior of the super-paramagnetic CNCs can also be combined with in situ photopolymerization technology both to generate visible structural colors of the microstructures and to tune the original color of the microstructures. [100]

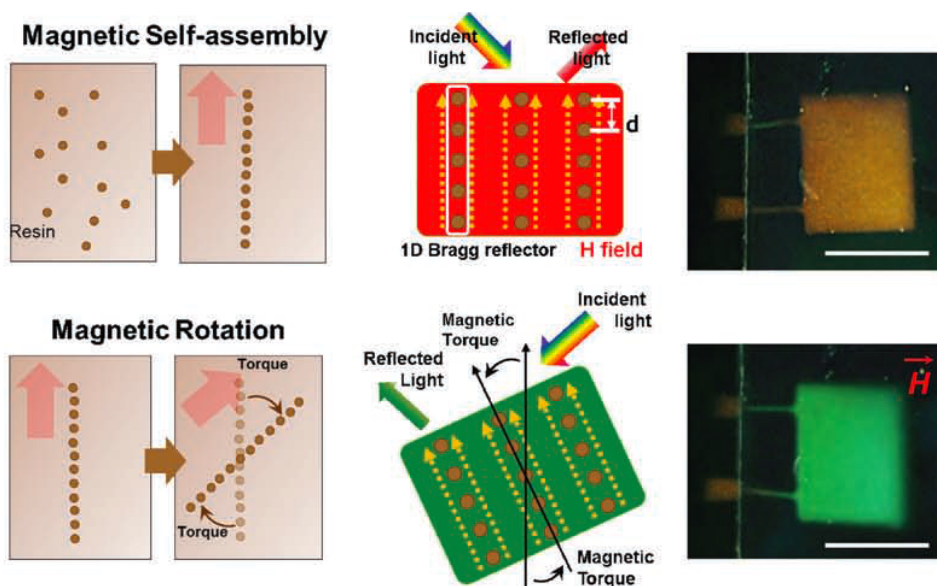


Figure 5.3 Principles of color generation and color change. The self-assembled magnetic nanoparticles reflect a specific wavelength because of their periodicity and form artificial magnetic easy axes to regulate the chromatic microactuator.

Firstly, self-assembled super-paramagnetic CNCs generate color because a chain-like nanostructure reflects a specific wavelength of light at a given interparticle distance. In other words, this chain-like nanostructure composed of several superparamagnetic CNCs plays the role of a one-dimensional Bragg

reflector, and the interparticle distance determines the color of the light diffracted from the chain-like nanostructure. Thus, the original color of the microstructure can be chosen by simply changing the interparticle distance between the CNCs, which varies with the applied magnetic field intensity. To maintain the generated color after the external magnetic field is turned off, I immobilize the assembled super-paramagnetic CNCs by solidifying a polymer resin using an optofluidic maskless lithography system.

5.3 Color Change of Microsurface

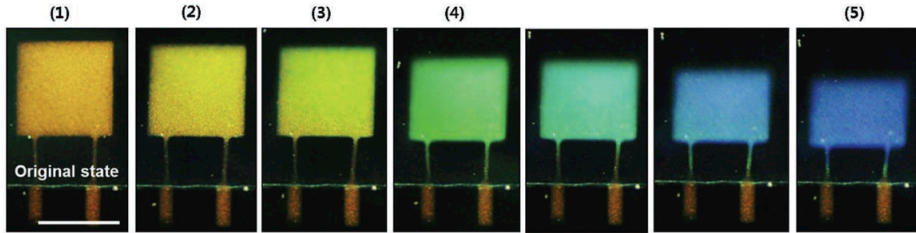


Figure 5.4 Red-colored microactuator and its color change. The reflective structural color is changed as the deflection angle of the microactuator changes, owing to the angular dependence of the structural color (scale bar: 50 μ m).

The first resulting microactuator appeared red in its original state. During the fabrication process, the intensity of the applied magnetic field determines the initial surface color of the microactuator by regulating the interparticle distance of the assembled super-paramagnetic CNCs. After the fabrication process is completed, the applied magnetic field for actuation whose intensity is enough to make the immobilized magnetic chains in the microactuator to be parallel to the magnetic field orientation (> 500 G). The tilting angles of the applied magnetic field for each actuation are exactly the same with the deflection angle of the microactuator. When the direction of the external magnetic field is changed, the microactuator transforms slightly, changing its color from red to green and blue.

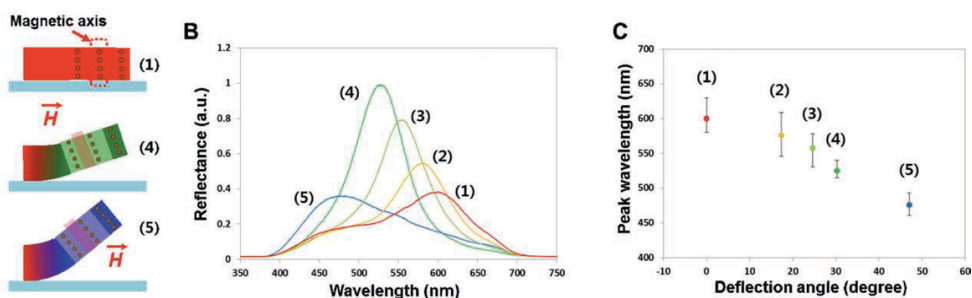


Figure 5.5 Spectra of the red microactuator. The self-assembled nanoparticles have a resonant peak at a green wavelength; therefore, the highest intensity occurs when the color of the microactuator becomes green. Bending angle determines the color of the microactuator.

Figure 5.5 shows the spectral change of the light reflected from the microactuator as the applied magnetic field direction is rotated from perpendicular to parallel to the substrate surface. The spectrum representing the green color has the peak with the highest intensity, because the chain-like periodic nano-structure has a resonance in the wavelength range of green light that depends on the geometric dimensions and the refractive index of the super-paramagnetic CNCs. The average peak wavelengths of the red-, green-, and blue-colored microstructures are about 600, 510, and 470 nm, respectively. The relationship between the deflection angle of the chromatic actuator and the peak wavelength is also shown in Figure 5.5. Moreover, I can control the color of the microactuator with a high level of precision, because the deflection angle can be analytically related to the tilting angle of the applied magnetic field using a simple model.

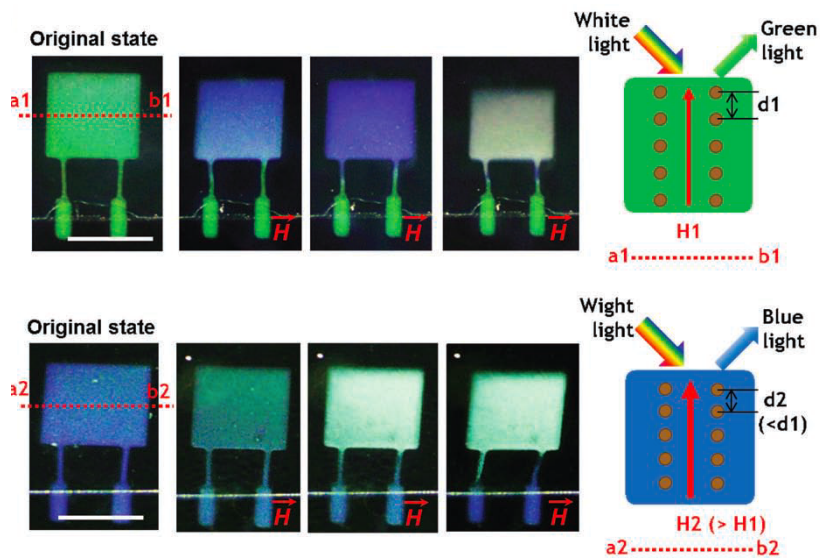


Figure 5.6 Green and blue microactuators. I can choose the original color of the microactuators by varying the intensity of the applied magnetic field during the fabrication process (scale bar: 50 μ m).

Similarly, the color of the blue and green microactuators is blue-shifted by the application of an external magnetic field as the deflection angle of the microactuator increases. Figure 5.6 show multiple colored micropixels, demonstrating the scalability of this system. [100]

5.4 Micropatterns

Figure 5.7 show multiple colored micropixels, demonstrating the scalability of this system. A single micropixel reflects two different colors that simultaneously change when a homogeneous magnetic field is applied. A simple checkerboard color pattern composed of six separate microstructures was also demonstrated on a polymer-coated glass substrate. The pattern changes from its original color pattern to another upon the application of a homogeneous magnetic field. This means that the combination of the self-assembly behavior of the superparamagnetic CNCs and the simple in situ fabrication method offers the potential of manufacturing a color pattern composed of many colorful micropixels on any substrate.

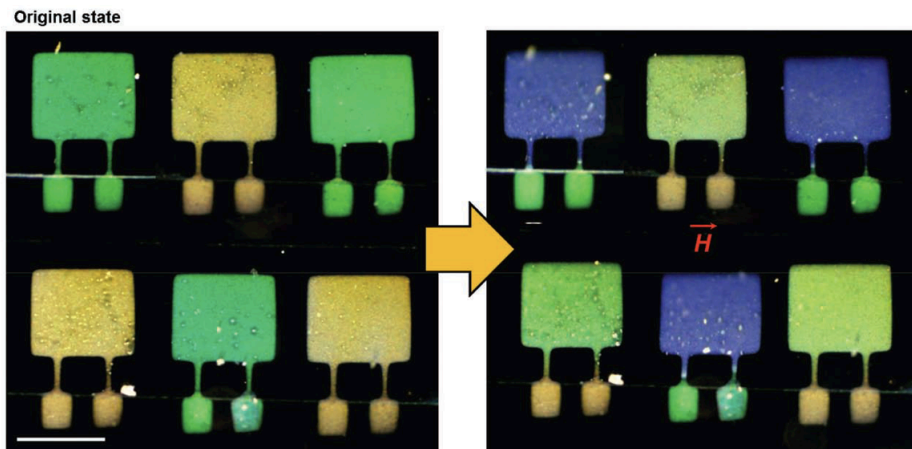


Figure 5.7 Color surface with multiple pixels of various colors. The surface is scalable, because the original color can be determined during the fabrication process within a half-second (scale bar: 50 μ m).

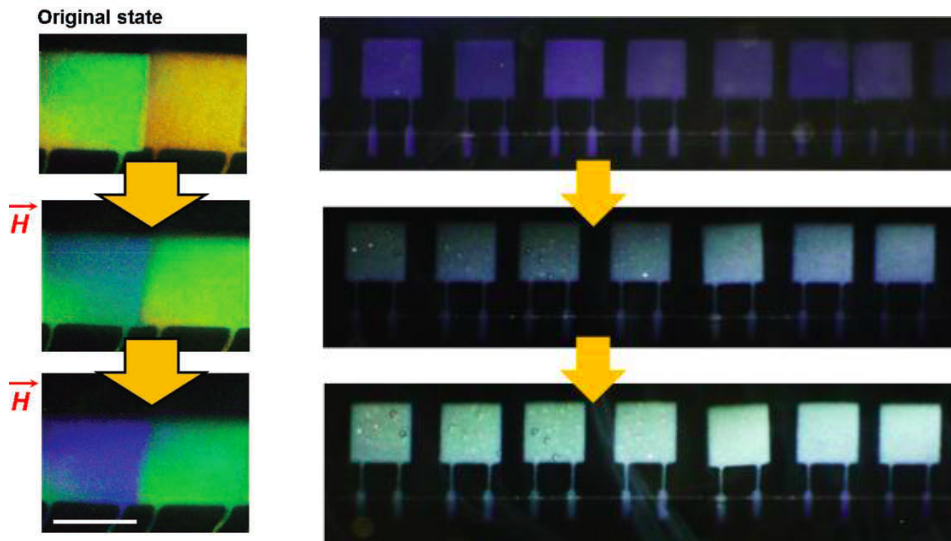


Figure 5.8 Synactuation of blue-colored microactuators. All seven microactuators begin with a blue color and change their color simultaneously upon the application of the external magnetic field.

When a chromatic microplate is too thin to maintain its mechanical stiffness, it can partially bend, showing an unexpected structural color gradient. This also occurs when a microactuator comes into contact with air by mistake during the resin-exchange process, because the polymeric nanocomposite is distorted as it dries upon contact with air. [90]

5.5 Conclusion

In chapter 5, a new type of magnetochromatic nanocomposite microactuator, capable of acting as the pixels in a color-changing surface that can be fabricated in situ using a simple method, is proposed. Notably, the optical and magnetic properties of the nanocomposite material provide the surface color and operability, respectively, in the microstructure fabricated in situ. This nanocomposite microstructure contains one-dimensionally assembled magnetic nanoparticles that both play a role as a one-dimensional Bragg reflector and establish a magnetic easy axis. The structural color is generated by these nanoscale Bragg scatterers and is changed by actuating the microstructure using its programmed magnetic axis. Using this scheme, I developed red-, blue-, and green-colored microactuators and changed their color by tilting the microactuators using an external magnetic field. I analyzed the magnetically driven flexure of a single microactuator and also fabricated a color-tunable micropattern composed of six pixels to show the potential of the scalability of this system. This strategy can be used to produce a color-changing surface based on soft materials that is very simple to fabricate and operate.

Conclusion and Future Work

In this dissertation, I introduce a new magnetic nanocomposite material system and in situ fabrication process that is not shape limited and allows the programming of heterogeneous magnetic anisotropy at the microscale. The key idea is to combine the self-assembling behavior of superparamagnetic nanoparticles, which have stronger magnetization than that of general paramagnetic materials, with a spatially modulated photopatterning process. By repetitively tuning the nanoparticle assembly and fixing the assembled state using photopolymerization, I fabricate microactuators for which all parts move in different directions under a homogeneous magnetic field. To show the feasibility of our concept, I demonstrate polymeric nanocomposite actuators capable of two-dimensional and three-dimensional complex actuations that have rarely been achieved using conventional microactuators. Our approach greatly simplifies the manufacturing process and also offers effective rules for designing novel and complex microcomponents using a nanocomposite material with engineered magnetic anisotropy.

I investigate the self-assembling behavior of both single domain magnetite nanoparticles and superparamagnetic nanoparticles using Monte Carlo simulation. First, I specify the magnetic I use to fabricate magnetic polymer composite: single domain magnetite nanoparticle with 50nm of averaged diameter and superparamagnetic magnetite nanoparticle with 280nm of averaged diameter. Second, I consider several particle interactions which affect to the self-assembling behavior of the magnetic nanoparticles including particle-field interaction, particle-

particle dipole interaction, magnetic anisotropy and steric layer repulsion. I refer several articles which analyze the magnetic self-assembly using Monte Carlo simulation and developed cluster-moving Monte Carlo simulation program with existing algorithm. I investigate the self-assembling behavior of the magnetite nanoparticles varying the intensity of the applied magnetic field during the chain formation and the concentration of the magnetic nanoparticles. The result shows that the well-defined magnetic chains are formed as both the intensity of the applied magnetic field and the magnetic nanoparticle concentration increase.

Also, a novel method to fabricate magnetic nanoparticle embedded polymer composite microstructure is introduced. Briefly, the combination of photocurable polymer and magnetic nanoparticles is photopolymerized to immobilize the various states of magnetic nanoparticles. I especially adopt a system called optofluidic maskless lithography system, which enables to fabricate various shapes of polymeric microstructures within a second. Also, I develop a model system for the magnetic polymer composite actuation. Based on the Monte Carlo simulation result, the torque, the derivative of system energy, of the magnetic chain embedded microstructure is calculated. And, the steady-state elastic modulus of the magnetic composite microbeam is induced by utilizing the simulated torque and cantilever bending experiment result. The torque from two dimensional Monte Carlo simulation result was expanded to calculate three dimensional composite microstructure. At equilibrium state, the magnetic torque equals to the mechanical restoring torque.

As an application, I introduce multiaxial microactuators. Polymeric microcomponents are widely used in microelectromechanical systems (MEMS) and lab-on-a-chip devices, but they suffer from the lack of complex motion, effective addressability and precise shape control. To address these needs, I fabricate

polymeric nanocomposite microactuators driven by programmable heterogeneous magnetic anisotropy. Spatially modulated photopatterning³ was applied in a shape-independent manner to microactuator components by successive confinement of self-assembled magnetic nanoparticles in a fixed polymer matrix. By freely programming the rotational axis of each component, I demonstrate that the polymeric microactuators can undergo predesigned, complex two- and three-dimensional motion.

Finally I also introduce a novel color changing microactuators based on the self-assembling behavior of the magnetic nanoparticles. I propose a color-tunable microactuator utilizing the optical and magnetic behaviors of one-dimensionally assembled super-paramagnetic nanoparticles that play the role of a one-dimensional Bragg reflector and establish a magnetic easy axis. By combining these properties with rapid photopolymerization, I develop red, blue, and green micropixels whose colors could be tuned by the application of an external magnetic field. This strategy offers very simple methods for the fabrication and operation of soft color-tunable surfaces with high resolution.

Bibliography

- [1] R. Nowosielski, Soft magnetic polymer-metal composites consisting of nanostructural Fe-basic powders, *Journal of Achievements in Materials and Manufacturing Engineering*, vol. 24, pp. 68-77, 2007.
- [2] A. C. Balazs, T. Emrick, and T. P. Russell, “Nanoparticle Polymer Composites: Where Two Small Worlds Meet,” *Science*, vol. 314, no. 5802, pp. 1107–1110, 2006.
- [3] Shi X, Hudson JL, Spicer PP, Tour JM, Krishnamoorti R, Mikos AG., Injectable nanocomposites of single-walled carbon nanotubes and biodegradable polymers for bone tissue engineering, *Biomacromolecules*, vol. 7, pp. 2237–2242, 2006.
- [4] S. Jiguet, A. Bertsch, H. Hofmann, and P. Renaud, “Conductive SU8 photoresist for microfabrication,” *Advanced Functional Materials*, vol. 15, no. 9, pp. 1511–1516, 2005.
- [5] S. Jiguet, A. Bertsch, M. Judelewicz, H. Hofmann, and P. Renaud, “SU-8 nanocomposite photoresist with low stress properties for microfabrication applications,” *Microelectronic Engineering*, vol. 83, no. 10, pp. 1966–1970, 2006.
- [6] A. Voigt, M. Heinrich, C. Martin, A. Llobera, G. Gruetzner, and F. Pérez-Murano, “Improved properties of epoxy nanocomposites for specific applications in the field of MEMS/NEMS,” *Microelectronic Engineering*, vol. 84, no. 5-8, pp. 1075–1079, 2007.
- [7] S. Jiguet, M. Judelewicz, S. Mischler, A. Bertch, and P. Renaud, “Effect of filler behavior on nanocomposite SU8 photoresist for moving micro-parts,” *Microelectronic Engineering*, vol. 83, no. 4-9, pp. 1273–1276, 2006.
- [8] C. S. Sikes, A. P. Wheeler, A. Wierzbicki, R. M. Dillaman, L. De Luca, *Biol. Bull.*, vol.194, pp. 304–316, 1998.
- [9] H. Colfen and S. Mann, Higher-Order Organization by Mesoscale Self-Assembly and Transformation of Hybrid Nanostructures, *Angew. Chem. Int. Ed.* vol. 42, pp. 2350–2365, 2003.

- [10] M. Suter, Photopatternable superparamagnetic nanocomposite for the fabrication of microstructures, Thesis, Eth Zurich, 2011.
- [11] P. M. Ajayan, L. S. Schadler, P. V. Braun, Nanocomposite science and technology, WILEY-VCH, 2003.
- [12] B. B. Nayak, Magnetic nanocomposite materials, Thesis, Indian institute of technology, 2006.
- [13] N.-T. Nguyen, S.-S. Ho, and C. L.-N. Low, "A polymeric microgripper with integrated thermal actuators," *Journal of Micromechanics and Microengineering*, vol. 14, no. 7, p. 969, 2004.
- [14] J. W. L. Zhou, C. Ho-Yin, T. K. H. To, K. W. C. Lai, and W. J. Li, "Polymer MEMS actuators for underwater micromanipulation," *Mechatronics, IEEE/ASME Transactions on*, vol. 9, no. 2, pp. 334–342, 2004.
- [15] N. Chronis and L. P. Lee, "Electrothermally Activated SU-8 Microgripper for Single Cell Manipulation in Solution," *Microelectromechanical Systems, Journal of Microelectromechanical Systems*, vol. 14, no. 4, pp. 857–863, 2005.
- [16] S. R. Quake and A. Scherer, "From Micro- to Nanofabrication with Soft Materials," *Science*, vol. 290, no. 5496, pp. 1536–1540, 2000.
- [17] F. Umbrecht, P. Wägli, S. Dechand, F. Gattiker, J. Neuenschwander, U. Sennhauser, and C. Hierold, "Wireless implantable passive strain sensor: design, fabrication and characterization," *Journal of Micromechanics and Microengineering*, vol. 20, no. 8, p. 085005, 2010.
- [18] V. Seidemann, S. Bütetfisch, and S. Büttgenbach, "Fabrication and investigation of in-plane compliant SU8 structures for MEMS and their application to micro valves and micro grippers," *Sensors and Actuators A: Physical*, vol. 97-98, pp. 457–461, 2002.
- [19] C. Goll, W. Bacher, B. Büstgens, D. Maas, R. Ruprecht, and W. K. Schomburg, "An electrostatically actuated polymer microvalve equipped with a movable membrane electrode," *Journal of Micromechanics and Microengineering*, vol. 7, no. 3, p. 224, 1997.
- [20] E. Smela, "Conjugated Polymer Actuators for Biomedical Applications," *Advanced*

- Materials, vol. 15, no. 6, pp. 481–494, 2003.
- [21] J. D. Madden, R. A. Cush, T. S. Kanigan, and I.W. Hunter, “Fast contracting polypyrrole actuators,” *Synthetic Metals*, vol. 113, no. 1-2, pp. 185–192, 2000.
- [22] N. S. Satarkar, A. M. Hawkins, and J. Z. Hilt, *Hydrogel Nanocomposites in Biology and Medicine: Applications and Interactions, Biological Interactions on Materials Surfaces*, DOI 10.1007/978-0-387-98161-1_16, 2009.
- [23] O. Cugat, G. Reyne, J. Delamare, and H. Rostaing, “Novel magnetic microactuators and systems (MAGMAS) using permanent magnets,” *Sensors and Actuators A: Physical*, vol. 129, no. 1-2, pp. 265–269, 2006.
- [24] I. J. Busch-Vishniac, “The case for magnetically driven microactuators,” *Sensors and Actuators A: Physical*, vol. 33, no. 3, pp. 207–220, 1992.
- [25] M. R. J. Gibbs, E. W. Hill, and P. J. Wright, “Magnetic materials for MEMS applications,” *Journal of Physics D-Applied Physics*, vol. 37, no. 22, pp. R237–R244, 2004.
- [26] O. Ergeneman, G. Dogangil, M. P. Kummer, J. J. Abbott, M. K. Nazeeruddin, and B. J. Nelson, “A magnetically controlled wireless optical oxygen sensor for intraocular measurements,” *Sensors Journal, IEEE*, vol. 8, no. 1, pp. 29–37, 2008.
- [27] L. Zhang, J. J. Abbott, L. Dong, B. E. Kratochvil, D. Bell, and B. J. Nelson, “Artificial bacterial flagella: Fabrication and magnetic control,” *Applied Physics Letters*, vol. 94, p. 064107, 2009.
- [28] A. G. Olabi and A. Grunwald, “Design and application of magnetostrictive materials,” *Materials & Design*, vol. 29, no. 2, pp. 469–483, 2008.
- [29] M. L. Johnson, J. Wan, S. Huang, Z. Cheng, V. A. Petrenko, D.-J. Kim, I. H. Chen, J. M. Barbaree, J. W. Hong, and B. A. Chin, “A wireless biosensor using microfabricated phage-interfaced magnetoelastic particles,” *Sensors and Actuators A: Physical*, vol. 144, no. 1, pp. 38–47, 2008.
- [30] Y. Yamanishi, Y. C. Lin, and F. Arai, “Magnetically modified PDMS microtools for micro particle manipulation,” *2007 IEEE/RSJ International Conference on Intelligent Robots and Systems*, Vol. 1-9, pp. 759–764, 2007.

- [31] F. Pirmoradi, L. Cheng, and M. Chiao, "A magnetic poly(dimethylsiloxane) composite membrane incorporated with uniformly dispersed, coated iron oxide nanoparticles," *J. Micromech. and Microeng.*, vol. 20, no. 1, pp. 015032, 2010.
- [32] W. Xue and T. Cui, "Carbon nanotube micropatterns and cantilever arrays fabricated with layer-by-layer nano self-assembly," *Sensors and Actuators A: Physical*, vol. 136, no. 2, pp. 510–517, 2007.
- [33] S. J. Leigh, C. P. Pursell, J. Bowen, D. A. Hutchins, J. A. Covington, and D. R. Billson, "A miniature flow sensor fabricated by microstereolithography employing a magnetite/acrylic nanocomposite resin," *Sensors and Actuators a-Physical*, vol. 168, no. 1, pp. 66–71, 2011.
- [34] N. Damean, B. A. Parviz, J. N. Lee, T. Odom, and G. M. Whitesides, "Composite ferromagnetic photoresist for the fabrication of microelectromechanical systems," *J. Micromech. and Microeng.*, vol. 15, no. 1, pp. 29–34, 2005.
- [35] K. L. Tsai, M. Ziaei-Moayyed, R. N. Candler, H. Wei, V. Brand, N. Klejwa, S. X. Wang, and R. T. Howe, "Magnetic, mechanical, and optical characterization of a magnetic nanoparticle-embedded polymer for microactuation," *J. Microelectromechanical Systems*, vol. 20, no. 1, pp. 65–72, 2011.
- [36] P. C. Gach, C. E. Sims, and N. L. Allbritton, "Transparent magnetic photoresists for bioanalytical applications," *Biomaterials*, vol. 31, no. 33, pp. 8810–8817, 2010.
- [37] Y. Tian, Y.-L. Zhang, J.-F. Ku, Y. He, B.-B. Xu, Q.-D. Chen, H. Xia, and H.-B. Sun, "High performance magnetically controllable microturbines," *Lab on a Chip*, vol. 10, no. 21, pp. 2902–2905, 2010.
- [38] S.-H. Kim, J. Y. Sim, J.-M. Lim, S.-M. Yang, "Magneto-responsive microparticles with nanoscopic surface structures for remote-controlled locomotion," *Angew. Chem. Int. Ed.*, vol. 49, pp. 3786–3790, 2010.
- [39] M. S. Saker, E. B. Steager, D. Y. Kim, M. J. Kim, G. J. Pappas, V. Kumar, "Single cell manipulation using ferromagnetic composite microtransporters," *Appl. Phys. Lett.*, vol. 96, 043705, 2010.
- [40] K. L. Tsai, M. Ziaei-Moayyed, R. N. Candler, H. Wei, V. Brand, N. Klejwa, S. X.

- Wang, and R. T. Howe, “Magnetic, mechanical, and optical characterization of a magnetic nanoparticle-embedded polymer for microactuation,” *Microelectromechanical Systems, Journal of*, vol. 20, no. 1, pp. 65–72, 2011.
- [41] P. C. Gach, C. E. Sims, and N. L. Allbritton, “Transparent magnetic photoresists for bioanalytical applications,” *Biomaterials*, vol. 31, no. 33, pp. 8810–8817, 2010.
- [42] D. J. Griffiths, *Introduction to electrodynamics*, Princeton Hall, 3rd edition.
- [43] J. W. Judy, *Batch-Fabricated Ferromagnetic Microactuators with Silicon Flexures*, Thesis, University of California, Berkeley, 1996.
- [44] Kim, S-H., Sim, J. Y., Lim, J. M. & Yang, S-M. Magneto-responsive microparticles with nanoscopic surface structures for remote-controlled locomotion. *Angew. Chem. Int. Edn.* 49, 3786-3790, 2010.
- [45] Khoo, M. & Liu, C. Micro magnetic silicon elastomer membrane actuator. *Sens. Actuat. A* 89, 259-266, 2000.
- [46] Judy, W. J. & Muller, R. S. Magnetic microactuation of torsional polysilicon structures. *Sens. Actuat. A* 53, 392-396, 1996.
- [47] Judy, W. J. & Muller, R. S. Magnetically actuated, addressable microstructures. *J. Microelectromech. Syst.* 6, 249-256, 1997.
- [48] Zhang, L. et al. Artificial bacterial flagella: Fabrication and magnetic control. *Appl. Phys. Lett.* 94, 064107, 2009.
- [49] Yellen, B. B. *Magnetically Programmable Transport and Assembly of Colloidal Particles*. Thesis, Drexel Univ., 2004.
- [50] N. B. Adelman, K. J. Beckman, D. J. Campbell, and A. B. Ellis, Preparation and Properties of an Aqueous Ferrofluid, *Journal of Chemical Education*, vol. 76, pp. 943-948, 1999.
- [51] R. M. Erb, H. S. Son, B. Samanta, V. M. Rotello, and B. B. Yellen, Magnetic assembly of colloidal superstructures with multipole symmetry, vol. 457, pp. 999-1002, 2009.
- [52] M. Boncheva, S. A. Andreev, L. Mahadevan, A. Winkleman, D. R. Reichman, M. G. Prentiss, S. Whitesides, and G. M. Whitesides, Magnetic self-assembly of three-

- dimensional surfaces from planar sheets, vol. 102, pp. 3924-3929, 2005.
- [53] D. Lorenzo, D. Fragouli, G. Bertoni, C. Innocenti, G. C. Anyfantis, P. D. Cozzoli, R. Cingolani, and A. Athanassiou, Formation and magnetic manipulation of periodically aligned microchains in thin plastic membranes, *Journal of Applied Physics*, vol. 112, 083927, 2012.
- [54] J. Kim, S. E. Chung, S-E. Choi, H. Lee, J. Kim and S. Kwon, "Programming magnetic anisotropy in polymeric microactuators", *Nature Materials*, vol. 10, pp. 747-752, 2011.
- [55] G. F. Goya, T. S. Berquo, F. C. Fonseca, and M. P. Morales, Static and dynamic magnetic properties of spherical magnetite nanoparticles, *Journal of Applied Physics*, vol. 94, pp. 3520-3528, 2003.
- [56] Y-W. Jun, J-W. Seo, and J. Cheon, Nanoscaling Laws of Magnetic Nanoparticles and Their Applicabilities in Biomedical Sciences, *Accounts of Chemical Research*, Vol. 41, pp. 179-189, 2008.
- [57] Diandra L. Leslie-Pelecky, Magnetic Properties of Nanostructured Materials, *Chem. Mater.*, vol.8, pp. 1770-1783, 1996.
- [58] H. Iida, K. Takayanagi, T. Nakanishi, T. Osaka, Synthesis of Fe₃O₄ nanoparticles with various sizes and magnetic properties by controlled hydrolysis, *Journal of Colloid and Interface Science*, vol. 314, pp. 274–280, 2007.
- [59] G. Allegraa, G. Raosa, M. Vacatello, Theories and simulations of polymer-based nanocomposites: From chain statistics to reinforcement, *Prog. Polym. Sci.*, vol. 33, pp. 683–731 2008.
- [60] J. Ge, Y. Hu, M. Biasini, W. P. Beyermann, and Y. Yin, Superparamagnetic Magnetite Colloidal Nanocrystal Clusters, *Angew. Chem.*, vol. 119, pp. 4420–4423, 2007
- [61] Adam J. Rondinone, Anna C. S. Samia, and Z. John Zhang, Superparamagnetic Relaxation and Magnetic Anisotropy Energy Distribution in CoFe₂O₄ Spinel Ferrite Nanocrystallites, *J. Phys. Chem. B*, vol. 103, pp. 6876-6880, 1999.
- [62] L.A. Dobrzański*, M. Drak, B. Ziębowicz, Materials with specific magnetic properties, *Journal of Achievements in Materials and Manufacturing Engineering*, vol. 17, pp. 37-40, 2006.

- [63] James E. Martin and Robert A. Anderson, Chain model of electrorheology, *J. Chem. Phys.*, vol. 104, pp. 4814-4827, 1996.
- [64] Y. Labaye, O. Crisan, L. Berger, J. M. Greneche, J. M. D. Coey, Surface anisotropy in ferromagnetic nanoparticles, *Journal of Applied Physics*, Vol. 91, doi: 10.1063/1.1456419, 2002.
- [65] G. Bertoni, B. Torre, A. Falqui, D. Fragouli, A. Athanassiou, and R. Cingolani, Nanochains Formation of Superparamagnetic Nanoparticles, *J. Phys. Chem. C*, vol. 115, pp. 7249–7254, 2011.
- [66] M. Aoshima, A. Satoh, Two-dimensional Monte Carlo simulations of a colloidal dispersion composed of polydisperse ferromagnetic particles in an applied magnetic field, *Journal of Colloid and Interface Science*, vol. 288, pp. 475–488, 2005.
- [67] S. E. Chung, W. Park, H. Park, K. Yu, N. Park, and S. Kwon, "Optofluidic maskless lithography system for real-time synthesis of photopolymerized microstructures in microfluidic channels," *Applied Physics Letters*, vol. 91, p. 041106, 2007.
- [68] S. E. Chung, W. Park, S. Shin, S. A. Lee, and S. Kwon, "Guided and fluidic self-assembly of microstructures using railed microfluidic channels," *Nature Materials*, vol. 7, pp. 581-587, 2008.
- [69] D. Dendukuri, P. Panda, R. Haghgooie, J. M. Kim, T. A. Hatton, and P. S. Doyle, "Modeling of oxygen-inhibited free radical photopolymerization in a PDMS microfluidic device," *Macromolecules*, vol. 41, pp. 8547-8556, 2009.
- [70] S. E. Chung, J. Kim, S. E. Choi, L. N. Kim, and S. Kwon, "In Situ Fabrication and Actuation of Polymer Magnetic Microstructures," *Journal of Microelectromechanical Systems*, DOI: 10.1109/JMEMS.2011.2159093, 2011.
- [71] L. L. Howell, *Compliant mechanisms*, John Wiley & Sons, 2001
- [72] F. Fahrni, M. W. J. Prins, L. J. van IJzendoorn, Magnetization and actuation of polymeric microstructures with magnetic nanoparticles for application in microfluidics, *Journal of Magnetism and Magnetic Materials*, vol. 321, pp. 1843–1850, 2009.
- [73] D. Bandopadhyaya, B. Bhattacharaya, and A. Dutta, Pseudo-rigid Body Modeling of IPMC for a Partially Compliant Four-bar Mechanism for Work Volume Generation,

- Journal of Intelligent Material Systems and Structures, vol. 20, pp. 51-61, 2009.
- [74] Y-J. Park, U. Jeong, J. Lee, S-R Kwon, H-Y. Kim, and K-J Cho, Kinematic Condition for Maximizing the Thrust of a Robotic Fish Using a Compliant Caudal Fin, IEEE Transactions on Robotics, doi:10.1109/TRO.2012.2205490, 2012.
- [75] S. E. Chung, S. A. Lee, J. Kim, and S. Kwon, "Optofluidic encapsulation and manipulation of silicon microchips using image processing based optofluidic maskless lithography and railed microfluidics," Lab on a Chip, vol. 9, pp. 2845-2850, 2009.
- [76] H. Lee, J. Kim, H. Kim, J. Kim, and S. Kwon, "Colour-barcoded magnetic microparticles for multiplexed bioassays," Nature Materials, vol. 9, pp. 745-749, 2010.
- [77] J. Ge, H. Lee, J. Kim, Z. Lu, H. Kim, J. Goebel, S. Kwon, and Y. Yin, "Magnetochromatic Microspheres: Rotating Photonic Crystals", Journal of American Society of Chemistry, vol. 131, pp. 15687-15694, 2009.
- [78] H. Kim, J. Ge, J. Kim, S.-e. Choi, H. Lee, H. Lee, W. Park, Y. Yin, and S. Kwon, "Structural colour printing using a magnetically tunable and lithographically fixable photonic crystal," Nature Photonics, vol. 3, pp. 534-540, 2009.
- [79] K. M. Kim, S.-y. Choi, H. J. Jeon, J. Y. Lee, D. J. Choo, J. Kim, Y. S. Kang, H.-O. Yoo, Macromol. Res., vol. 16, pp. 169–177, 2008.
- [80] O. B. Ayyub, J. W. Sekowski, T.-I. Yang, X. Zhang, R. M. Briber, P. Kofinas, Biosens. Bioelectron., vol. 28, pp. 349–354, 2011.
- [81] Y. Lu, H. Xia, G. Zhang, C. Wo, J. Mater. Chem., vol. 19, pp. 5952–5955, 2009.
- [82] J.-T. Sun, C.-Y. Hong, C.-Y. Pan, Soft Matter, vol. 8, pp. 3753, 2012.
- [83] X. Wang, J. K.-P. Ng, P. Jia, T. Lin, C. M. Cho, J. Xu, X. Lu, C. He, Macromolecules, vol. 42, pp. 5534–5544, 2009.
- [84] M. Brehmer, J. Lub, P. v. d. Witte, Adv. Mater., vol. 10, pp. 1438, 1998.
- [85] J. Shin, P. V. Braun, W. Lee, Sensors Actuators B, vol. 150, pp. 183–190, 2010.
- [86] D. K. Cullen, K. D. Browne, Y. Xu, S. Adeeb, J. A. Wolf, R. M. McCarron, S. Yang, M. Chavko, D. H. Smith, J. Neurotrauma, vol. 28, pp. 2307–2318, 2011.
- [87] S. Colodrero, M. Ocana, H. Miguez, Langmuir, vol. 24, pp. 4430–4434, 2008.
- [88] Q. Zhao, A. Haines, D. Snoswell, C. Keplinger, R. Kaltseis, S. Bauer, I. Graz, R. Denk,

- P. Spahn, G. Hellmann, J. J. Baumberg, *Appl. Phys. Lett.*, vol. 100, 101902, 2012.
- [89] C. I. Aguirre, E. Reguera, A. Stein, *Adv. Funct. Mater.*, vol. 20, pp. 2565-2578, 2010.
- [90] W. Caseri, *J. Mater. Chem.*, vol. 20, pp. 5582–5592, 2010.
- [91] G. Carotenuto, G. La Peruta, L. Nicolais, *Sensors Actuators B*, vol. 114, pp. 1092, 2006.
- [92] S. T. Dubas, V. Pimpan, *Mater. Lett.*, vol. 62, pp. 3361, 2008.
- [93] Z. H. Fang, C. Punckt, E. Y. Leung, H. C. Schniepp, I. A. Aksay, *Appl. Opt.*, vol. 49, pp. 6689–6696, 2010.
- [94] K. Ueno, J. Sakamoto, Y. Takeoka, M. Watanabe, *J. Mat. Chem.*, vol. 19, pp. 4778–4783, 2009.
- [95] M. A. Haque, T. Kurokawa, G. Kamita, Y. Yue, J. P. Gong, *Chem. Mater.* vol. 23, pp. 5200–5207, 2011.
- [96] T. Kinoshita, S. Hayashi, Y. Yokogawa, *J. Photochem. Photobiol. A: Chem.*, vol. 145, pp. 101–106, 2001.
- [97] Y. Takeoka, M. Watanabe, *Langmuir*, vol. 19, pp. 9104–9106, 2003.
- [98] J. Kim, L. He, Y. Song, Y. Yin and S. Kwon, "Lithographic compartmentalization of emulsion droplet templates for microparticles with multiple nanostructured compartments", *ChemComm*, vol. 48, pp. 6091–6093, 2012.
- [99] J. Kim, Y. Song, L. He, H. Kim, H. Lee, W. Park, Y. Yin, and S. Kwon, "Real-Time Optofluidic Synthesis of Magnetochromatic Microspheres for Reversible Structural Color Patterning", *Small*, vol. 7, pp. 1163-1168, 2011.
- [100] J. Kim, S-E. Choi, H. Lee and S. Kwon, "Magnetochromatic Microactuators for Micropixelated Color-changing Surface", *Advanced Materials*, vol. 25, pp. 1415–1419, 2013.

국문 초록

우주 공학 기술, 생명 공학 기술, 로봇 공학 기술 등이 발전하며 다양한 미세 복합 시스템들이 전 세계적으로 활발히 연구되고 있다. 미세 복합 시스템은 외부 환경에 따라 지능적으로 반응하며 다양한 기능을 수행할 수 있는 지능형 미세 소자들의 기능에 의해 그 역할이 결정되는데 기존의 소자들은 외부 환경에 대한 반응이 매우 단순하여 복잡한 기능을 수행하는데 많은 한계를 보여 왔다. 이를 해결하기 위해서는 미세 환경에서도 다양한 반응을 유도할 수 있도록 물질의 특성을 인공적으로 제어할 수 있는 지능형 신소재의 개발이 필연적으로 요구된다.

지능형 신소재를 개발하기 위해서 여러 연구 분야에서 다양한 제작 방법들이 시도되어 왔다. 나노 입자들을 매질 내에 가둬으로써 전기적, 화학적 혹은 물리적 특성을 전체적으로 향상시키는 나노 복합 소재나 외부의 전기적 신호에 반응하여 움직임은 보여주는 전기활성 고분자 (electroactive polymer) 소재 등이 그 대표적인 예이다. 하지만 이러한 기존의 소재들은 소재의 물성을 자유롭게 제어하거나 프로그래밍할 수 없기 때문에 외부 자극에 대한 반응이 한 방향으로 휘어짐과 같이 매우 단순하고 반응 속도가 느리다. 또한 실제 기능을 수행하는 소자를 제작하기 위해 매우 복잡한 공정 과정을 거쳐야 하며 구동을 위한 전기 기기를 소재에 직접 접촉시켜야 하므로 전기 화학적 환경에 매우 민감한 시스템에서는 구동시키기가 어렵다는 문제점들을 가지고 있다.

본 논문에서는 이와 같은 문제점을 해결하기 위하여 기존의 나노 공정들과는 비교할 수 없을 정도로 매우 간단한 접근 방법으로 소재 내의 다양한 영역에 나노크기 수준으로 자기 이방성을 인공적으로 프로그래밍할 수 있는 기술을 개발하였다. 초상자성 나노입자의 자기 조립 특성을 이용해 자기 이방성을 유도하고 고분자 광경화 기술을 이용하여 유도된 자기 이방성을 소재 내의 다양한 영역에 프로그래밍 하였으며, 개발된 소재를 이용해 신개념 마이크로 소자 및 생체 모사적 마이크로 로봇을 구현하였다.

자기 이방성이란 물질 내에서 일종의 자축 (magnetic axis)과 같은 역할을 수행하는 자기적 성질로 외부에서 자기장을 걸어주게 되면 물질이 자기 이방성의 방향으로 에너지를 갖게 된다. 자기 나노입자들은 외부 자기장을 걸어주었을 때 자기력선 방향을 따라 저절로 쇠사슬 모양으로 정렬되는 구조적 변화를 보여주는데, 이러한 구조적 변화가 나노입자가 포함된 물질의 자기 이방성을 결정하게 된다. 이러한 물리적 현상에 기반하여, 빛을 쬐어주면 굳는 액체를 나노입자와 조합한 후 나노 입자의 자기 조립 방향을 제어함과 동시에 이러한 구조적 변화를 매질 내에 국소적으로 고정시킬 수 있는 독자적인 플랫폼을 개발하였다. 또한, 자성 나노입자의 자기 조립 특성을 Monte-Carlo 시뮬레이션으로 분석하고 이를 통해 자기 이방성이 프로그래밍된 소재로 제작된 액츄에이터의 구동 원리를 밝히고 모델을 정립하였다. 이 기술을 이용해 소재 내 원하는 영역마다 자기 이방성을 순차적으로 프로그래밍할 수 있으며 그와 동시에 다양한 모양으로 미세 소자를 구성하는 부품을 제작할 수 있다.

본 연구에서 개발한 자기 이방성을 프로그래밍할 수 있는 나노 복합 소재는 자기 나노입자의 자기 조립 특성과 본 연구실의 독자적 기술인 고분자 마이크로 입자 생성 기술을 이용하여 개발되었다. 이 기술을 이용하면 소재 내의 다양한 영역에 나노미터 크기 수준으로 인공적 자기 이방성을 프로그래밍할 수 있다. 그 제작 방법과 구동 환경이 매우 간단한 것에 비해 기존의 소재가 구현하기 어려운 복잡한 기능들을 수행할 수 있고, 외부의 기기들과 직접적으로 접촉할 필요가 없는 자기력을 사용하기 때문에 전기 화학적 주변 환경에 민감한 우주 공학이나 생명 공학에 사용되는 정밀 소자들을 제작하는데 매우 유용할 것이라 예상된다.

주요어: 고분자 기반 자성 나노복합체, 미세입자 구동, 자기조립, 광미세유체 리소그래피

학번: 2010-20779